# POLY(QUINONE-HYDRAZINE) BASED COMPOSITES FOR ENERGY STORAGE APPLICATIONS

Thesis Submitted for the Award of the Degree of

## **DOCTOR OF PHILOSOPHY**

in

## **CHEMISTRY**

By

Pooja

**Registration Number: 42000383** 

**Supervised By** 

Dr. Harish Mudila (19331)

**Department of Chemistry** 

**Associate Professor** 

**Faculty of Technology and Sciences** 



LOVELY PROFESSIONAL UNIVERSITY, PUNJAB
2025

**DECLARATION** 

I, hereby declared that the presented work in the thesis entitled "Poly(quinone-

hydrazine) based composites for energy storage applications" in fulfilment of

degree of **Doctor of Philosophy** (Ph. D.) is outcome of research work carried out by

me under the supervision of Dr. Harish Mudila working as Associate Professor in the

Chemical Engineering and Physical sciences, of Lovely Professional University,

Punjab, India. In keeping with general practice of reporting scientific observations, due

acknowledgements have been made whenever work described here has been based on

findings of other investigator. This work has not been submitted in part or full to any

other University or Institute for the award of any degree.

(Signature of Scholar)

Name of the scholar: Pooja

Registration No.: 42000383

Department/school: Chemical Engineering and Physical sciences

Lovely Professional University,

Punjab, India

i

**CERTIFICATE** 

This is to certify that the work reported in the Ph. D. thesis entitled "Poly(quinone-

hydrazine) based composites for energy storage applications" submitted in

fulfillment of the requirement for the award of degree of **Doctor of Philosophy (Ph.D.)** 

in the Chemical Engineering and Physical sciences, is a research work carried out by

Pooja, 42000383 is bonafide record of his/her original work carried out under my

supervision and that no part of thesis has been submitted for any other degree, diploma

or equivalent course.

(Signature of Supervisor)

Name of supervisor: Dr. Harish Mudila

Designation: Associate professor

Department/school: Chemical Engineering and Physical sciences

University: Lovely Professional University, Punjab

ii

#### **Abstract**

Although many materials, including carbonaceous and metallic materials, have been used to generate high electrochemical and electrical energy, none of these materials are perfect at producing energy with high efficiency; therefore, the need for new and efficient materials is always a push for vitality capacity.

To address future as well as present energy storage device concerns, conducting polymers (CPs) had a specific place where polyaniline, polypyrrole, polyindole, and other types of CPs were employed either alone or in combination. Whereas anthraquinone, benzoquinone, and their derivatives have been widely employed, quinone-based materials are new for producing high energy for operating these storage devices. A few of the studies even indicate the polymerized Quinone structure for energy storage. The study's main objective was to synthesize a polyazine that is poly(quinone-hydrazine) from quinone and hydrazine hydrate (NH<sub>2</sub>NH<sub>2</sub>.H<sub>2</sub>O) with an acidic catalyst for energy storage devices. Its composites were also prepared with graphene oxide (GO) and reduced graphene oxide (rGO) in different ratios, showing better energy storage applications.

A brown-coloured poly(quinone-hydrazine)/polyazine (PAZ) was synthesised by the polycondensation of p-benzoquinone and hydrazine hydrate with the help of catalyst ZnCl<sub>2</sub> at 110-113°C for 13 hrs. The resulting polymer was rinsed with Chloroform and acetic acid, which were used to remove the unaltered p-benzoquinone, and 1M NH<sub>4</sub>OH to eliminate the excess catalyst from the reaction product. Fourier transform infrared (FTIR) spectroscopy, scanning electron microscopy (SEM), and X-ray diffraction (XRD) were utilised to corroborate the structural characterizations, and thermogravimetric analysis (TGA) and differential scanning calorimetry (DSC) were employed to inspect the

thermal behaviour. The electrochemical behaviour of the PAZ was estimated through electrochemical methods involving galvanostatic charge/discharge (GCD), cyclic voltammetry (CV), and electrochemical impedance spectroscopy (EIS) using a carbon paste electrode (CPE) as a substrate in 1M H<sub>2</sub>SO<sub>4</sub> solution. With the scanning rate of 10 mV/s, the specific capacitance of PAZ has been measured with a maximum value of 35.42 F/g and a minimum value of 4.8 F/g with a scanning rate of 100 mV/s. The energy density for PAZ was recorded as 2.76 Wh/kg when measured at 1 A/g. Similarly, the energy density was found to be 4.41Wh/kg with 0.5 A/g, and 3.94 Wh/kg with 0.25 A/g current density. Similarly, the power density was determined to be 499.99 W/kg at 1 A/g, 249.99 W/Kg at 0.5 A/g, and 124.99 W/kg at a current density of 0.25 A/g. PAZ's extended conjugation and wide surface area, which promote better charge transfer and efficient charge carrier interaction, are responsible for its notable electroactive performance. The Bode plot and EIS studies indicate the typical behaviour of the conducting polymer with a significant phase angle and impedance. The synthesized PAZ's potential as a supercapacitor material is demonstrated by the electrochemical investigations.

Although PAZ has specific properties (such as high power density and specific capacitance) that make it an appropriate choice for supercapacitors, performance is constrained by the possibility of a low power density. Therefore, certain carbonaceous elements are added to the conducting polymer matrix to combat this. Because of its potential for functionalization and flaws, graphite oxide (GO), a carbonaceous substance, can be employed as a good starting material for the creation of composites with conducting polymers. GO sheets contain functional groups such as C-O-C, -COOH, and -OH. Due to their affordability, time efficiency, and improved conductivity from their electroactive components, compounds containing GO and their composites have been modified in various ways. Furthermore, there are other conducting

polymer-GO nanocomposites that are already being investigated for energy storage applications because of their small particle sizes and intercalation properties. As a result, the idea of using conducting polymer-GO for energy storage devices has recently attracted a lot of attention. The expanding uses of PAZ and GO have encouraged the authors to develop a substance that would be a good fit for developing extremely sophisticated energy storage devices. Using a simple in-situ polymerization technique, this work produces composites (PGs) with varying PAZ to GO ratios. The prepared composites were characterised by FTIR, SEM, XRD, TGA, and DSC techniques. The electrochemical properties were assessed using GCD, CV, and EIS methods. Through CV analysis, the extreme specific capacitance was 247.20 F/g with a scanning rate of 10 mV/s, and the lowest value was 33.53 F/g with a scan rate of 100 mV/s for GO. The extreme specific capacitance for PG-1 was 77.48 F/g, for PG-2 was 140.20 F/g, for PG-3 was 332.05 F/g, for PG-4 was 475.61, and PG-5, was 407.56 F/g with a scanning rate of 10 mV/s. When measured at 100 mV/s scan rate, the specific capacitance values were 10.52 F/g for PG-1, 18.90 F/g for PG-2, 45.30 F/g for PG-3, 63.10 F/g for PG-4, and 55.11 F/g for PG-5. PG-4 exhibited the maximum specific capacitance, which declined as the GO content escalated in PG-5. According to GCD results, GO exhibited 22.39 F/g specific capacitance, 5.06 Wh/kg energy density, and 856.33 W/kg power density when measured at 1A/g current density. In contrast, PG-4 showed energy and power densities of 10.35 Wh/kg and 1007.02 W/kg, respectively, with reduced impedance facilitating better charge transport at 1 A/g.

Reduced graphene oxide (rGO), another carbon-based material, has been recognized as an exceptional choice for supercapacitor applications owing to its vast surface area as well as its good electrical conductivity and electric double-layer capacitance. Due to the impressive conductivity properties of PAZ and rGO, and the growing

applications of these materials, the authors have motivated us to develop a novel material that could potentially serve as a good choice for fabricating highly advanced energy storage devices.

In this study, composites featuring varied PAZ to rGO ratios were fabricated via a straightforward in-situ polymerization method. Furthermore, the rGO was synthesized by reducing GO in the presence of the reducing agent, ascorbic acid. The resulting rGO and PrGs were characterized by the FTIR, XRD, SEM, TGA, and DSC techniques. The electrochemical behaviour was evaluated by the GCD, CV, and EIS techniques. The extreme value of specific capacitance for rGO is 383.21 F/g with a scanning rate of 10 mV/s, and the minimum value 48.77 F/g noted at 100 mV/s. The extreme value of specific capacitance was noted as 158.76 F/g for PrG-1, 312.10 F/g for PrG-2, 689.21 F/g for PrG-3, and 432.21 F/g for PrG-4 with a 10 mV/s scanning rate. The lowest specific capacitance was found to be 20.11 F/g for PrG-1, 43.34 F/g for PrG-2, 112.54 F/g for PrG-3, and 54.22 F/g for PrG-4 with 100 mV/s scanning rate. Based on the above calculation, it was analysed that PrG-3 had the highest specific capacitance value, which began to decline when the amount of rGO in the composite PrG-4 increased. The specific capacitance was 90.11 F/g along with 12.52 Wh/kg energy density, and 500 W/kg power density noted for rGO at 1A/g current density. The measured values for PrG-3 were 235.31 F/g for specific capacitance, 32.68 Wh/kg for energy density, and 499.99 W/kg for power density under 1 A/g current density. The Nyquist plot of PrG-3 didn't not show any semicircle, which clearly suggests that this compound had either no barrier to charge transmission or low faradaic resistance.

 Among all the PAZ composite materials, the PrG-3 composite exhibits significantly greater specific capacitance, high energy density compared to the polymer alone, and PG-4 exhibits high specific capacitance, high power density. Therefore, the PG-4 and PrG-3 composite electrode represents a promising candidate for the development of future safe and cost-effective electrochemical supercapacitors and batteries intended for energy storage and conversion applications. Based on their electrochemical behaviour, it was observed that the composite of PAZ with GO, i.e., the PG-4 composite electrode, may be a promising candidate for the development of future safe and reasonably priced electrochemical supercapacitors, and PrG-3 may be useful for batteries.

# Acknowledgement

Dedicated to my little sweetheart

Apurva Yadav

Looking back on the omega portion of this PhD adventure, I am incredibly grateful for the unwavering support and encouragement I have received from so many individuals. Though this thesis may be the culmination of many years of my work, I would like to sincerely thank everyone who helped make it possible.

First and foremost, I would like to express my deepest gratitude to my supervisor, **Dr. Harish Mudila**, for their invaluable guidance, support, and encouragement throughout this research journey. Their expertise and insights have been instrumental in shaping this work, and I am deeply appreciative of the time and effort they have dedicated to helping me succeed.

I am immensely grateful to my husband, **Arun Yadav**, whose love, patience, and understanding have been a constant source of strength. His unwavering belief in my abilities and his support during the long hours of research and writing have been invaluable. Without his encouragement, this journey would not have been possible.

A special thank you to my beloved daughter, **Apurva Yadav**, whose laughter and love have been a source of joy and motivation. Balancing motherhood and academic work has been challenging, but her presence has brought light and purpose to this journey.

To my parents, **Sh. Udayveer Yadav and Smt. Krishna Yadav**, I extend my heartfelt appreciation for their endless love, sacrifices, and the strong foundation they provided me. Their belief in education and their constant support have been the cornerstone of my academic pursuits. I am forever indebted to them for their encouragement and for always being there.

I would also like to express my sincere gratitude to my brother, **Nikhil Yadav**, and my sister, **Priya Yadav**, for their constant encouragement

and support. Their belief in me and their words of motivation have strengthened me throughout this journey.

I am also deeply thankful to my in-laws for their understanding, patience, and encouragement. Their support, both practical and emotional, has been a tremendous help in allowing me to focus on my research.

I am especially grateful to my grandfather, **Sh. Bohtram Yadav**, whose wisdom and encouragement have always inspired me to pursue my dreams. I also wish to honor the loving memory of my late grandmother, **Smt. Singari Yadav**, whose blessings and values continue to guide me every step of the way. She always wished to see me grow as a well-educated person.

A special acknowledgment to the Chemistry department of LPU and CIF Jalandhar for providing the resources and support essential to completing this research. I am also grateful to all the faculty members and administrative staff for their assistance and encouragement during my time here.

Lastly, I extend my gratitude to all those who contributed to this work directly or indirectly. Your support and kindness have left a lasting impact, and I am forever grateful.

Thank you doesn't seem sufficient, but it is said with appreciation and respect to all of them for their support and encouragement.

This thesis is dedicated to everyone who believed in me and stood by my side through every step of this journey.

I convey special acknowledgment to my daughter, Apurva Yadav.

## **Table of Contents**

Chapter-1		
INTRODUCT	TION	01-15
1.1	Introduction of Conducting Polymer	1-3
1.2	Properties of CPs	3-5
1.3	Quinone-Based Conducting Material	5-7
1.4	Quinone-based materials for energy storage	7-8
References  Chapter-2		9-15
LITERATUR	E REVIEW	16-49
2.1	Quinones-based supercapacitors	18-24
2.2	Quinone-based conducting polymers	24-29
2.3	Quinone/Graphene composites as supercapacitors	29-32
2.4	Azine-based conducting polymers	32-36
References		39-49
Chapter-3		
MATERIALS	S AND METHODS	50-71
3.1	Materials	50
	Synthesis	51

3.2.1	Synthesis of Poly(quinone-hydrazine) (Polyazine, PAZ)	51-52
3.2.2	Synthesis of Graphene Oxide (GO)	52-53
3.2.3	Synthesis of Reduced Graphene Oxide (rGO)	53
3.2.4	Fabrication of Polyazine/Graphene Oxide Composite (PAZ/GO or PGs)	53-54
3.2.5	Fabrication of Polyazine (PAZ)/ reduced Graphene Oxide(rGO) Composite (PAZ/rGO or PrGs)	55
3.2.6	Fabrication of electrode on carbon paste electrode (CPE)	55-56
3.3	Characterization techniques	56-57
3.3.1	Fourier transform infrared spectroscopy (FTIR)	57-59
3.3.2	X-ray diffraction (XRD) technique	59-60
3.3.3	Thermal Properties	60
3.3.3.1	Thermogravimetric analysis (TGA)	60-61
3.3.3.2	Differential Scanning Calorimetry (DSC)	61-62
3.3.4	Scanning Electron Microscopy (SEM)	62-63
3.4	Electrochemical Characterisation	64
3.4.1	Cyclic voltammetry (CV)	64-65
3.4.2	Galvanostatic charge-discharge (GCD)	65-66
3.4.3	Electrochemical Impedance Spectroscopy (EIS)	66-67

# **Chapter-4**

RESULT AND I	DISCUSSION	72-129
4.1	FOURIER TRANSFORM INFRARED SPECTROSCOPY (FTIR)	72
4.1.1	FTIR of Polyazine (PAZ)	72-73
4.1.2	FTIR of Graphene Oxide (GO)	73
4.1.3	FTIR of Reduced graphene oxide (rGO)	74
4.1.4	FTIR of Polyazine composite with GO (PG)	75-76
4.1.5	FTIR of composite of Polyazine with reduced Graphene Oxide (PrG)	75-77
4.2	MORPHOLOGICAL STUDIES	77
4.2.1	XRD of PAZ	77-79
4.2.2	XRD of GO	79-80
4.2.3	XRD of rGO	80-81
4.2.4	XRD of the composite of PAZ with GO (PG)	81
4.2.5	XRD of a composite of PAZ with rGO (PrG)	82-83
4.3	SCANNING ELECTRON MICROSCOPY (SEM)	84
4.3.1	SEM of PAZ	84
4.3.2	SEM of GO	85
4.3.3	SEM of rGO	85-86
4.3.4	SEM of the composite of PAZ with GO (PG)	86-87
4.3.5	SEM of the composite of PAZ with rGO (PrG)	87
4.4	THERMAL PROPERTIES	87-88
4.4.1	TGA of PAZ	88-89

4.4.2	TGA of GO	89-90
4.4.3	TGA of rGO	90-91
4.4.4	TGA of PG along with PAZ and GO	91-92
4.4.5	TGA of PrG along with PAZ and rGO	92-93
4.5	DIFFERENTIAL SCANNING	93
	CALORIMETRY (DSC)	
4.5.1	DSC of PAZ	93-94
4.5.2	DSC of GO	94-95
4.5.3	DSC of rGO	95-96
4.5.4	DSC of PG, PAZ and GO	96-97
4.5.5	DSC of PrG along with PAZ and rGO	97-98
4.6	ELECTROCHEMICAL STUDIES	98-99
4.6.1	CYCLIC VOLTAMMETRY (CV)	99
4.6.1.1	CV of PAZ	99-101
4.6.1.2	CV of GO	101-103
4.6.1.3	CV of rGO	103-104
4.6.1.4	CV of composites of PAZ with GO (PGs)	104-107
4.6.1.5	CV of composites of PAZ with rGO	107-108
	(PrGs)	
4.6.2	GALVANOSTATIC CHARGE-	108-109
	DISCHARGE (GCD)	
4.6.2.1	GCD of PAZ	109-110
4.6.2.2	GCD of GO along with PAZ and PG-4	111-112
4.6.2.3	GCD of rGO, PAZ and PrG-3	112-113
4.6.3	ELECTROCHEMICAL IMPEDANCE	114
	SPECTROSCOPY (EIS)	
4.6.3.1	EIS of PAZ	114-116
4.6.3.2	EIS of PAZ, GO and PG-4	116-118
4.6.3.3	EIS of PAZ, rGO and PrG-3	118-120

References		121-129	
Chapter-5			
SUMMARY AND FUTURE OUTLOOK130-134			
5.1	Summary	130-134	
5.2	Future outlook	134	

- List of Publications
- List of Conferences
- List of workshops attended

#### **List of Tables**

Table:1	Some quinone-based materials for energy	37-38
	storage devices	
Table:2	Materials Used in the Synthesis Process	50
Table:3	Composition and weight ratio of PGs	54
Table:4	Composition and weight ratio of PrGs	55
Table:5	Specific capacitance of GO at various	102
	scan rates	
Table:6	Specific capacitance of rGO at various	104
	scan rates	
Table:7	Specific capacitance of the PAZ, GO, and	106
	PGs at various scan rates	
Table:8	Specific capacitance of the PAZ, rGO, and	108
	PrGs at various scan rates	
Table:9	Specific capacitance, energy, and power	110
	density of PAZ at varying current densities	
Table:10	Specific capacitance, energy, and power	111
	density of PAZ, GO, and PG-4 at the	
	current density of 1 A/g	
Table:11	Specific capacitance, energy, and power	113
	density of PAZ, rGO, PrG-3 at the current	
	density of 1A/g	

# **List of Figures**

Figure 1	Energy band gap diagram for materials	4
Figure 2(A)	The Synthesis process of PAZ	52
Figure 2(B)	Dark brown coloured PAZ	52
Figure 3(A)	Synthesis of GO	53
Figure 3(B)	Synthesis of rGO	53
Figure 4(A)	In-situ Composite formation of PAZ/GO	54
	(PGs)	
Figure 4(B)	In-situ Composite formation of	54
	PAZ/rGO (PrGs)	
Figure 5	Fabrication of a carbon paste electrode	56
	for electrochemical studies	
Figure 6	Block diagram of the FTIR working	58
	process	
Figure 7(A)	FTIR instrument of the Perkin Elmer	59
	company	
Figure 7(B)	Bruker powder X-ray diffractometer	59
Figure 8(A)	TGA instrument used for current	61
	research	
Figure 8(B)	DSC Instrument used to measure	61
	thermal transitions	
Figure 9	SEM instrument used for	63
	morphological study of prepared	
	materials	
Figure 10	Instrument for electrochemical	64
	characterization	
Figure 11	FTIR spectrum of PAZ	72
Figure 12	FTIR spectrum of GO	73
Figure 13	FTIR spectrum of rGO	74
Figure 14	FTIR spectrum PAZ, GO, and PG	76

Figure 15	FTIR spectrum of PAZ, rGO, and PrG	77
Figure 16	XRD of PAZ	78
Figure 17	XRD of GO	80
Figure 18	XRD of rGO	81
Figure 19	XRD of PAZ, GO, and PG	82
Figure 20	XRD of PAZ, rGO and PrG	83
Figure 21(A-	SEM images of PAZ at 500, 5000, and	84
C)	25000 magnification	
Figure 22(A-	SEM images of GO at 500, 5000, and	85
C)	25000 magnification	
Figure 23(A-	SEM images of rGO at 500, 5000, and	86
C)	25000 magnification	
Figure 24(A-	SEM images of PG at 500, 5000, and	87
C)	25000 magnification	
Figure 25(A-	SEM images of PrG at 500, 5000, and	87
C)	25000 magnification	
Figure 26	TGA plot of PAZ	88
Figure 27	TGA plot of GO	89
Figure 28	TGA plot of rGO	90
Figure 29	TGA plot of PAZ, GO, and PG composite	92
Figure 30	TGA plot of PAZ, rGO, and PrG	93
	composite	
Figure 31	DSC curve of PAZ	94
Figure 32	DSC curve of GO	95
Figure 33	DSC curve of rGO	96
Figure 34	DSC curve of PAZ, GO, and PG	97
	composite	
Figure 35	DSC curve of PAZ, rGO, and PrG	98
	composite	
Figure 36	CV of PAZ at a varying scan rate	100
Figure 37	CV curve of GO at various scan rates	102

Figure 38	CV of rGO at a varying scan rate	104
Figure 39	CV of PGs at 10 mV/s scan rate	105
Figure 40	CV of PrGs at 10 mV/s scan rate	107
Figure 41	GCD curve for PAZ at varying current	110
	density	
Figure 42	GCD curves of PAZ, GO, and	112
	representative PG-4 at 1 A/g	
Figure 43	GCD curves of PAZ, rGO, and	113
	representative PrG-3 at 1 A/g	
Figure 44	Nyquist plot of PAZ	115
Figure 45	Bode plot of the prepared PAZ	115
	representing the typical relation	
	between impedance, frequency, and	
	phase angle	
Figure 46	Nyquist plot of PAZ, GO, and	117
	representative PG-4	
Figure 47	Bode plot of PAZ, GO, and	118
	representative PG-4	
Figure 48	Nyquist plot of PAZ, rGO, and PrG-3	119
Figure 49	Bode plot of PAZ, and PrG-3	120

1.1 Introduction of Conducting Polymers: Energy is essential because it powers everything around us, from natural processes to human-made systems. Without energy, nothing can function or exist in the way we experience it. Energy is the foundation of life, technology, and human progress. Energy makes modern life convenient and efficient [1]. Energy is essential for maintaining life, promoting economic expansion, and developing modern innovations. In its many forms—kinetic, potential, chemical, thermal, electrical, and nuclear—it can be characterized as the ability to carry out work. According to the rule of conservation of energy, energy in nature can only be changed from one form to another; it can't be created or destroyed. The availability of energy represents one of the main issues of the twentyfirst century since the world's population is growing and industrialization is happening at an unprecedented rate. The primary energy sources are still standard fossil fuels like oil, natural gas, and coal but their usage is linked to environmental depletion, climate change and emission of greenhouse gases [2,3]. Research on sustainable and renewable sources, such energy biomass, wind, hydropower, and cutting-edge energy storage technologies, has increased as a result of these difficulties. Energy is a environmental and socioeconomic issue in addition to being a physical term. Reducing reliance on fossil fuels while maintaining long-term sustainability, environmental preservation and economic stability is the goal of the global shift to clean and renewable energy. As a result, energy research is essential to solving global issues including sustainable developement, climate change, and technological advancement [4].

Without energy, devices won't function. Some devices (like medical equipment) are critical for saving lives. Modern apps (mobile

applications), operating systems, and background processes require energy to operate smoothly. Every action (touch, scroll, call, gaming, video playback) requires processing power, which consumes energy. The battery supplies energy to the screen, processor, speakers, and other hardware. A battery needs energy because it stores and provides power to devices. Phones, laptops, and cars need energy from batteries to function [1, 5]. Some batteries (like in UPS systems) store energy for later use in case of a power outage. Metals are used for energy storage because they have high electrical conductivity, durability, and energy density. They allow efficient energy transfer within batteries and power systems. Metals are strong and resistant to wear, making them reliable long-term energy storage. They can withstand multiple charge/discharge cycles without breaking down [6, 7]. Metals are being replaced by conducting polymers (CPs) in batteries because polymers offer several advantages, including lightweight properties, flexibility, and environmental benefits. Polymers like polyaniline (PANI), polypyrrole (PPY), polythiophene (PTH), polyindole (PIND), polyazine (PAZ) etc. can conduct electricity efficiently. They can replace metal electrodes while maintaining good energy flow. CPs are shaping the future of batteries, making them safer, lighter, and greener [8, 9].

The CPs are usually known as 'conjugated polymers' due to their alternating single and double-bond characteristics. It is observed that in a pure state, conjugated polymers act as semiconductors or insulators. Electrons can delocalize across the system due to their unique chain conjugation, allowing them to be shared by several atoms [10]. Delocalized electrons can flow across the system and act as charge carriers, resulting in conductive properties. The delocalization of electrons determines the electrical conductivity of any material. In metals, the electrons can readily surmount the energy barrier between the conduction and valence bands, resulting in a low band gap and high conductivity. However, metals exhibit certain drawbacks, such as high

cost and susceptibility to corrosion. These days, supercapacitors and rechargeable batteries are considered effective sources for electrochemical energy storage owing to their exceptionally high power density, energy density, and remarkable cyclic stability. In this regard, metals and their oxides, sulfides, and other pseudocapacitive and supercapacitive materials have been thoroughly studied to attain high energy and power densities, making them essential components of energy storage systems. Nevertheless, these materials based on transition metals are relatively expensive, have finite supplies, and are linked to certain environmental issues [11-14]. Consequently, there is a need for a material that can substitute metals with their high or appreciable conductivity without the limitations associated with these metals. This requirement can be met by certain organic materials known as conductive polymers, also referred to as synthetic metals [15, 16].

**1.2. Properties of CPs:** A variety of CPs have been produced in the laboratory through various synthetic routes. These CPs encompass well-known polymers such as PPY [17], polyacetylene (PACE) [18], PTH [19], PANI [20], PIND [21], PAZ [22], etc., and their derivatives. These CP's or organic polymers generally contain sigma ( $\sigma$ ) and pi ( $\pi$ ) bonds where the  $\sigma$  bond is localized and  $\pi$  bonds can be delocalized and this delocalization of  $\pi$  bonds if present in conjugation is responsible for the conduction of electricity in the large molecules [23]. When the polymers are undoped, they have a broad bandgap and are either insulating or semiconducting. Delocalized charge carriers are produced by either reduction or oxidation reactions that change these polymers into electrically conductive or doped forms [17]. To achieve conductivity, the polymeric backbone of conducting polymers requires oxidation or reduction to introduce charge, which is facilitated through the incorporation of anionic or cationic species referred to as dopants. Anions and cations transfer charge from one location to another in response to an electrical field, enhancing conductivity [18, 19]. The energy gap is typically around 2 eV or more, preventing charge carriers' thermal excitation (Fig. 1). A substance is categorized as an insulator if its electrical conductivity is less than  $10^{-7}$  S/cm, and as a conductor if value lies above  $10^3$  S/cm. Conversely, the semiconductor's conductivity is determined by the bandgap, type, and degree of doping and ranges from  $10^{-4}$  to 10 S/cm [20, 24].

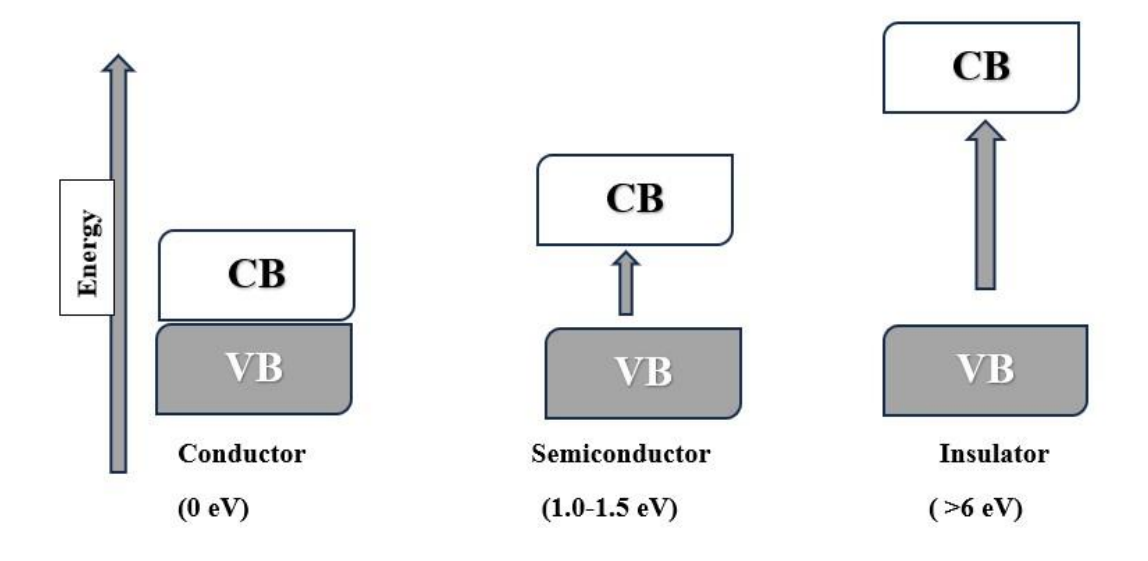


Figure 1: Energy band gap diagram for materials

The conductivity of various polymers mainly depends upon  $sp^2$  hybridized linear carbon chains. Polymers exhibit unique electrical properties due to decoupling the  $p_z$  electron from the backbone sigma-orbital **[25].** CPs demonstrate potential as candidates for a diversity of electronic applications, such as shielding against electromagnetic interference, electro-optical devices, flexible "plastic" transistors like electroluminescent polymer displays, photovoltaic solar cells, polymer light-emitting diodes, and electrochemical systems like chemical sensors, biochemical sensors, and rechargeable batteries. Organic substances have shown great promise as cathode materials for LIBs and supercapacitors because they have special qualities and benefits above their more conventional inorganic equivalents. This

paper examines the application of organic substances as cathode materials in energy storage systems, with a particular emphasis on supercapacitors and batteries [26-29].

The study of CPs has been garnering increasing attention due to their remarkable characteristics, including high electrical conductivity, non-corrosive properties, flexibility, tunability, facile processing, chemical, thermal, and mechanical durability, efficient charge transport, biocompatibility, adaptability, rigidity, and lightweight construction. Moreover, CPs are fabricated using low-cost materials, making them a viable substitute for metals in various applications [30,31]. Along with the various CPs, the quinone-based conductive polymers have demonstrated high redox potential and long-term cycling stability. These properties, along with their fast redox kinetics and stable structure, make them a promising option for supercapacitors and rechargeable batteries [32].

1.3. Quinone-Based Conducting Materials: Due to its outstanding redox characteristics, quinone is crucial in naturally occurring electrochemical processes, such as electron transfer in photosynthesis, thereby aiding in the conversion and storage of biological energy. The chemistry behind this natural process has inspired scientists to incorporate this concept to improve current energy storage technologies [33, 34]. It is noteworthy that quinone-based materials serve as cathode materials with high voltage and capacity, which can experience voltage hysteresis, thereby surpassing the energy in similar high-voltage cells. The significant redox potential of quinone-based materials positions them as a viable option for use in both monovalent and multivalent battery systems [34, 35]. The wide range of potentials in which this material can function allows it to be utilized as both an anode and a cathode material.

Research has identified power density, energy density, and cycle stability as significant challenges for materials used in energy storage, particularly concerning CPs, which often face setbacks due to their limitations. In addition to these, various conducting polymeric materials encounter numerous other issues. Studies on quinone derivatives, such as naphthoquinone and benzoquinone, have primarily focused on the Li system. However, the solubility of quinone derivatives in the electrolyte poses a significant obstacle to their use in battery and supercapacitor applications [32]. Furthermore, the formation of polymers from quinones, which exhibit a high reduction-oxidation potential, is a complex process. However, research advancements have successfully overcome these challenges, resulting in desirable electrochemical performances through specific modifications to the synthetic methods [36, 37]. To enhance its electrochemical properties and energy storage capacities, quinone has been hybridized with a variety of inorganic and organic substances in previous studies [33].

Quinones have great potential as capacity-carrying functions because of their high theoretical capacity, quick charge transfer process, strong redox stability, and structural variety. Roughly high discharge capacity, high discharge capacity, and good cycling stability may be attained, according to a recent study on quinone-based battery materials [38]. Several research studies have been conducted in buffered, unbuffered, and aprotic solvents to investigate the redox behaviour of quinone. The general structure of quinone and its associated derivatives includes two carbonyl groups, which facilitate the transfer of two protons and electrons within the system. Quinone has been observed to display a single redox peak (reduction of quinone to hydroquinone and vice-versa) in a buffered medium, with a linear relationship between the peak potential and the solution pH. In contrast, the redox potential of quinone is significantly impacted in unbuffered solutions due to the oxidation and reduction processes occurring at the electrode-solution interface. This causes acidic and basic entities to have a significant impact on quinone-based materials'

electrochemical activity. Therefore, it is recommended to utilize pH-buffered aqueous solutions for studying the electrochemical properties of quinone-based systems [39].

Relative to conventional metal-based redox batteries, redox flow batteries engineered with quinone and its derivatives demonstrate advantages, including the ability to deliver high energy densities and significant redox potentials.

1.4. Quinone-Based Materials for Energy Storage: Similarly, quinones have been widely utilized as an efficient material for storing energy in various electroactive materials because of their high energy density. Quinone and its derivative compounds are being employed in supercapacitors and rechargeable batteries for energy storage applications, owing to their distinct properties, such as high energy density, excellent cyclic stability, and improved capacity retention. Numerous studies have been conducted to examine the advantages and drawbacks of quinone and its derivative compounds. These quinonebased materials possess a substantial number of carbonyl structures with low molecular weight, resulting in enhanced specific capacity [35]. Increased aromatic character was observed to reduce the redox potential, whereas ortho-quinones and para-quinones exhibited the highest and lowest redox potentials, respectively. Functionalization of the molecular structure can modulate the HOMO-LUMO energy gap, thereby influencing the electrical conductivity of quinone compounds [40,41].

1,4-benzoquinones have become attractive options, owing to their favorable attributes, including high energy density, robust specific capacity, affordability, and environmental friendliness. Likewise, the Mg-Benzoquinone cell has demonstrated efficient and comparatively elevated energy density, rendering it a compelling contender for the development of future rechargeable metal-organic batteries [42, 43].

Despite being used as a viable contender for energy storage materials, 1,4-benzoquinone continues to have several drawbacks that prevent it from being widely used in energy storage systems. The solubility of 1,4-benzoquinone is higher when compared to naphthoquinone and anthraquinone. Due to this high solubility and its relatively limited oxidative stability, the use of benzoquinone as a cathode-active material is somewhat restricted [42].

PAZ (a quinone-based polymer) has been the focus of considerable research attention owing to its distinctive electronic, electrochemical, and redox characteristics. Quinone-based polymers, including PAZ, have excellent redox activity, making them ideal for organic batteries, supercapacitors, and redox flow batteries. These materials offer high capacity, quick charge/discharge rates, and extended cycle life compared to conventional inorganic electrodes. PAZs' mechanical flexibility and electronic properties make them useful for next-generation wearable technologies, such as flexible batteries and electronic textiles. With the growing demand for lightweight, efficient, and sustainable materials, PAZ-based quinone polymers are expected to play a critical role in the development of green energy storage, catalysis, and next-generation electronics. The research community has extensively studied the PAZ (from benzoquinone and hydrazinehydrate) conducting material to investigate its potential applications in electrochemical energy storage. Conjugated PAZ constitutes a novel class of semiconductor materials with significant promise for use in organic thin-film transistors. Efficient azine bond formation techniques, including a condensation process involving hydrazine and a pconjugated dialdehyde or diketone, can be used to create these compounds. It is discovered that the azine linkage is a unique and strong electron-withdrawing element that can be utilized to lower the LUMO energy level and offer electron mobility characteristics [44].

#### References

- [1] Pramanik, P. K. D., Sinhababu, N., Mukherjee, B., Padmanaban, S., Maity, A., Upadhyaya, B. K., Holm-Nielsen, J. B., & Choudhury, P. (2019). Power Consumption Analysis, Measurement, Management, and Issues: A State-of-the-Art Review of Smartphone Battery and Energy Usage. *IEEE Access*, 7, 182113-182172. doi:10.1109/access.2019.2958684
- [2] Chu, S., & Majumdar, A. (2012). Opportunities and challenges for a sustainable energy future. *Nature*, 488(7411), 294–303. doi.org/10.1038/nature11475
- [3] Ahmad, T., & Zhang, D. (2020). A critical review of comparative global historical energy consumption and future demand: The story told so far. *Energy Reports*, 6, 1973–1991. doi.org/10.1016/j.egyr.2020.07.020
- [4] Sims, R. E. H., Rogner, H. H., & Gregory, K. (2003). Carbon emission and mitigation cost comparisons between fossil fuel, nuclear and renewable energy resources for electricity generation. *Energy Policy*, 31(13), 1315–1326. doi.org/10.1016/S0301-4215(02)00192-1
- [5] Aghmadi, A., & Mohammed, O. A. (2024). Energy Storage Systems: Technologies and High-Power Applications. *Batteries*, 10(4), 141. doi:10.3390/batteries10040141
- [6] Kiai, M. S., Eroglu, O., & Aslfattahi, N. (2023). Metal-Ion Batteries: Achievements, Challenges, and Prospects. *Crystals*, 13(7), 1002. doi:10.3390/cryst13071002
- [7] Lobato-Peralta, D. R., Okoye, P. U., & Alegre, C. (2024). A review on carbon materials for electrochemical energy storage applications: State of the art, implementation, and synergy with metallic compounds for supercapacitor and battery electrodes. *Journal of Power Sources*, 617, 235140. doi:10.1016/j.jpowsour.2024.235140

- [8] Saal, A., Hagemann, T., & Schubert, U. S. (2020). Polymers for Battery Applications—Active Materials, Membranes, and Binders. *Advanced Energy Materials*, 11(43), 2001984. doi:10.1002/aenm.202001984
- [9] Oladele, I. O., Adelani, S. O., Taiwo, A. S., Akinbamiyorin, I. M., Olanrewaju, O. F., & Orisawayi, A. O. (2025). Polymer-based nanocomposites for supercapacitor applications: a review on principles, production and products. RSC Advances, 15, 7509-7534. DOI: 10.1039/D4RA08601E
- [10] Shahid, M. A., Rahman, M. M., Hossain, M. T., Hossain, I., Sheikh, M. S., Rahman, M. S., Uddin, N., Donne, S. W., & Hoque, M. I. U. (2025). Advances in Conductive Polymer-Based Flexible Electronics for Multifunctional Applications. *Journal of Composites Science*, 9(1), 42. doi:10.3390/jcs9010042
- [11] Kumar, M., Samal, S. K., & Maharana, T. (2024). Conducting Polymers: An Approach Towards Flexible Supercapacitors. *Polymer-Plastics Technology and Materials*, 64(3), 309–328. doi.org/10.1080/25740881.2024.2406507
- [12] Zhou, L., Li, C., Liu, X., Zhu, Y., Wu, Y., & Ree, T. V. (2018). Metal oxides in supercapacitors. In Yuping W. *Metal Oxides in Energy Technologies*, 169–203. doi:10.1016/b978-0-12-811167-3.00007-9
- [13] Adil, M., Abdelkareem, M. A., Sayed, E. T., Rodrigue, C., Ramadan, M., & Olabi, G. A. (2022). Progress of Metal Chalcogenides in Supercapacitors. In *Reference Module in Materials Science and Materials Engineering*, 24-433. doi: 10.1016/B978-0-12-815732-9.00153-4
- [14] Ajloo D., Yoonesi B., & Soleymanpour A. (2010). Solvent Effect on the Reduction Potential of Anthraquinones Derivatives. The Experimental and Computational Studies. *International Journal of*

- Electrochemical Science, 5(4), 459 477. Doi:10.1016/S1452-3981(23)15298-9
- [15] An, J. Y., Lee, H. S., Kim, J., Ryu, S. W., Park, B. C., & Kahng, Y. H. (2021). Doping of graphene with polyethylenimine and its effects on graphene-based supercapacitors. *Journal of Applied Physics*, 129(9), 094904. doi:10.1063/5.0035891
- [16] Kaloni, T. P., Schreckenbach, G., & Freund, M. S. (2016). Bandgap modulation in polythiophene and polypyrrole-based systems. *Scientific Reports*, 6, 36554. doi:10.1038/srep36554
- [17] Mudila, H., Joshi, V., Rana, S., Zaidi, M. G. H., & Sarfaraz, A. (2014). Enhanced electrocapacitive performance and high-power density of polypyrrole/graphene oxide nanocomposites prepared at reduced temperature. *Carbon Letters*, 15(3), 171–179. doi: 10.5714/CL.2014.15.3.171
- [18] Seo, J., Lee, S. Y., & Bielawski, C. W. (2019). Unveiling a masked polymer of dewar benzene reveals trans-poly(acetylene). *Macro-molecules*, 52(8), 2923–2931.doi:10.1021/acs.macro mol.8b02754
- [19] Hong, X., Liu, Y., Li, Y., Wang, X., Fu, J., & Wang, X. (2020). Application progress of polyaniline, polypyrrole, and polythiophene in lithium-sulfur batteries. *Polymers*, 12(2), 331. doi: 10.3390/polym12020331
- [20] Shen, Y., Xue, H., Wang, S., Wang, Z., Zhang, D., Yin, D., Wang, L., & Cheng, Y. (2021). A highly promising high-nickel low-cobalt lithium layered oxide cathode material for high-performance lithium-ion batteries. *Journal of Colloid and Interface Science*, 597, 334–344. doi:10.1016/j.jcis.2021.04.008
- [21] Mudila, H., Prasher, P., Kumar, M., Kumar, A., Zaidi, M. G. H., & Kumar, A. (2019). Critical analysis of polyindole and its composites in

- supercapacitor application. *Materials for Renewable and Sustainable Energy*, 8(9), 2851. doi:10.1007/s40243-019-0149-9
- [22] Hong, W., Sun, B., Aziz, H., Park, W.-T., Noh, Y.-Y., & Li, Y. (2012). A conjugated polyazine containing diketopyrrolopyrrole for ambipolar organic thin film transistors. *Chemical Communications*, 48(67), 8413. doi:10.1039/c2cc33998f
- [23] Ramya, R., Sivasubramanian, R., & Sangaranarayanan, M. V. (2013). Conducting polymers-based electrochemical supercapacitors-Progress and prospects. *Electrochimica Acta*, 101, 109–129. doi:10.1016/j.electacta.2012.09.116
- [24] Das, T. K., & Prusty, S. (2012). Review on conducting polymers and their applications. *Polymer-Plastics Technology and Engineering*, 51(14), 1487–1500. doi:10.1080/03602559.2012.710697
- [25] Zhang, K., Zhang, Y., & Shi, L. (2020). A review of linear carbon chains. *Chinese Chemical Letters*, 31(7), 1746-1756. doi:10.1016/j.cclet.2020.03.019
- [26] Andezai, A. & Iroh, J. O. (2025). Review: Overview of Organic Cathode Materials in Lithium-Ion Batteries and Supercapacitors. *Energies*, 18(3), 582. doi.org/10.3390/en18030582.
- [27] Hasan, B. M., Parvez, M. M., Abir, A. Y., & Ahmad, F. M. (2025). A review on conducting organic polymers: Concepts, applications, and potential environmental benefits. *Heliyon*, 11(3), e42375. doi.org/10.1016/j.heliyon.2025.e42375
- [28] Adeosun, W. A., Katowah, D. F., Asiri, A. M., & Hussein, M. A. (2021). Conducting terpolymers and its hybrid nanocomposites variable trends. review. From synthesis applications. Α to *Polymer-Plastics* Technology Materials, 60(3), 271–285. and doi.org/10.1080/25740881.2020.1811316

- [29] Zhigerbayeva, G., Aliyev, A., Magazov, Y., Kudryashov, V., Adilov, S., & Nuraje, N. (2025). Efficient template free polymerization of continuously porous hybrid conducting polymers for highly stable flexible micro pseudocapacitors. *Scientific Reports*, 15, 9577. doi.org/10.1038/s41598-025-93663-5
- [30] Miao, L., Liu, L., Li, Y., Lü, Y., Cheng, F., Chen, J., & Shang, Z.-F. (2018). The structure–electrochemical property relationship of quinone electrodes for lithium-ion batteries. *Physical Chemistry Chemical Phys*ics, 20, 13478–13484. doi:10.1039/C8CP00597D
- [31] Nellaiappan, S, Shalini Devi, K. S., Selvaraj, S., Krishnan, U. M., & Yakhmi, J. V. (2021). Chemical, gas, and optical sensors based on conducting polymers. In: Shahabuddin, S., Pandey, A. K., Khalid, M., & Jagadish, P. (eds) Advances in hybrid conducting polymer technology. *Engineering materials*, 159–200.
- [32] Son, E. J., Kim, J. H., Kim, K., & Park, C. B. (2016). Quinone and its derivatives for energy harvesting and storage materials. *Journal of Materials Chemistry A*, 4(29), 11179–11202. doi:10.1039/c6ta03123d
- [33] Pillai, A.M., Salini, P., John, B., & Devassy, M. T. (2025). Recent advancements in Quinone-based cathode materials for high-energy density lithium-ion batteries. *Journal of Energy Storage*, 109,115152. doi.org/10.1016/j.est.2024.115152
- [34] Bitenc, J., Pavčnik, T., Košir, U., & Pirnat, K. (2020). Quinone-Based Materials as Renewable High Energy Density Cathode Materials for Rechargeable Magnesium Batteries. *Materials*, 13(3), 506. doi:10.3390/ma13030506.
- [35] Han, C., Li, H., Shi, R., Zhang, T., Tong, J., Li, J. Q., & Li, B. (2019). Organic Quinones Towards Advanced Electrochemical Energy Storage: Recent Advances and Challenges. *Journal of Materials Chemistry A*, 7, 23378-23415. doi:10.1039/c9ta05252f.

- [36] Song, Z., Qian, Y., Zhang, T., Otani, M., & Zhou, H. (2015). Poly (benzoquinonyl sulfide) as a high-energy organic cathode for rechargeable Li and Na batteries. *Advanced Science*, 2,1500124(1-9). doi:10.1002/advs.201500124
- [37] Bitenc, J., Pirnat, K., Mali, G., Novosel, B., Vitanova, A.R., & Dominko, R. (2016). Poly(hydroquinoyl-benzoquinonyl sulfide) as an active material in Mg and Li organic batteries. *Electrochemistry Communications*, 69, 1–5. doi:10.1016/j.elecom.2016.05.009
- [38] Wang, H., Emanuelsson, R., Liu, H., Mamedov, F., Strømme, M., & Sjodin, M. (2021). A conducting additive-free high potential quinone-based conducting redox polymer as lithium-ion battery cathode. *Electrochimica Acta*, 391, 138901. doi:10.1016/j.electacta.2021.138901
- [39] Ansari, S. P., & Dar, R. A. (2025). Quinones as redox-active materials for energy applications. *Trends and application*, 209-228. doi.org/10.1016/B978-0-443-24126-0.00012-3
- [40] Navarro-Suárez, A. M., Carretero-González, J., Rojo, T., & Armand, M. (2017). Poly(quinone-amine)/nanocarbon composite electrodes with enhanced proton storage capacity. *Journal of Materials Chemistry A*, 5(44), 23292–23298. doi:10.1039/c7ta08489g.
- [41] Ding, Y., Li, Y., & Yu, G. (2016). Exploring Bio-inspired Quinone-Based Organic Redox Flow Batteries: A Combined Experimental and Computational Study. *Chem*, 1(5), 790–801. doi:10.1016/j.chempr.2016.09.004
- [42] Er, S., Suh, C., Marshak, M. P., & Aspuru-Guzik, A. (2015). Computational design of molecules for an all-quinone redox flow battery. *Chemical Science*, 6(2), 885–893. doi:10.1039/c4sc03030c
- [43] Zhong, F., Yang, M., Ding, M., & Jia, C. (2020). Organic Electroactive Molecule-Based Electrolytes for Redox Flow Batteries:

Status and Challenges of Molecular Design. *Frontiers in Chemistry*, 8. doi:10.3389/fchem.2020.00451

[44] Hong, W., Sun, B., Aziz, H., Park, W. T., Noh, Y. Y., & Li, Y. (2012). A conjugated polyazine containing diketopyrrolopyrrole for ambipolar organic thin film transistors. *Chemical Communications*, 48(67), 8413. doi:10.1039/C2CC33998F

Growing the world's expanding energy needs and the diminishing supply of non-renewable energy resources have made it essential to look into alternative sources of energy such as wind, tidal, biomass, geothermal and solar. These resources are predicted to make up a significant portion of the world's energy supply soon. All of these renewable energy sources are naturally inconsistent and spread across a wide geographic region. The thrust and demand for effective energy storage technology to enable the quick deployment of renewable energy. Supercapacitors and rechargeable batteries stand out as among the most intriguing methods for storing energy due to their high power density, and other desirable features [1-4]. Lithium-ion batteries, for instance, have experienced widespread success since their introduction in the 1990s. Graphite is commonly used as the anode material, while LiCoO<sub>2</sub>, LiFePO<sub>4</sub>, LiMn<sub>2</sub>O<sub>4</sub>, and LiNi<sub>x</sub>Co<sub>y</sub>Mn<sub>1-x-y</sub> are prevalent cathode materials in contemporary commercial LIBs. Additionally, there is a substantial research focus on sodium-ion batteries (SIBs), which exhibit battery chemistry analogous to lithium-ion batteries. NaFePO<sub>4</sub>, Na<sub>2</sub>FePO<sub>4</sub>F, and other suitable cathode components for SIB are facilitated by the abundance of sodium resources [5]. Numerous materials, including metal oxides, selenides, sulfides, phosphides, and carbonaceous substances (hard carbon, graphite, etc.) have been extensively researched, leading to a diverse array of results for anodes. As can be seen above, a significant number of transition metal-based inorganic chemicals are needed to produce today's rechargeable batteries and supercapacitors. Although substantial advancements have been achieved, escalating concerns regarding resources and the environment have arisen due to the high cost and limited reserves of these inorganic transition metal-based materials [6-8]. On the other hand, inexpensive and sustainable constituents

including C, N, O, H, and S make up organic electrode materials, which offer a great chance to advance current energy storage methods. Furthermore, many organic substances can be produced from their derivatives or directly taken from natural, renewable sources [9, 10]. The physical as well as electrochemical features of organic materials, including their specific capacity, electrical conductivity, solubility, voltage, and mechanical qualities, can be easily altered due to their flexible composition. Growing concerns about resource depletion and environmental issues have driven research on organic electrode materials in recent decades. The organic electrode materials described in the literature can be divided into categories depending on their structural features (Like multiple bonds between carbon-carbon and carbon-nitrogen). Additionally, these materials encompass organic radicals, conductive polymers, carbonyl-containing compounds, organosulfur compounds, and other organic species [11-13]. Derivatives of organic material for electrodes with similar redox-active cores have been the subject of study owing to their similar electrochemical behavior and potential for improved performance. However, significant research has been done to enhance the electrochemical properties among the previously identified organic electrodes. Despite having excellent electronic materials for conductivity, conductive polymers usually have two major drawbacks: insufficient stability during cycles due to dopant buildup during cycling, and a low accessible doping level, which results in limited specific capacity. Various techniques, such as morphological optimization, copolymerization, and hybridization with a robust substrate, have been employed with varying degrees of success to modify the energy storage characteristics [14, 15].

Organic electrode materials offer novel possibilities for creating the upcoming phase of long-lasting and environmentally friendly LIBs and SIBs since they are affordable, renewable, adaptable, redox stable, and structurally diverse. High solubility in organic electrolytes, low discharge potential as positive materials, and poor electrical conductivity are only a few of the difficulties electroactive organic compounds encounter in real-world LIB/SIB applications. The most attractive options for LIBs/SIB electrodes are quinone organic materials due to their high theoretical capacity, good reaction reversibility, and abundant resource availability [16, 17]. Because of their structural diversity, affordability, and sustainability, organic carbonyl compounds are attractive substitutes for conventional inorganic battery materials. However, the poor electric conductivity and dissolution of these carbonyl compounds prevent them from being used as materials for energy storage. In this case, the conducting redox polymer concept is used to functionalize the carbonyl moiety over CPs. To enable the electrochemical reduction and oxidation of carbonyl-containing functional groups, a conducting polymer is used, which inhibits dissolution and offers electron transport channels.

**2.1. Quinones-based supercapacitors:** Quinones exhibit desirable qualities as active materials for energy storage applications, including high theoretical capacity, robust redox behavior, rapid charge transport kinetics, and structural diversity [18-20]. Quinones are a category of carbonyl-containing compounds characterized by an unsaturated sixmembered cyclic structure and two nearby (or separated) carbonyl groups. There have been reports of several kinds of organic cathode active materials working well as alternatives to traditional inorganic ones. Benzoquinone derivatives are cathode-active materials that belong to the carbonyl class and provide two-electron reversible redox reactions (Scheme 1.).

Scheme 1. Benzoquinone shows Reversible redox reactions involving 2e's

Their huge specific capacity, good electrochemical reversibility, molecular diversity, and structural tailor ability develop them into potentially inexpensive, renewable, and high-energy-density electrode components [21-23]. Future applications involving electric cars have major challenges due to current energy storage technologies' insufficient high energy storage capacity, long cyclic durability, and quick charge/discharge rates. The energy density is the result of multiplying a specific capacity by the output voltage. The molecule mass and the number of e's transferred throughout the redox process are the primary determinants of specific capacity. Higher numbers of carbonyl groups and a lower molecular weight of quinone molecules allow for higher theoretical capacities.

The enhancement of energy density and cycling performance can be achieved through the utilization of a specific category of organic compounds known as Quinones, characterized by the presence of two or more carbonyl groups within unsaturated six-membered rings. Quinones have many favorable qualities, including cheap cost, high energy density, sustainability, structural tunability, and good environmental stability, which make them suitable materials for supercapacitors. The low intrinsic electrical conductivity, rapid self-discharge, and dissolving of quinones within the electrolyte throughout the charge-discharge procedure are some of the severe drawbacks of quinones. The main reason quinone and its derivatives are used with

carbon materials is to give double-layer capacitance—a combination of the faradaic and non-faradaic processes-a redox contribution [24]. The redox-active quinone/hydroquinone in the aqueous H<sub>2</sub>SO<sub>4</sub> electrolyte to functionalize a carbon-based supercapacitor and show its charge storage capabilities. An exceptional specific capacitance of 5017 F/g along with 30.6 Wh/Kg energy density (higher than carbon-based supercapacitors i.e. 10.1 Wh/Kg) was demonstrated by the anode and cathode of the as-fabricated electrode materials in a three-electrode supercapacitor device [25].

Quinone compounds exhibit a wide range of molecular configurations, and by adding the right functional groups, their redox characteristics can be modified. Popular methods for altering the redox capability involve the use of electron-gaining and electron-releasing functional groups. The introduction of electron-donating moieties typically decreases the redox potential, while the incorporation of electrongaining functionalities (such as Bromo, and per-fluoro butyl) can raise the redox potential. This is because these properties exert a notable influence on the reduction potential, which is controlled by the energy of LUMO [26]. The study showed that when aromaticity in LIBs grows, the redox potential in the sequence of 1,4-benzoquinone (1,4-BQ), 1,4naphthoquinone (1,4-NQ),1,10-anthraquinone and (1,10-AQ)diminishes. Additionally, it is observed that by raising the more substituent groups, greater redox potential shifts are possible. However, the addition of more functional groups typically increases molecular weight rather than the number of active sites which reduces specific capacity. This makes it simple to modify their specific capacity through molecular engineering. Changing the relative location of carbonyl functional groups is a practical way to modulate the potential for redox reactions without reducing the theoretical capacity. Quinone electrode voltage is significantly impacted by the relative positions of carbonyl groups. The redox potentials of the quinone species follow an

increasing trend, with para-quinones exhibiting the lowest values, followed by discrete-quinones, and ortho-quinones demonstrating the highest redox potentials [27, 28].

Studies have shown that various quinone compounds and also their derivatives demonstrate great potential as electrode materials in LIBs. Among the quinone family, 1,4-BQ is considered the most fundamental member. With an estimated specific capacity around as much as 496 mAh/g with 2.8 V redox potential vs Li/Li<sup>+</sup>, it can take two electrons and is more significant as compared to conventional inorganic cathode electrode materials like LiFePO<sub>4</sub> (170 mAh/g) and LiCoO<sub>2</sub> (140 mAh/g) [29, 30]. Furthermore, quinone compounds show great promise in attaining high-rate performance and high cyclic stability because of the quinone moiety's fast redox kinetics and stable structure. Because of their steadily growing molecular weight, the predicted specific capacity of 9,10-AQ was reduced to 258 mAh/g and that of 1,4-NQ to 339 mAh/g, compared to 1,4-BQ's 496 mAh/g [21].

In rechargeable LIBs, derivatives of 2,2'-bis-p-benzoquinone (BBQ) and 1,4,5,8-naphthodiquinone (NDQ) were used as cathode active materials. The cells that used 2,2'-BBQ derivatives performed better than the cells that used BQ derivatives. The initial capacity values of 157 Ah/kg (at 2.8V), 326 Ah/kg (at 2.9V), and the 20th capacity values of 59 Ah/kg, and discharge 170 Ah/kg were demonstrated by the BQ and 2,2'-BBQ based cells respectively. In comparison to the 2,2'-BBQ-based cell, the 1,4,5,8-NDQ-based cell had a greater initial capacity that was comparable to that of the latter. However, its 20th discharge capacity was only 67 Ah/kg, and its 20th to 1st capacity ratio was much lower at 19%. It was observed that the resulting derivatives of 2,2'-BBQ, a benzoquinone dimer that included four carbonyl groups, were intended to function as four-electron acceptors [31].

The highly polarized amino and carbonyl functionalities found in 2,5diamino-1,4-benzoquinone (DABQ) strengthen the intermolecular hydrogen bonding, and this bonding is shown to be strong enough to provide an unusually restricted dissolution in organic battery fluids. Three important variables that directly affect the cycle stability of solid electrode cells are the solubility of DABQ, the electrolyte's solvation state, and the electrolyte's polarity. Relative to organic battery materials with similar compositions, such as 1,4-BQ, the galvanostatic cycling tests demonstrate exceptional cycling stability and an enhanced electrolyte formulation, attaining a reversible 2e-reaction with 388 mAh/g theoretical capacity. Combining this with conductive carbon frameworks, H-bond interaction binders, and/or non-polar electrolyte solvents may result in a novel approach to insoluble tiny organic battery materials that have applications [32]. The  $R_2$ -BQ (where R = Methyl(Me), Iso-Propyl (i-Pr), and t-Butyl (t-Bu)) charge-discharge behaviour and cycling durability were evaluated over eight cycles. The Me2-BQbased cell exhibited a first discharge capacity of 226 Ah/kg, which was significantly lower than the anticipated value of 394 Ah/kg. Furthermore, its cyclability was suboptimal, as demonstrated by the 57% ratio between the 15th discharge capacity and the initial discharge capacity. On the other hand, the i-Pr2-BQ and t-Bu2-BQ cells demonstrated excellent cycle retention; the corresponding ratios of the 15th to the 1st discharge capacity were 73% (the 1st cycle's capacity was 128 Ah/kg, and the 15th cycle's capacity was 94 Ah/kg) and 96% (the 1st cycle's capacity was 165 Ah/kg, and the 15th cycle's capacity was 158 Ah/kg). In a typical rechargeable LIBs system, the cell utilizing t-Bu<sub>2</sub>-BQ-based material demonstrated superior performance compared to other BQ-based cathode active materials. The cyclability order, which corresponds to the steric bulk, is t-Bu<sub>2</sub>-BQ > i-Pr<sub>2</sub>-BQ > Me<sub>2</sub>-BQ. These findings showed that adding large functional groups to BQ-based cells enhances their cyclability [33].

The 5,8-dihydroxy-1,4-naphthoquinone lithium salt and 5,8dihydroxy-1,4-naphthoquinone dilithium salt exhibited promising initial discharge capabilities when utilized as positive electrodes in rechargeable LIBs. The first discharge capacity of the dilithium salt was larger at 247 mAh/g (2.1 V versus Li+/Li) compared to that of the lithium salt, which showed an initial discharge capacity of 170 mAh/g (2.2 V versus Li+/Li). The discharge capabilities that were found align with their two-electron redox characteristics [34]. The electrochemical behaviour of 5,7,12,14-pentacenetetrone and 9,10-AQ as cathode materials for LIBs was compared by Yao et al. The initial discharge capacity of the 9,10-AQ electrode was 217 mAh/g, or 84% of the expected value of 257 mAh/g. This electrode displayed an electric discharge peak at roughly 2.1 V in comparison to the Li/Li+ reference. 9,10-AQ was soluble in the electrolyte, and due to this, the capacity rapidly decreased to 49 mAh/g after 100 cycles. Given that all 4 CO sites may be decreased, 5,7,12,14-pentacenetetrone demonstrated a greater initial discharge capacity of 236 mAh/g, or 74% of the predicted value of 317 mAh/g. In the ensuing cycle performance evaluation, 5,7,12,14-pentacenetetrone also showed better cycle life than AQ, retaining a capacity of 183 mAh/g after 100 cycles. This indicates that the  $\pi$ -system's expansion successfully lowers the solubility [21].

The properties of NQ as a possible cathode material for innovative LIBs systems are encouraging. 1H-naphtho[2,3-d]imidazole-4,9-dione (NID) and 2,3-diamino-1,4-naphthoquinone (DNQ), two NQ-derivatives, were synthesized on a massive scale, producing tens of grams of product. Both DNQ and NID displayed redox behaviors that were mostly similar to those of unmodified NQ, including the reduction that transforms the C=O groups into enolates and vice versa. The electrochemical characteristics of the resultant compounds might be effectively modulated by altering the ring shape of NQ. Among the NQ derivatives, Li-DNQ demonstrated the highest first discharge capacity

of 250 mAh/g (363 mAh cm<sup>-3</sup>), and after 500 cycles at 0.2C, its retention capacity was 99%. Shows an energy density of 575 Wh/Kg and a power density of 21000 W/Kg. Additionally, when running at a 20C rate, the Li-DNQ cell showed a 47% discharge capacity (117 mAh/g and 170 mAhcm<sup>-3</sup>). Cycling performance shows 100% retention of initial capacity at different rates below 50C. This stands in complete opposition to the Naphthoquinone cathode's findings, which revealed non-reversible redox behaviour and a notable decrease in capacity (55 mAh/g, 78 mAhcm<sup>-3</sup>) at 20C. The remarkable rate performance of Li-DNQ cells is explained by the quick charge and ion transport capabilities of DNQ, which are a result of its remarkably narrow band gap and large lithium diffusion coefficient when compared to NQ [35]. The disodium salt of 2,5-dihydroxy-1,4-benzoquinone (Na<sub>2</sub>DBQ) was suitable as an anode (negative) electrode material for SIBs. Na<sub>2</sub>DBQ may demonstrate outstanding electrochemical performance without any alterations, including a high capacity (265 mAh/g at 0.1 C), extended cycle life, high specific capacity (160 mAh/g at a 5 C rate), and a high average discharge voltage of 1.2 V. These findings confirm the use of organic carbonyl (-C=O) containing compounds in SIBs as an active electrode material [36].

**2.2. Quinone-based conducting polymers:** In rechargeable batteries, any electroactive organic or polymer that undergoes reversible redox reactions can be employed to create an organic electrode material. Conjugated carbonyl compounds have become the most intriguing electroactive materials because of their high cyclic stability, energy, and power density. They have been the subject of considerable research for about half a century. Based on their molecular structure, these compounds can be categorized as small organic molecules, organic polymers, or organic salts, while their electroactive groups can include

quinones, dihydrides, carboxylates, diketones, and others. Carboxylates exhibit a comparatively low redox potential (1.0 V), whereas conjugated carbonyl compounds have redox potential between 1.5 and 3.0 V vs Li<sup>+</sup>/Li [21]. The benzoquinone electrode is regarded as a groundbreaking material for LIBs owing to its numerous advantages, such as its high theoretical specific capacity, ready availability, and environmentally benign nature. Nevertheless, the two main obstacles to the practical use of BQ as a cathode are its dissolution in organic electrolytes and its low discharge plateaus. Here, triphenylaminebenzoquinone monomer and its polymer (poly triphenylaminebenzoquinone) are synthesised as cathode active material for LIBs using triphenylamine with a high working voltage and benzoquinone having high theoretical capacity [37]. Redox-active quinone moieties within a quinone-based porous organic polymer were proposed as a novel material for cathode electrodes for rechargeable aqueous zinc-ion batteries (ZIBs). This polymer was synthesized via the Diels-Alder reaction in the absence of heavy metals. The high porosity of the material facilitates efficient diffusion of charge carriers (Zn<sup>2+</sup>/H<sup>+</sup>) through the pores, enabling effective use of the redox-active quinone functionalities throughout the charge and discharge processes. The fused-aromatic conjugated skeleton of the material additionally offers enhanced intrinsic conductivity and strong physicochemical stability. The redox-active quinone-based organic polymer exhibits exceptional cyclic stability, maintaining its capacity and rate performance over an extended period. Specifically, it demonstrates a remarkable cyclical lifespan of a maximum of 30,000 cycles (at 2.0 A/g, initial 66% capacity retention), accompanied by robust initial capacity retention and a reversible specific capacity of 120 mAh/g (at 0.1 A/g) [38].

Most of the quinone polymers that have been reported are mainchain type polymers synthesized via polycondensation reactions. Three types of polyanthraquinone polymers were synthesized using the monomers 1,5-dichloroanthraquinone and 1,4-dichloroanthraquinone. One of the polymers exhibited an impressively high discharge capacity of 263 mAh/g when measured at a rate of 0.2C current. Furthermore, this polymer retained remarkable quick discharge/charge ability, retaining 98%, 96%, 91%, 84%, 78%, and 69% of its initial capacity at current rates of 0.5C, 1C, 2C, 5C, 10C, and 20C, respectively [39, 40]. Organic polymers are commonly fabricated by grafting onto a backbone chain or linking monomer units with a variety of organic moieties, ether, including methylene, imine, and thioether groups. Understanding the relationship between monomer units and the connecting link, along with quinone polymer composition and electrochemical properties, is essential. Presently, quinone polymers joined by a thioether bond have garnered significant research interest. The lithium salt of poly(2,5-dihydroxy-p-benzoquinonyl sulfide) shows a high reversible capacity of 268 mAh/g after 1500 cycles. Additionally, it is discovered that the thioether bond promotes rapid electron transfer because of the p-electron delocalization between the quinonyl rings and the lone pair of sulfur, in addition to guaranteeing the structural integrity of the quinone polymer during the redox processes [40]. Poly(2,5-dihydroxyaniline) was chemically synthesized with а theoretical capacity of 443 mAh/g and inherent electrical conduction. The conjugated structure of polyaniline facilitates electrical conduction, while quinone moieties the redox-active contribute the electrochemical performance of the material. The polymer's preliminary discharge capacity was estimated to be 270 mAh/g, and it had two distinct redox peak values around 2.3 V and 2.6 V against the Li/Li+. Nevertheless, there remains potential for further enhancement of the cycle life [41]. Poly(benzoquinonyl sulfide) (PBQS), a novel polymerbased cathode material, has been reported for use in rechargeable LIBs or SIBs. The energy density of PBQS is remarkably high, exceeding that of the majority of Li or Na insertion cathodes, possessing a value of 734

Wh/kg (2.67 V × 275 mAh/g) in LIBs and 557 Wh/kg (2.08 V × 268 mAh/g) in SIBs. Furthermore, in LIBs, PBQS demonstrates excellent rate performance (5000 mA/g, 72%) and exceptional long-term cycling stability (1000 cycles, 86%). Along with the intriguing battery efficiency, research on the structure-property relationship between PBQS and BQ and the electrochemical composition differences between Li–PBQS and Na–PBQS batteries provides valuable information for developing better SIBs and LIBs that surpass conventional LIBs [42].

Poly(2,5-dihydroxyl-1,4-benzoquinonyl sulfide) (PDBS) a cathode active material, was recently developed and is currently undergoing testing for application in LIBs. The electrochemical studies show that PDBS has a starting capacity for discharge of 350 mAh/g, which remains intact at 184 mAh/g through 100 cycles of charge and discharge at 15mA/g current density within the 1.5-3.6 V voltage range. Excluding few cycles, the PDBS material demonstrates exceptional rate performance, outstanding cycling stability, and a discharge/charge coulombic efficiency exceeding 98%. The high coulombic efficiency and robust cycling behavior of the material can be attributed to its highly reversible carbonyl groups that facilitate energy storage, as well as the stable thioether linkages that stabilize the polymer's structure [43]. The cathode and anode of a new all-plasticelectrode LIBs can be only one flexible, ladder-like heterocyclic, bifunctional polyquinone (C<sub>6</sub>O<sub>2</sub>S<sub>2</sub>)<sub>n</sub>. Considering its unique structural characteristics, this kind of polymer cathode has a 624 Wh/kg energy density and endures 1000 charge-discharge cycles. Additionally, the symmetric full-battery as-fabricated exhibits a noteworthy capacity (249 mAh/g), an amazing energy density (276 Wh/kg), and a remarkable capacity retention (119 mAh/g at 1 A/g after 250 cycles) [44]. Another polymer Poly(2,3-dithiino-1,4-benzoquinone) having a ladder-type structure, was created using a straightforward 100 polymerization method in two steps. Over cycles, the electrochemical performance showed that this polymer could retain 98.4% of its large reversible specific capacity (681 mAh/g) [45]. An interesting organic electrode chemical called poly (2-chloro-3,5,6-trisulfide-1,4-benzoquinone) (PCTB) was studied as an active component for rechargeable LIBs. It was created by using thioether bonds to polymerize chloranil. This material has a lot of potential and excellent lithium-storage capabilities due to the C-Cl groups that compose its structure. When used as the positive electrode, PCTB showed an average voltage of 2.72 V and a discharge capacity of 138.65 mAh/g (at 30 mA/g current density) [46].

The dilithiated 2,5-dihydroxy-1,4-benzoquinone ( $[Li_2(C_6H_2O_4)]$ (DLHB), work as a cathode active material in LIBs, exhibited two distinct reduction and oxidation maxima at 1.7 V and 2.7 V, respectively, relative to the Li/Li<sup>+</sup> reference. Furthermore, the DLHB electrode's GCD testing showed a coulombic effectiveness of 93.18% throughout the first cycle and a starting capacity for discharge was 176 mAh/g [47]. According to recent studies on quinone-based battery materials, it is possible to obtain good cycling stability, a high discharge capacity, and a moderately high voltage output. Calix [6] quinone (C6Q), an organic three-dimensional cyclic oligomer, exhibits high-capacity performance as a cathode active component in rechargeable LIBs. When paired with a lithium metal anode, this battery configuration yielded a 2.7 V voltage and a 425 mAh/g discharge capacity [48]. Quinizarin (Qz) having high potential, is employed as a group that carries capacity. A battery cell with a discharge capacity of 65 mAh/g at 1.5 C (at 3.3 V) and a 74% retention of capacity through 500 cycles is coupled with a lithium metal electrode [49]. Inspired by the extremely active material pyrene-4,5,9,10-tetraone in the redox process, authors have developed two new organic cathode materials, poly(2,7-ethynylpyrene-4,5,9,10tetraone) [PEPT] and poly(pyrene-4,5,9,10-tetraone) [PPTO]. Both cathodes demonstrate impressive energy densities of up to 507 and 530

Wh/kg, respectively, along with substantial reversible capacities of 244 and 234 mAh/g, owing to their ability to accommodate four Li⁺ ions. The PEPT cathode, in particular, following the incorporation of C≡C, exhibits excellent capacity retention of 110 mAh/g after 1000 cycles (at 800mA/g) and significantly enhanced rate performance under high current densities. This is attributed to the increased conjugation and planarity of the PEPT structure. The authors propose that this synthetic approach may provide a practical pathway to develop novel organic cathodes for the next generation of organic batteries, delivering both excellent stability and energy density [50].

Proton trap technology involves an organic cathode active material composed of poly(3,4-ethylenedioxythiophene) with different functional groups like hydroquinone and pyridine. This approach produces electrode materials suitable for both LIBs and SIBs chemistries by leveraging the quinone-hydroquinone redox conversion. Even though material lithiation is required, these polymers exhibit high intrinsic potentials when mixed with lithium, yielding a reversible output voltage of greater than 3.5 V. Compatibility with various anode components is made possible by the proton trapping in the cathode material, which effectively separates the anode's cycle chemistry from the quinone oxidation, and reduction chemistry confers insensitivity to the electrolyte cation type. Furthermore, the conducting polymer backbone facilitates the construction of electrical conductivity without the need for additional chemicals. The ideal copolymer quinone to pyridine (1:2 ratio) had a theoretical capacity of 62 mAh/g, of which 25-30 mAh/g (45%) was attained. Keep in mind that this capacity was determined by the electrode's total deposited mass, which EDX indicates contains sizable amounts of dopant and counter ions [51].

**2.3. Quinone/Graphene composites as supercapacitors:** Apart from the methods of polymerization and solidification, merging quinone

compounds with conductive materials like graphene, carbon nanotubes, porous carbon, conducting polymer, etc., provides a practical approach to reducing quinone compound dissolution while simultaneously improving electrical conductivity. Composed of sp<sup>2</sup> hybridized carbon atoms arranged in a honeycomb structure, graphene constitutes a thick layer of single atoms of graphite material. Its exceptional physical and chemical characteristics have garnered global interest. These features encompass exceptional electron mobility (2.5×10<sup>5</sup> cm<sup>2</sup>/Vs), great mechanical strength, high thermal and chemical stability, and a sizable specific surface area (2630 m<sup>2</sup>/g). These attributes render it an ideal 2D structural component for the preparation of quinone-graphene composites intended for energy applications. The estimated findings indicate that the predominant interaction between graphene and quinone is strong physisorption using binding energy from 1.10 eV to 1.56 eV. This could increase cycle stability by suppressing the dissolution in nonaqueous electrolytes. Due to increased electron transport during hybridization with graphene, cycle stability was substantially improved, and specific capacity and rate capability [21].

Poly(imide-benzoquinone) fabricated via in-situ polymerization on graphene serves as a cathode material for LIBs. The transfer of charges from graphene to poly(imide-benzoquinone) and unhindered passage of electrons and Li+ ions through the numerous redox-active groups of carbonyl are made possible by the structural design, both of which are essential for battery operation. In addition to maintaining greater than 86% of its starting capacity after 300 cycles of charge-discharge, the material exhibits impressive reversible specific capacities of 271.0 at 0.1 C and 193.1 mAh/g at a 10 C charge rate. During the discharging and charging cycle, the carbonyl functionalities of the corresponding quinone and imide moieties subsequently admit 2 lithium ions and 8 lithium ions, respectively [52]. Poly-(9,10-

phenanthrenequinone) (PFQ) is polymerized in situ on rGO. The voltage of the PFQ compound containing both carbonyl groups at the ortho configuration was 400 mV higher than that of their para counterparts. The specific capacity of the PFQ/rGO composite was 153 mAh/g by applying a current density of 0.05 A/g. The resulting value surpassed the 136 mAh/g exhibited by the pristine PFQ. The PFQ/rGO compound demonstrated excellent rate performance and excellent capacity retention, retaining 91% of initial capacity during 500 cycles at 5C [53].

Poly(anthraquinonyl sulfide) was evenly distributed on the graphene sheets' surface via straightforward in situ polymerization using a 0.5 M H<sub>2</sub>SO<sub>4</sub> aqueous solution for an electrode material in electrochemical capacitors. Remarkable cycle stability and two prominent redox peaks at about 0 V were displayed by poly(anthraquinonyl sulfide) / graphene sheets. Even when operating at an extremely high current density of 5000 mA/g, Poly(anthraquinonyl sulfide) /graphene sheets maintained a capacitance of 305 F/g(86 mAh/g), and their specific capacitance was 349 F/g at a current density of 500 mA/g. Because of the quick transfer of charge and redox reaction that occur when graphene sheets are added to the composite, poly(anthraquinonyl sulfide) / graphene sheets exhibit excellent electrode characteristics [54]. Also, a heterojunction system was formed from graphene and hydroquinone dimethyl ether, showing a large specific capacitance of 523 F/g at 1.0 A/g along with good cyclic stability. Supercapacitors have attractive capacitive properties, and the device with the greatest efficiency has a negligible capacitance decay and may provide a power density of 8000 W/Kg along with 32.4 Wh/Kg The electrochemically energy density [55]. active 2,6diaminoanthraquinone is joined in an imine linkage with 1,3,5benzenetricarboxaldehyde as a bridge to form a new polymer PDAQ with a distinct structure. Strong  $\pi$ - $\pi$  interactions between the rGO and PDAQ enhance cycling stability, while a large  $\pi$ -conjugation

system and high density of C=O in the structural unit of the PDAQ result in excellent electrochemical properties. At 5 mV/s, PDAQ/rGO-0.3 demonstrates an excellent specific capacitance of up to 622 F/g with a remarkable energy density of 32.97 Wh/kg at a power density of 605.57 W/Kg, and has potential in supercapacitors [56].

The poly(anthraquinonyl sulfide)/graphene composites containing 6 and 26 weight percent graphene were fabricated. With the addition of 6 and 26 % weight graphene, the poly(anthraquinonyl sulfide /graphene composite's electronic conductivity significantly increased (2.9×10<sup>-5</sup> S/cm to 6.4×10<sup>-3</sup> S/cm). This composite material shows discharge capacities of 165 and 187 mAh/g with a 0.1C rate, when graphene weight percentages were 26% and 6%, respectively. The composite, having 26% graphene content, exhibited impressive electrochemical performance. It retained over 90% of its discharge capacity at a rate of 0.1C, which translates to a specific capacity of about 100 mAh/g at a higher rate of 10C [57]. Lin et al. reported the preparation of nitrogen-enriched, self-supporting, single-layer graphene-like holey conjugated polymer materials (NGHCPs). The uniform hexagonal micropores and graphene-like subunits make up the 2D NG-HCP nanosheets. 2D NG-HCP demonstrated an extremely high discharge capacity of 1320 mAh/g after 600 cycles (performed at 0.02 A/g). Nevertheless, it's mysterious how the charge storage works [58].

**2.4. Azine-based conducting polymers:** Azines are 2,3-diaza counterparts of 1,3-butadiene, commonly referred to as diimines with N-N linkage **[59]**. Dimethylketazine, the first example of an azine compound, was synthesized in 1891 by researchers Curtius and Thun through the combination of two acetone molecules with the compound hydrazine. Because of their many different chemical, biological, and material properties, azines have attracted more and more interest. The

conventional approach to synthesizing azines entails the condensation of hydrazine with aldehydes and ketones **[60]**. Azines were initially evaluated as potential conducting polymers following the publication of an extended Hückel calculation regarding the azine analog of polyacetylene by Euler and Hauer, which determined the material's band gap. According to the band gap value, polyazines may function as weak conductors, but oxidative doping may cause them to become conducting. Polyazine,  $(-N=C(R_1)-C(R_2)=N-)$ , was later created as a novel kind of CP that, when doped with iodine, provided an electrically conducting material that was stable in the air **[61, 62]**.

The scientific community has recently examined polyazine conducting materials to investigate their potential use in electrochemical energy storage systems. A brand-new family of semiconductor materials called conjugated polyazines has a lot of promise for application in organic thin-film transistors. Convenient synthetic methods involving the formation of azine linkages, such as a condensation reaction between hydrazine and a  $\pi$ -conjugated diketone/dialdehydes, can be employed to prepare these materials. It is found that the azine linkage is a special and potent electron-withdrawing element that may be utilized to lower the LUMO energy level and offer electron mobility characteristics **[63]**.

Heterochain polymers have significant characteristics and are used in many fields. Polyazines and polyazomethines are especially relevant because dicarbonylic chemicals can result in conjugated systems. To prepare poroplasts, the polyazines readily remove nitrogen through the creation of thermostable polyolefins. Hydrazine was polycondensed with various quinone derivatives, including 5-chloroacenaphthenequinone, 5,6-dinitroacenaphthenequinone, and 5-nitroacenaphthenequinone, to synthesize new polyazine materials. The researchers investigated the influence of the quinone/hydrazine ratio

and the catalyst on the viscosity of the polymer solution in dimethylformamide and the yields of soluble and insoluble products. The resulting polyazines exhibit electrical conductivity and paramagnetic properties due to their extended, alternating double-bond structure. Hydrazine is added to the nucleophilic dicarbonylic component during the polycondensation process and then eliminated. The observed electrical conductivity for this polyazine was  $10^{-15}$ - $10^{-13}$  S/cm [64].

Azine-based polymers with two reversible oxidations at 2.9 and 3.3 V vs. Li/Li+, which are attractive potentials. In a Li-ion half-cell configuration, an end-capped, cross-linked azine-based polymer offered adequate cyclic stability, 133 mAh/g specific capacity, and improved performance with a 100 C rate [65]. The material (Poly(3-vinyl-Nmethylphenothiazine)) exhibited remarkably high-rate performance and exceptional cycling durability, maintaining 93% of its initial capacity after 10,000 cycles at a 10 C rate, facilitated by  $\pi$ - $\pi$  interactions and supramolecular charge transport mechanisms [66]. Hydrazine hydrate's condensation with several acetophenone derivatives in less than three hours, ketazines with good-to-excellent yields were formed as a result of smooth operation at room temperature with ethanol and nickel-based heterogeneous **[67]**. 4-hydroxy-3catalyst methoxybenzaldehyde azine, Poly(4-hydroxy-3-methoxybenzaldehyde azine) was made to examine electrical and optical conductivity, whereas azine and polyazine, obtained from different combinations, have been used to study conductive behavior. Azine and polyazine electrical conductivities are measured, as is the conductivity variation with the iodine doping period. The undoped azine and polyazine have respective electrical conductivities of  $4.68 \times 10^{-11}$  and  $7.68 \times 10^{-11}$  S/cm. Prolonged doping is necessary to attain optimal electrical conductivity. Azine and polyazine have maximum or saturated conductivity values of  $8.83 \times 10^{-9}$  and  $3.44 \times 10^{-7}$  S/cm, respectively. Polyazine is a good

option for gas-sensing applications since its conductivity rises with iodine doping time **[68]**. Using the polycondensation process, polyazine derived from quinones is another family of CPs first reported in the 1980s **[69, 70]**.

Triazine and anthraquinone moieties were combined to create a new polymer that was employed as the anode component in LIBs. The polyanthraquinone-triazine polymer's extremely conductive conjugated moieties and structural characteristics enable sophisticated lithium accumulation chemistry and quick electron transport. This comprises interfacial storage that contributes to the capacity output and a 17e-redox process with 1450 mAh/g specific capacity (theoretical). The polymer electrode exhibits remarkable reversible capacities of 760 mAh/g and 1770 mAh/g at 1A/g and 200 mA/g current density respectively, with 100% Coulombic efficiency throughout the cycles. The covalent organic framework polymer shows promise as a workable material for anodes for cutting-edge high-powered battery technologies because of these beneficial properties [71].

The nitrogen-doped graphene and nitrogen-doped carbon electrodes were prepared via a three-electrode configuration and demonstrated a 289 and 238 F/g specific capacitance respectively, at 0.2 A/g current density. In contrast to pure mesoporous carbon lacking nitrogen dopants, the 91.6% specific capacitance of Nitrogen-Doped Carbon was enhanced at 0.5 A/g. A symmetrical two-electrode cell was also used to examine the as-made electrode's performance. The findings showed that the as-made electrodes provided great cycling performance (91% retention after 1000 cycles) and outstanding rate capability. These findings show that the nitrogen-doped carbon/nitrogen-doped graphene electrode shown makes a very interesting option for a supercapacitor with higher performance [72].

Through polycondensation of 9,10-phenanthrenequinone, 9,10anthraguinone, 2-chloroanthraguinone, and 1-chloroanthraguinone, with hydrazine hydrate and disulphinylhydrazine, another polyazine molecule was created. It has been determined how zinc chloride in DMF solvent causes the polycondensation reaction between phenanthrenequinone and hydrazine hydrate. These polyazines' electrical conductivity varies from 10<sup>-10</sup> to 10<sup>-6</sup> ohm<sup>-1</sup>cm<sup>-1</sup>, and the amount of paramagnetic species varies from 10<sup>18</sup> to 10<sup>21</sup> spin/g present in the materials, both demonstrating their semiconducting characteristics [73]. A brown-colored polymer(polyazine) was synthesized by the polycondensation of p-benzoquinone and hydrazine hydrate with a catalytic amount of ZnCl<sub>2</sub>, showing 35.42 F/g specific capacitance with a scanning rate of 10 mV/s, and has decent energy, power density of 4.41 Wh/Kg, and 249.99 W/Kg, respectively. The findings indicate that PAZ may be used as a suitable material for supercapacitor applications [74].

Table:1 Some quinone-based materials for energy storage devices

Energy Storage Material	Electrolyte	Specific Capacitance (mAh/g)	Ene rgy Den sity (Wh /Kg)	Power Density (W/Kg)	Refer ences
5,8-dihydroxy- 1,4- naphthoquino ne lithium salt	Lithium hexafluorophosp hate	170			[34]
5,8-dihydroxy- 1,4- naphthoquino ne dilithium salt	Lithium hexafluorophosp hate	247			[34]
2,3-diamino- 1,4- naphthoquino ne	1 M LiPF <sub>6</sub> in Ethyl carbonate/Dimet hyl carbonate	250	575	21000	[35]
Disodium salt of 2,5-dihydroxy-1,4-benzoquinone	1 M NaClO <sub>4</sub> in Ethyl carbonate/Dimet hyl carbonate	265			[36]
Poly(benzoquin onyl sulfide) in Li ion batteries		275	734		[42]
Poly(benzoquin onyl sulfide) in Na ion batteries		268	557		[42]
Poly(anthraqui nonyl sulfide)	1 M H <sub>2</sub> SO <sub>4</sub>	86			[54]
Polyquinone (C6O2S2)n		249	624		[44]
Poly(2,3- dithiino-1,4- benzoquinone)		681			[45]
Poly (2-chloro- 3,5,6- trisulfide-1,4- benzoquinone)		138.65			[46]
Dilithiated 2,5-dihydroxy-1,4-benzoquinone		176			[47]

Calix [6] quinone	lithium bis(trifluorometh	425			[48]
	ane)sulfonimide in succinonitrile				
Quinizarin	LiClO <sub>4</sub> /MeCN/H <sub>2</sub> O	65			[49]
Poly(2,7- ethynylpyrene- 4,5,9,10- tetraone)		244	507	2961	[50]
Poly(pyrene- 4,5,9,10- tetraone)		234	530	1622	[50]
Poly-(9,10- phenanthreneq uinone)/rGO	1 M trifluoromethane sulfonimide lithium salt dissolved in a mixture of 1,3- dioxolane and dimethoxyethane	153	430	1600	[53]
Poly(anthraqui nonyl sulfide)/graph ene(6%) composites	N-methyl-2- pyrrolidone	165			[57]
Polyanthraqui none-triazine	Mixture of ethylene carbonate and dimethyl carbonate	760 at 1A/g			[71]
Hydroquinone Dimethyl Ether + Graphene Heterojunction	1 M H <sub>2</sub> SO <sub>4</sub>	523 F/g	32.4	8000	[55]
PDAQ/rGO		622	32.9 7	605.57	[56]

## References

- [1] Georgious, R., Refaat, R., Garcia, J., & Daoud, A. A. (2021) Review on Energy Storage Systems in Microgrids. *Electronics*, 10(17), 2134. doi:10.3390/electronics10172134
- [2] Aghmadi, A., & Mohammed, O. A. (2024). Energy Storage Systems: Technologies and High-Power Applications. *Batteries*, 10(4), 141. doi:10.3390/batteries10040141
- [3] Faisal, M., Hannan, M. A., Ker, P. J., Hussain, A., Mansor, M. B., & Blaabjerg, F. (2018). Review of Energy Storage System Technologies in Microgrid Applications: Issues and Challenges. *IEEE Access*, 6, 35143–35164. doi:10.1109/access.2018.2841407
- [4] Karaman, C., Bengoa, L. N., Gil, R. M. G., & Romero, P. G., (2025). Quinone Quest: Unraveling electrochemical performance in quinone-anchored 3D graphene architectures for high-energy supercapacitors. *Electrochemica Acta*, 512, 145414. doi.org/10.1016/j.electacta.2024.145414
- [5] Shobana, M. K. (2019). Metal oxide coated cathode materials for Liion batteries A review. *Journal of Alloys and Compounds*, 802, 477-487. doi:10.1016/j.jallcom.2019.06.194.
- [6] Alemu, A. M., Worku, K. A., & Getie, Z. M. (2023). Recent Advancement of Electrically Rechargeable Di-Trivalent Metal-Air Batteries for Future Mobility. *Results in Chemistry*, 6, 101041. doi:10.1016/j.rechem.2023.101041
- [7] Njema, G. G., Ouma, O. B. R., & Kibet, K. J. (2024). A Review on the Recent Advances in Battery Development and Energy Storage Technologies. *Journal of Renewable energy*. doi:10.1155/2024/2329261

- [8] Forouzandeh, P., Kumaravel, V., & Pillai, S. C. (2020). Electrode Materials for Supercapacitors: A Review of Recent Advances. *Catalysts*, 10(9), 969.doi:10.3390/catal10090969
- [9] Gannett, C. N., Melecio-Zambrano, L., Theibault, M. J., Peterson, B. M., Fors, B. P., & Abruña, H. D. (2021). Organic electrode materials for fast-rate, high-power battery applications. *Materials Reports: Energy*, 1(1), 100008. doi:10.1016/j.matre.2021.01.003
- [10] Banerjee, A., Khossossi, N., Luo, W., & Ahuja, R. (2022). Promise and reality of organic electrodes from materials design and charge storage perspective. *Journal of Materials Chemistry A*, 10, 15215-15234. doi:10.1039/D2TA00896C
- [11] Banerjee, T., & Kundu, R. (2024). Mini-Review on Organic Electrode Materials: Recent Breakthroughs and Advancement in Metal Ion Batteries. *Energy and Fuels*, 38(14), 12487-12509. doi:10.1021/acs.energyfuels.4c02201
- [12] Wu, Z., Liu, Q., Yang, P., Chen, H., Zhang, Q., Li, S., Tang, Y., & Zhang, S. (2022). Molecular and Morphological Engineering of Organic Electrode Materials for Electrochemical Energy Storage. *Electrochemical Energy Reviews*, 5, 26. doi:10.1007/s41918-022-00152-8
- [13] Le, T. H., Kim, Y., & Yoon, H. (2017). Electrical and Electrochemical Properties of Conducting Polymers. *Polymers*, 9(4), 150. doi: 10.3390/polym9040150.
- [14] Mishra, K. A. (2018). Conducting Polymers: Concepts and Applications. *Journal of Atomic, Molecular, Condensate and Nano Physics*, 5(2), 159-193. doi:10.26713/jamcnp.v5i2.842
- [15] Dube, A., Malode, J. S., Alodhayb, N. A., Mondal, K., & Shetti, P. N. (2025). Conducting polymer-based electrochemical sensors: Progress, challenges, and future perspectives. *Talanta Open*, 100395. doi:10.1016/j.talo.2024.100395.

- [16] Wu, Y., Zeng, R., Nan, J., Shu, D., Qiu, Y., & Chou, S-L. (2017). Quinone Electrode Materials for Rechargeable Lithium/Sodium Ion Batteries. *Advanced Energy Materials*, 7(24), 1700278. doi:10.1002/aenm.201700278
- [17] Lu, Y., Zhang, Q., Li, L., Niu, Z., & Chen, J. (2018). Design Strategies toward Enhancing the Performance of Organic Electrode Materials in Metal-Ion Batteries. *Chem*, 4(12), 2786-2813. doi:10.1016/j.chempr.2018.09.005.
- [18] Gupta, N., & Linschitz, H. (1997). Hydrogen-bonding and protonation effects in electrochemistry of quinones in aprotic solvents *Journal of the American Chemical Society*, 119, 6384–6391. doi:10.1021/ja970028j.
- [19] Häupler, B., Wild, A., & Schubert, U. S. (2015). Carbonyls: powerful organic materials for secondary batteries. *Advanced Energy Materials*, 5, 1402034. doi:10.1002/aenm. 201402034.
- [20] Luo, Z., Liu, L., Zhao, Q., Li, F., & Chen, J. (2017). An Insoluble Benzoquinone-Based Organic Cathode for Use in Rechargeable Lithium-Ion Batteries. *Angewandte Chemie International Edition*, 56, 12561–12565. doi:10.1002/anie.201706604
- [21] Han, C., Li, H., Shi, R., Zhang, T., Tong, J., Li, J. Q., & Li, B. (2019). Organic Quinones Towards Advanced Electrochemical Energy Storage: Recent Advances and Challenges. *Journal of Materials Chemistry A*, 7, 23378-23415. doi:10.1039/c9ta05252f.
- [22] Song, Z., & Zhou, H. (2013). Towards sustainable and versatile energy storage devices: an overview of organic electrode materials. *Energy and Environmental Science*, 6(8), 2280. doi:10.1039/c3ee40709h
- [23] Yokoji, T., Kameyama, Y., Sakaida, S., Maruyama, N., Satoh, M., & Matsubara, H. (2015). Steric Effects on the Cyclability of Benzoquinone-

- type Organic Cathode Active Materials for Rechargeable Batteries. *Chemistry Letters*, 44(12), 1726–1728. doi:10.1246/cl.150836
- [24] Ega, S. P., & Srinivasan, P. (2022). Quinone materials for supercapacitor: Current status, approaches, and future directions. Journal of Energy storage, 47, 103700. doi.org/10.1016/j.est.2021.103700
- [25] Bhosale, S. V., & Bhosale, S. V.(2025). Advancements in supercapacitors: breaking barriers and enabling amazing applications. Royal Society of Chemistry, 16, 10159-10227. DOI: 10.1039/D5SC01955A
- [26] Yokoji, T., Matsubara, H., & Satoh, M. (2014). Rechargeable organic lithium-ion batteries using electron-deficient benzoquinones as positive-electrode materials with high discharge voltages. *Journal of Materials Chemistry A*, 2(45), 19347–19354. doi:10.1039/c4ta02812k
- [27] Zhou, Y., Wei, Q., Xiao, L., Meng, C., Yin, Q., Song, S., He, Y., Qiang, R., Yang, Y., Li, Z., & Hu, Z. (2024). Quinone-Enriched Polymer with a Large π-Conjugated Structure for High-Energy Supercapacitors: Synthesis and Electrochemical Assessment. *Batteries and Energy Storage*, 38(8), 7399–7411. doi.org/10.1021/acs.energyfuels.4c00778
- [28] Liang, Y., Zhang, P., Yang, S., Tao, Z., & Chen, J. (2013). Fused Heteroaromatic Organic Compounds for High-Power Electrodes of Rechargeable Lithium Batteries. *Advanced Energy Materials*, 3(5), 600–605. doi:10.1002/aenm.201200947
- [29] Dong, T., Zhang, J., Xu, G., Chai, J., Du, H., Wang, L., Wen, H., Zang, X., Du, A., Jia, Q., Zhou, X., & Cui, G. (2018). A multifunctional polymer electrolyte enables ultra-long cycle-life in a high-voltage lithium metal battery. *Energy and Environmental Science*, 11(5), 1197–1203. doi:10.1039/c7ee03365f

- [30] Xu, D., He, Y.-B., Chu, X., Ding, Z., Li, B., He, J., Du, H., Qin, X., & Kang, F. (2014). Synthesis of Lithium Iron Phosphate/Carbon Microspheres by Using Polyacrylic Acid Coated Iron Phosphate Nanoparticles Derived from Iron (III) Acrylate. *Chem Sus Chem*, 8(6), 1009–1016. doi:10.1002/cssc.201403060
- [31] Yokoji, T., Kameyama, Y., Maruyama, N., & Matsubara, H. (2016). High-capacity organic cathode active materials of 2,2'-bis-p-benzoquinone derivatives for rechargeable batteries. *Journal of Materials Chemistry A*, 4(15), 5457–5466. doi:10.1039/c5ta10713j
- [32] Sieuw, L., Jouhara, A., Quarez, E., Auger, C., Gohy, J.-F., Poizot, P., & Vlad, A. (2018). H-bond Stabilized Quinone Electrode Material for Li-Organic Batteries: the Strength of Weak Bonds. *Chemical Science*, 10, 418-426. doi:10.1039/c8sc02995d
- [33] Yokoji, T., Kameyama, Y., Sakaida, S., Maruyama, N., Satoh, M., & Matsubara, H. (2015). Steric Effects on the Cyclability of Benzoquinone-type Organic Cathode Active Materials for Rechargeable Batteries. *Chemistry Letters*, 44(12), 1726–1728. doi:10.1246/cl.150836
- [34] Yao, M., Numoto, T., Araki, M., Ando, H., Takeshita, H. T., & Kiyobayashi, T. (2014). Long Cycle-life Organic Electrode Material based on an Ionic Naphthoquinone Derivative for Rechargeable Batteries. *Energy Procedia*, 56, 228–236. doi:10.1016/j.egypro.2014.07.153
- [35] Lee, J., Kim, H., & Park, M. J. (2016). Long-Life, High-Rate Lithium-Organic Batteries Based on Naphthoquinone Derivatives. *Chemistry of Materials*, 28(7), 2408–2416. doi:10.1021/acs.chemmater.6b00624
- [36] Zhu, Z., Li, H., Liang, J., Tao, Z., & Chen, J. (2015). The disodium salt of 2,5-dihydroxy-1,4-benzoquinone as anode material for

- rechargeable sodium ion batteries. *Chemical Communications*, 51(8), 1446–1448. doi:10.1039/c4cc08220f
- [37] Zhou, A., Li, Z., Li, D., Cheng, C., Chen, X., Wang, Q., Kasera, A. A., Li, J., Hou, Q., & Zeng, R. (2024). Triphenylamine-Supported Benzoquinone Polymer as High Performance Cathode for Lithium-Ion Batteries. *Chemistry Select*, 9(19), e202400538. doi:10.1002/slct.202400538
- [38] Buyukcakir, O., Yuksel, R., Begar, F., Erdogmus, M., Arsakay, M., Lee, S. H., Kim, S. O., & Ruoff, R. S. (2023). Ultralong-Life Quinone-Based Porous Organic Polymer Cathode for High-Performance Aqueous Zinc-Ion Batteries. *ACS Applied Energy Materials*, 6 (14), 7672-7680. doi: 10.1021/acsaem.3c01163
- [39] Song, Z., Qian, Y., Gordin, M. L., Tang, D., Xu, T., Otani, M., Zhan, H., Zhou, H., & Wang, D. (2015). Polyanthraquinone as a Reliable Organic Electrode for Stable and Fast Lithium Storage. *Angewandte Chemie International Edition*, 54(47), 13947–13951. doi:10.1002/anie.201506673
- [40] Song, Z., Qian, Y., Liu, X., Zhang, T., Zhu, Y., Yu, H., Otani, M., & Zhou, H. (2014). A quinone-based oligomeric lithium salt for superior Li–organic batteries. *Energy & Environmental Science*, 7(12), 4077–4086. doi:10.1039/c4ee02575j
- [41] Vlad, A., Arnould, K., Ernould, B., Sieuw, L., Rolland, J., & Gohy, J.-F. (2015). Exploring the potential of polymer battery cathodes with electrically conductive molecular backbone. *Journal of Materials Chemistry A*, 3(21), 11189–11193. doi:10.1039/c5ta01500f
- [42] Song, Z., Qian, Y., Zhang, T., Otani, M., & Zhou, H. (2015). Poly(benzoquinonyl sulfide) as a High-Energy Organic Cathode for Rechargeable Li and Na Batteries. *Advanced Science*, 2(9), 1500124. doi:10.1002/advs.201500124

- [43] Liu, K., Zheng, J., Zhong, G., & Yang, Y. (2011). Poly(2,5-dihydroxy-1,4-benzoquinonyl sulfide) (PDBS) as a cathode material for lithium ion batteries. *Journal of Materials Chemistry*, 21(12), 4125. doi:10.1039/c0jm03127e
- [44] Xie, J., Wang, Z., Xu, Z. J., & Zhang, Q. (2018). Toward a High-Performance All-Plastic Full Battery with a'Single Organic Polymer as Both Cathode and Anode. *Advanced Energy Materials*, 8(21), 1703509. doi:10.1002/aenm.201703509
- [45] Xie, J., Wang, Z., Gu, P., Zhao, Y., Xu, Z. J., & Zhang, Q. (2016). A novel quinone-based polymer electrode for high performance lithiumion batteries. *Science China Materials*, 59(1), 6–11. doi:10.1007/s40843-016-0112-3
- [46] Wei, W., Li, L., Zhang, L., Hong, J., & He, G. (2018). A benzoquinone-based cathode for Li-organic batteries. *Materials Letters*, 213, 126–130. doi:10.1016/j.matlet.2017.11.035
- [47] Xiang, J., Chang, C., Li, M., Wu, S., Yuan, L.,&Sun, J. (2008). A Novel Coordination Polymer as Positive Electrode Material for Lithium Ion Battery. *Crystal Growth and Design*, 8(1), 280–282. doi:10.1021/cg070386q
- [48] Huang, W., Zheng, S., Zhang, X., Zhou, W., Xiong, W., & Chen, J. (2020). Synthesis and application of Calix [6] quinone as a high-capacity organic cathode for plastic crystal electrolyte-based lithiumion batteries. *Energy Storage Material*, 26, 465–471. doi:10.1016/j.ensm.2019.11.020.
- [49] Wang, H., Emanuelsson, R., Liu, H., Mamedov, F., Strømme, M., & Sjödin, M. (2021). A conducting additive-free high potential quinone-based conducting redox polymer as lithium-ion battery cathode. *Electrochimica Acta*, 391, 138901. doi:10.1016/j.electacta.2021.138901

- [50] Xie, J., Chen, W., Long, G., Gao, W., Xu, Z. J., Liu, M., & Zhang, Q. (2018). Boosting the performance of organic cathodes through structure tuning. *Journal of Material Chemistry A*, 6, 12985–12991. doi:10.1039/C8TA03857K
- [51] Åkerlund, L., Emanuelsson, R., Renault, S., Huang, H., Brandell, D., Strømme, M., & Sjodin, M. (2017). The Proton Trap Technology-Toward High Potential Quinone-Based Organic Energy Storage. *Advanced Energy Materials*, 7(20), 1700259. doi:10.1002/aenm.201700259
- [52] Luo, Z., Liu, L., Ning, J., Lei, K., Lu, Y., Li, F., & Chen, J. (2018). A Microporous Covalent-Organic Framework with Abundant Accessible Carbonyl Groups for Lithium-Ion Batteries. *Angewandte Chemie International Edition*, 57(30), 9443–9446. doi:10.1002/anie.201805540
- [53] Pirnat, K., Bitenc, J., Vizintin, A., Krajnc, A., & Tchernychova, E. (2018). Indirect Synthesis Route toward Cross-Coupled Polymers for High Voltage Organic Positive Electrodes. *Chemistry of Materials*, 30(16), 5726–5732. doi:10.1021/acs.chemmater.8b02329
- [54] Lee, W., Suzuki, S., Miyayama, M. (2014). Electrochemical Properties of Poly(Anthraquinonyl Sulfide)/Graphene Sheets Composites as Electrode Materials for Electrochemical Capacitors. *Nanomaterials (Basel*), 4(3), 599-611. doi: 10.3390/nano4030599
- [55] Wang, J., Wang, Z., Li, Z., Liu, N., Luo, Y., Chu, Y., Jiang, L., Zhao, F. G., Zhang, K., Liu, X., Shen, Y. (2023). High-energy-density flexible graphene-based supercapacitors enabled by atypical hydroquinone dimethyl ether. *J Colloid Interface Science*, 648, 231-241. doi: 10.1016/j.jcis.2023.05.194.
- [56] Zhou, Y., Wei, Q., Xiao, L., Meng, C., Yin, Q., Song, S., He, Y., Qiang, R., Yang, Y., Li, Z., & Hu, Z. (2024). Quinone-Enriched Polymer

- with a Large π-Conjugated Structure for High-Energy Supercapacitors: Synthesis and Electrochemical Assessment. *Energy & Fuels*, 38(8), 7399–7411. doi.org/10.1021/acs.energyfuels.4c00778
- [57] Song, Z., Xu, T., Gordin, M. L., Jiang, Y.-B., Bae, I.-T., Xiao, Q., Zhan, H., Liu, J., & Wang, D. (2012). Polymer–Graphene Nanocomposites as Ultrafast-Charge and -Discharge Cathodes for Rechargeable Lithium Batteries. Nano Letters, 12(5), 2205 -2211. doi:10.1021/nl2039666
- [58] Lin, Z.-Q., Xie, J., Zhang, B-W., Jie-Wei Li, J.-W., Weng, J., Song, R.-B., Huang, X., Zhang, H., Li, H., Liu, Y., Zhichuan J. Xu, Z. J., Huang, W., & Zhang, Q. (2017). Solution-processed nitrogen-rich graphene-like holey conjugated polymer for efficient lithiumion storage. *Nano Energy*, 41, 117-127. doi:10.1016/j.nanoen.2017.08.038
- [59] Safari, J., & Gandomi-Ravandi, S. (2014). Structure, synthesis and application of azines: a historical perspective. *RSC Advances*, 4(86), 46224-46249. doi:10.1039/C4RA04870A
- [60] Chourasiya, S. S., Kathuria, D., Wani, A., & Bharatam, V. P. (2019). Azines: Synthesis, Structure, Electronic Structure and their Applications. *Organic and Biomolecular Chemistry*, 17, 8486-8521. doi:10.1039/C90B01272A
- [61] Wen, J., Wu, A., Wang, M., & Zhu, J. (2015). Rhodium (III)-Catalyzed Directed ortho-C-H Bond Functionalization of Aromatic Ketazines via C-S and C-C Coupling. *The Journal of Organic Chemistry*, 80(21), 10457–10463. doi:10.1021/acs.joc.5b01154
- [62] Kesslen, E. C., & Euler, W. B. (1995). Synthesis and characterization of pyridine end-capped oligoazines. *Tetrahedron Letters*, 36(27), 4725–4728. doi:10.1016/0040-4039(95)00888-j
- [63] Hong, W., Sun, B., Aziz, H., Park, W.-T., Noh, Y.-Y., & Li, Y. (2012). A conjugated polyazine containing diketopyrrolopyrrole for

- ambipolar organic thin film transistors. *Chemical Communications*, 48(67), 8413. doi:10.1039/c2cc33998f
- [64] Păstrăvanu, M., Dumitriu, M., & Lixandru, T. (1981). Synthesis and properties of new polyazines—I. *European Polymer Journal*, 17(2), 197–201. doi:10.1016/0014-3057(81)90055-0
- [65] Acker, P., Speer, E. M., Jan S. Wössnera, S. J. & Esser, B. (2020). Azine-based polymers with a two-electron redox process as cathode materials for organic batteries. *Journal of Materials Chemistry A*, 8(22), 11195-11201. doi:10.1039/D0TA04083E
- [66] Kolek, M., Otteny, F., Schmidt, P., Mück-Lichtenfeld, C., Einholz, C., Becking, J., Schleicher, E., Winter, M., Bieker, P. & Esser, B. (2017). Ultra-high cycling stability of poly(vinylphenothiazine) as battery cathode material resulting from π-π interactions. *Energy Environmental Sci*ence, 10, 2334-2341. doi:10.1039/c7ee01473b
- [67] Medjahed, N., Kibou, Z., Berrichi, A., Bachir, R., & Choukchou-Braham, N. (2022). Synthesis of Bis-Hydrazine Using Heterogeneous Catalysis. *Chemistry Proceedings*, 8(1), 88. doi:10.3390/ecsoc-25-11706
- [68] Dineshkumar, S., & Muthusamy, A. (2017). Investigation of aggregation-induced emission in 4-hydroxy-3-methoxybenzaldehyde azine and polyazine towards application in (opto) electronics: synthesis, characterization, photophysical and electrical properties. *Designed Monomers and Polymers*, 20 (1), 234-249. doi:10.1080/15685551.2016.1231039
- [69] Pooja, Mudila, H., & Kumar, A. (2023). Quinone based conducting materials for efficient energy storage. *AIP Conf. Proc.*, 2800, 020114. doi:10.1063/5.0162875

- [70] Păstrăvanu, M., Dumitriu, M., & Lixandru, T. (1986). Synthesis and properties of new polyazines—III. European Polymer Journal, 22 (7), 565-567. doi:10.1016/0014-3057(86)90184-9
- [71] Kang, H., Liu, H., Li, C., Sun, L., Zhang, C., Gao, H., Yin, J., Yang, B., You, Y., Jiang, K. C., Long, H., & Xin, S. (2018). Polyanthraquinone-Triazine A Promising Anode Material for High-Energy Lithium-Ion Battery. *ACS Applied Materials and Interfaces*, 10 (43), 37023–37030. doi:10.1021/acsami.8b12888
- [72] Li, M., & Xue, J. (2014). Integrated Synthesis of Nitrogen-Doped Mesoporous Carbon from Melamine Resins with Superior Performance in Supercapacitors. *The Journal of Physical Chemistry C*, 118(5), 2507–2517. doi:10.1021/jp410198r
- [73] Păstrăvanu, M., Dumitriu, M., & Lixandru, T. (1983). Synthesis and properties of new polyazines—II. *European Polymer Journal*, 19(7), 633–637. doi:10.1016/0014-3057(83)90191-x
- [74] Pooja, Kumar, A., & Mudila, H. (2024). Studying Possibilities of Poly(Benzoquinone-Hydrazine) for Electrochemical Energy Storage Application. *ES Energy and Environment*, 26, 1302. doi:10.30919/esee1302

This section outlines the experimental procedures involved in the synthesis of polyazine (PAZ), GO (graphene oxide), rGO (reduced graphene oxide), and their respective composites. Additionally, it details the chemical requirements for the present research study. It also covers the general procedures of several physicochemical techniques used for the polymer's characterization and methodology for the investigation of their electrochemical behaviour.

## 3.1 Materials

Table 2. Materials Used in the Synthesis Process

Chemical Name	Chemical	Company	
	Formula		
p-Benzoquinone (98%)	C <sub>6</sub> H <sub>4</sub> O <sub>2</sub>	Loba Chemie	
Hydrazine hydrate (99%)	$NH_2NH_2.H_2O$	Loba Chemie	
Chloroform (99.8%)	CHCl <sub>3</sub>	Loba Chemie	
Zinc chloride (extra pure)	$\mathrm{ZnCl}_2$	Loba Chemie	
Para-Xylene (99%)	$C_8H_{10}$	Alpha chemika	
Graphite	С	Loba Chemie	
Hydrochloric acid	HC1	Loba Chemie	
Conc. Sulphuric acid (98%)	$H_2SO_4$	Loba Chemie	
Potassium permanganate (99%)	$KMnO_4$	Loba Chemie	
Hydrogen Peroxide (30%)	$H_2O_2$	Loba Chemie	
Ascorbic acid	$C_6H_8O_6$	Loba Chemie	
Ethanol (99.9%)	$C_2H_5OH$	Analytical	
Ammonia (25%)	$NH_3$	Loba Chemie	
Distilled water	$H_2O$	N/A	

**3.2. Synthesis:** The PAZ, GO, rGO, and composites were synthesised by modifying the reported methods.

## **3.2.1 Synthesis of Poly(quinone-hydrazine) (Polyazine, PAZ):** Polycondensation of *p*-benzoquinone with hydrazine hydrate (mol ratio, 1:2) was carried out in the presence of ZnCl<sub>2</sub>. Utilizing a magnetic stirrer, 21.6 g of p-Benzoquinone was mixed in 100 mL of xylene at room temperature in a round-bottom flask, which was further supplied with anhydrous ZnCl<sub>2</sub> (0.3 g). The solution was further stirred for the next 10 minutes, to which hydrazine hydrate (12 g or 11.6 ml) was gradually (dropwise) introduced into the reaction mixture. After the complete incorporation of hydrazine hydrate, the reaction mixture's temperature was elevated to 110-115°C and further stirred for the next 13 hours [1].

A systematic representation of the reaction has been shown in Scheme 2. An insoluble mass (brown) with a good yield (79%) was obtained after the reaction time. Afterward, this insoluble fraction was washed with 1M NH<sub>4</sub>OH (formed by dissolving 7 ml NH<sub>3</sub> in 200 ml H<sub>2</sub>O) to remove the excess of ZnCl<sub>2</sub>, while for removing the unreacted benzoquinone from the reaction mixture, chloroform was used. This polyazine was (poly-*p*-benzoquinone azine) formed as complexes (dimers and oligomers) and was treated by washing in hot acetic acid, followed by filtration and precipitation in water to remove the smaller chains as shown in Fig 2(A, B).

Scheme 2. General representation of the preparation of PAZ





Figure 2. (A) The synthesis process of PAZ (B), Dark brown coloured PAZ

3.2.2 Synthesis of Graphene Oxide (GO): Graphite was used as the starting material to synthesize GO. 5 gm graphite (99.99 wt%) and 115 mL of conc. H<sub>2</sub>SO<sub>4</sub> was taken in a 1L vessel maintained at 5±0°C in an ice bath with continuous stirring for ½ hour. Thereafter, 15 g KMnO<sub>4</sub> as an oxidant was added gradually (1g/min) into the reaction mixture while maintaining the temperature at 5±0°C for the next 3 hours. The reaction temperature was gradually allowed to be raised to 35°C by removing the ice bath and kept maintained for another 1 hour with vigorous stirring as shown in Fig. 3(A). After that, deionized water (DI, 200ml) was introduced into the reaction mixture, which led to a temperature increase to 98°C because of the exothermic heat of the hydration process. The reaction vessel was maintained at 98°C temperature for 1 hour while continuously stirring. Afterward, the reaction was halted by adding 200 mL of DI along with 50 mL of H<sub>2</sub>O<sub>2</sub> (10% v/v). The resulting brown product was separated from the solution through vacuum filtration. The obtained GO powder underwent five washes with a diluted HCl (5%, 200 ml) solution and additional rinsing with deionized water to eliminate any remaining Mn ions and acid, and was then dried in a vacuum oven at 60°C for 12 hours [2-4].

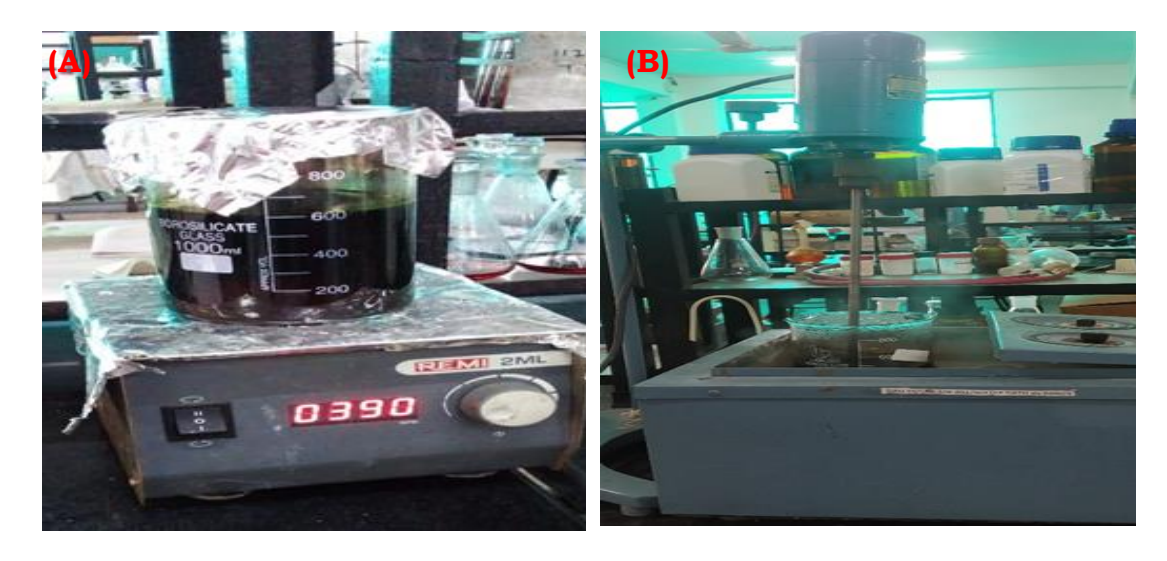


Figure 3. (A) Synthesis of GO, and (B) Synthesis of rGO

3.2.3 Synthesis of Reduced Graphene Oxide(rGO): rGO was synthesised from GO in the presence of a reducing agent ascorbic acid. Initially, 1gm of GO (in powder form) was mixed in a liter of distilled water. Subsequently, 10 grams of ascorbic acid were introduced into the resulting mixture, then this mixture was magnetically stirred for two hours at 60°C using a magnetic stirrer, as shown in Fig (B). The resulting reduced product underwent centrifugation at 4000 r/sTo oxidize any remaining ascorbic acid, an excess of 30% H<sub>2</sub>O<sub>2</sub> was added to the mixture and stirred for an hour at 60°C. Following this, the resulting black material was isolated through vacuum procedure(filtration), washed three times each with ethanol and distilled water, and then dried at 120°C for 24 hours [5].

**3.2.4 Fabrication of Polyazine/Graphene Oxide Composite** (PAZ/GO or PGs): The Polyazine/graphene oxide (PAZ/GO or PGs) composites were prepared by an in-situ method. A definite amount of PAZ was taken, which was further added with varying amounts of GO

to give the desired compositions as represented in Table 3. GO and PAZ in the requisite amount were mixed in a 2 ml ethanol solution, and after mixing, they were sonicated for about 1 hour at room temperature (RT) (Fig. 4 (A)). After mixing the individual components to form composites, those powdered materials were dried with the help of a vacuum oven for further characterization and electrochemical studies [3, 6]. The weight ratios of PAZ and GO were adjusted to 3:1, 2:1, 1:1, 1:2, and 1:3, and the resulting composite materials were designated as PAZ/GO or PGs.

Table 3. Composition and weight ratio of PGs

Symbols	PG-1	PG-2	PG-3	PG-4	PG-5
Weight ratio PGs	3:1	2:1	1:1	1:2	1:3
Amount of PAZ (gm)	0.05	0.05	0.05	0.05	0.05
Amount of GO (gm)	0.0166	0.025	0.05	0.1	0.15

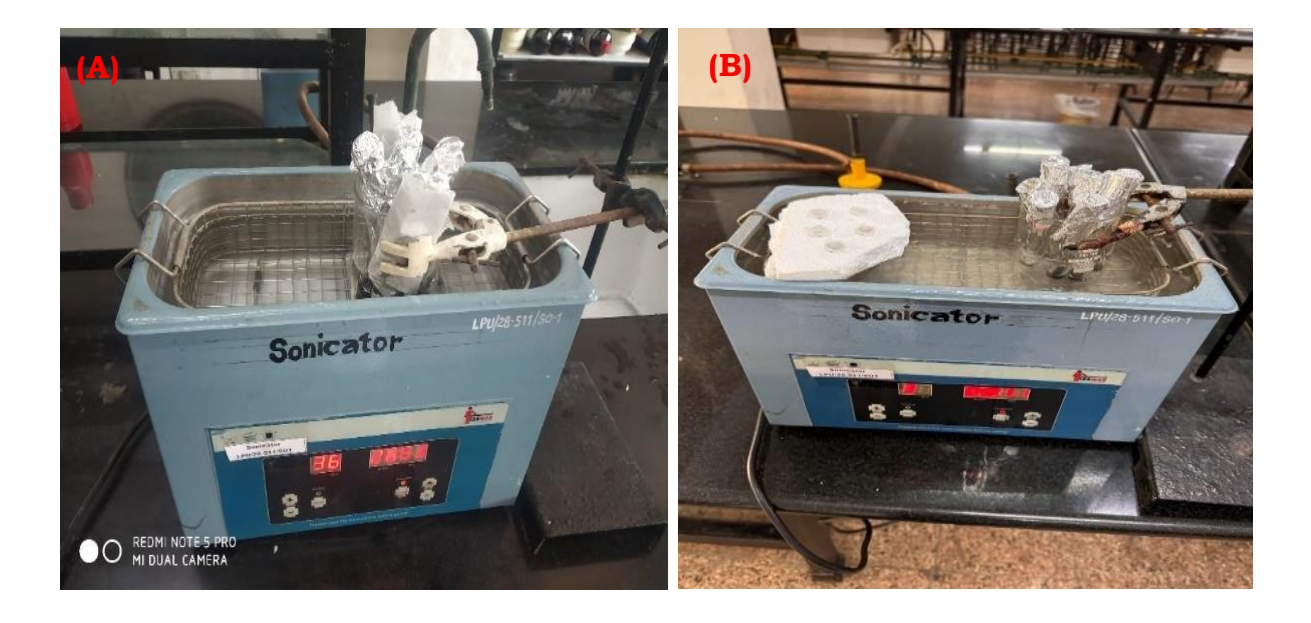


Figure 4. (A) In situ Composite formation of PAZ/GO (PGs) and (B) In situ Composite formation of PAZ/rGO (PrGs)

# 3.2.5 Fabrication of Polyazine (PAZ)/ reduced Graphene Oxide(rGO)

Composite (PAZ/rGO or PrGs): The in-situ approach was used to make the PAZ/rGO (PrGs) composites. A specific amount of PAZ was taken and then mixed with different amounts of rGO to produce the appropriate compositions, as shown in Table 4. Fig. 4(B) demonstrates the dissolution of rGO and PAZ in 2 mL of ethanol solution, followed by sonication for one hour at ambient temperature. For additional characterisation and electrochemical research, the powdered materials were baked in a vacuum oven after the constituent parts had been combined to create composites [7]. The proportion of PAZ to rGO in the composite materials was systematically varied, with weight ratios of 3:1, 2:1, 1:1, and 1:2, and the resulting composites were designated as PAZ/rGO or PrGs.

Table 4. Composition and weight ratio of PrGs

Symbols	PrG-1	PrG-2	PrG-3	PrG-4
Weight ratio PAZ/r-GO	3:1	2:1	1:1	1:2
Amount Of PAZ (gm)	0.05	0.05	0.05	0.05
Amount Of rGO (gm)	0.0166	0.025	0.05	0.1

**3.2.6 Fabrication of electrode on carbon paste electrode (CPE):** In a mortar and pestle, 10g of graphite powder and 3.6 ml of paraffin oil were thoroughly mixed to prepare the carbon paste as shown in fig 5. The CPE was fabricated by tight packing the hollow glass tube body with the requisite amount of prepared carbon paste, the fabricated CPE surface was turned smooth, uniform, and shiny by grating it against a clean A4 paper surface [8].

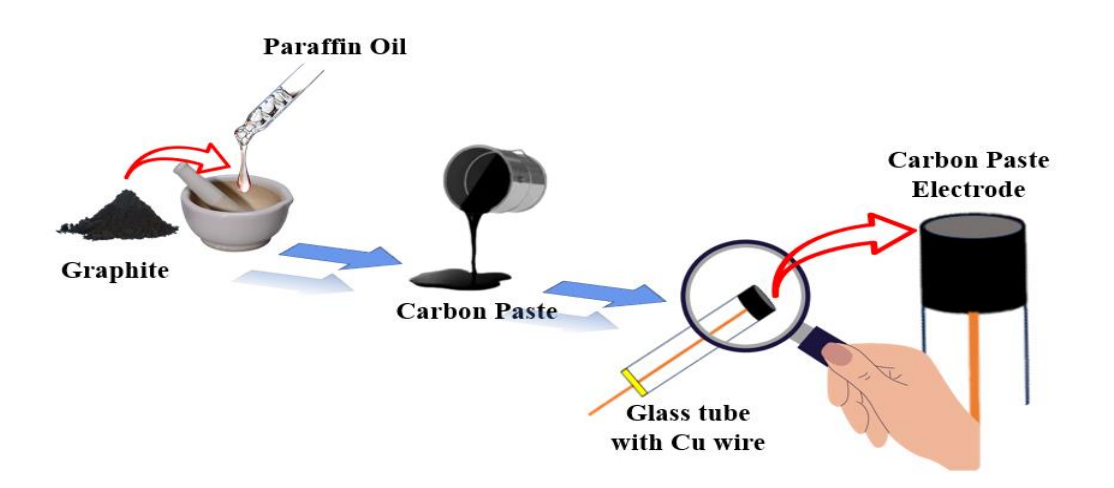


Figure 5. Fabrication of a carbon paste electrode for electrochemical studies

A copper wire (50 mm × 2 mm) was placed inside the body of the glass tube, ensuring contact of the copper wire with the filled carbon paste, while another end was extended out to create an electrical contact.

**3.3 Characterization techniques:** This section provides a detailed explanation of the characterisation methods utilized for conducting polymer PAZ, GO, rGO, and their composites. Fourier Transform **Infrared (FTIR) Spectroscopy** was used to examine and characterize the chemical makeup of prepared materials. This technique operates by quantifying the absorption or transmission of infrared radiation through a specimen. X-ray diffraction (XRD) is a powerful analytical method employed to investigate the crystallographic structure, chemical composition, and physical characteristics of materials. This method operates by directing X-ray beams at a sample and analyzing the diffraction patterns that arise when the X-rays interact with the atomic planes within the crystalline structure. A Scanning Electron Microscope (SEM) was employed to investigate the surface characteristics and structural morphology of materials at remarkably high magnifications. This instrument operates by directing a focused beam of electrons onto a sample and detecting the signals generated by

the interaction between the charged particles and the sample material. Differential Scanning Calorimetry (DSC) and Thermogravimetric Analysis (TGA) were utilised to examine the thermal properties and behaviour of all the prepared materials. These techniques are often complementary, offering information about the material's composition, stability, and phase changes during the process. Cyclic Voltammetry (CV), Galvanostatic Charge-Discharge (GCD), and Electrochemical Impedance Spectroscopy (EIS) techniques were utilized to analyze the properties and electrochemical behaviour of the materials.

**3.3.1 Fourier transform infrared (FTIR) spectroscopy:** FTIR spectroscopy is a method of analysis utilized to identify and investigate the chemical composition and molecular structure of substances by quantifying their absorption of infrared radiation (as shown in the block diagram, i.e., Fig. 6). It measures the absorption of particular infrared light frequencies, producing a distinctive fingerprint for detection and study. Various bonds absorb different wavelengths of infrared radiation because they vibrate at different frequencies. The resulting spectrum creates a distinct molecular fingerprint with each of its distinct absorption bands concerning position and strength. FTIR provides significant information regarding the polymer's chemical composition and functional groups.

Molecules exhibit distinctive vibrational patterns. The mid-infrared (mid-IR) spectrum can be divided into two key regions. One is the fingerprint region spanning 650 to 1500 cm<sup>-1</sup>, and the second one is the functional group region ranging from 1500 to 4000 cm<sup>-1</sup>. In the region of the highest wavenumber (2500-4000 cm<sup>-1</sup>), all single bonds (O-H, N-H, and C-H) can be detected; in the mid wavenumber region (1500-2500 cm<sup>-1</sup>), multiple bonds can be detected; and in the lower wavenumber region (600-1500 cm<sup>-1</sup>), whole vibrations in molecules resulting in a

complex pattern can be detected. These characteristics are specific to a given molecule. Among dispersive spectrometers, this model is preferred due to its advanced features, including exceptional sensitivity, rapid operation, high precision, user-friendliness, and non-destructive sample analysis [9, 10].

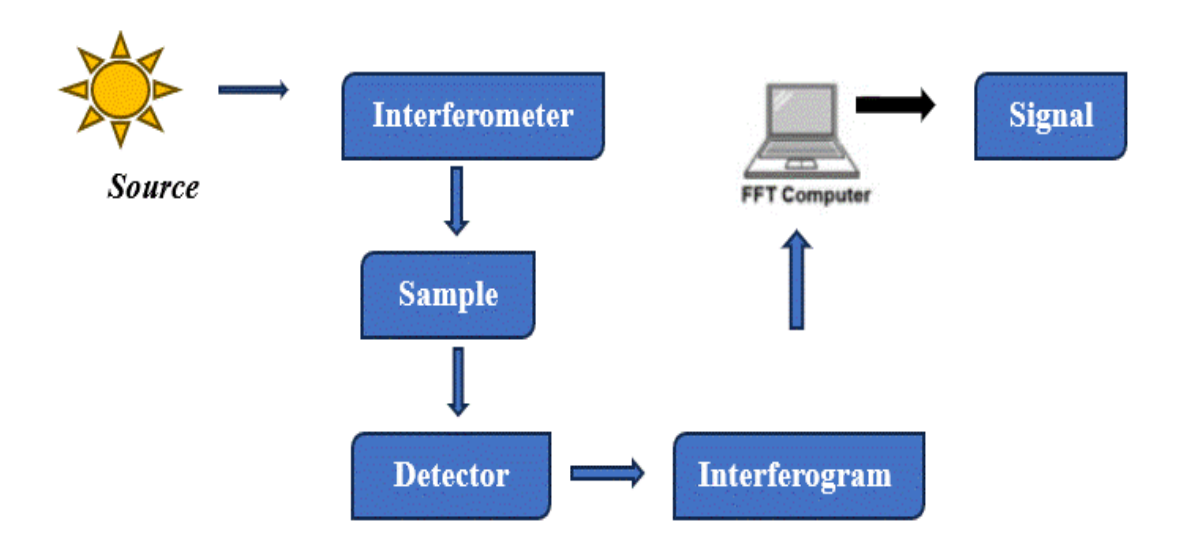


Figure 6. Block diagram of the FTIR working process

Much of the research on polymer characterization in historically significant assets uses FTIR spectroscopy, which is a quick, easy, and non-invasive method [11].

The FTIR spectra were obtained using a Perkin Elmer spectrometer (Fig 7(A)) under a scan range of 8300-350 cm<sup>-1</sup>(0.5 cm<sup>-1</sup> resolution), equipped with a Diamond ATR accessory, and Spectrum 10 software was used for determining the IR spectra of the material and its composites with GO and rGO. The resulting spectrum displays the intensity of absorption versus the frequency (usually in cm<sup>-1</sup>) or wavelength (microns). The observed peaks in the spectral data correspond to specific vibrational frequencies of the molecular components present in the analyzed sample.

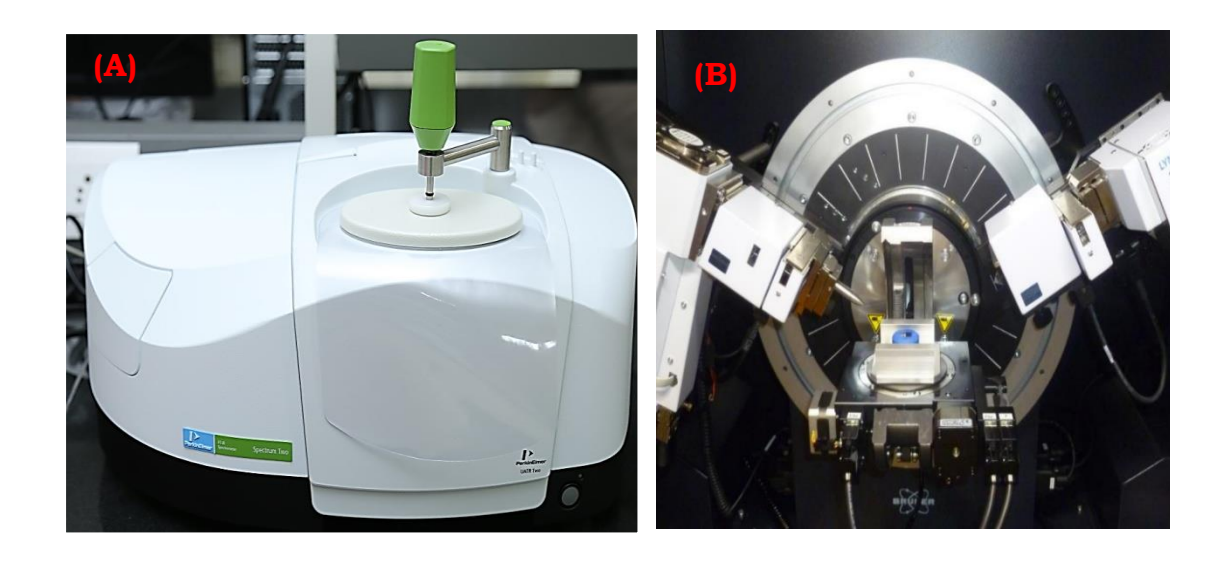


Figure 7 (A). FTIR instrument of the Perkin Elmer company, (B).

Bruker powder X-ray diffractometer

**3.3.2 X-ray diffraction (XRD) technique:** An essential method for characterizing materials is X-ray diffraction (XRD). It has historically been applied to analyze the crystallographic properties of many different materials, including polymers. PAZ, GO, rGO, and composites have all had their crystalline and amorphous structures investigated using XRD. Due to its ease of use, dependability, capacity to yield quantitative data, and non-destructive characteristics, the approach has become increasingly popular. A Bruker powder X-ray diffractometer (Fig.7(B)) technique was leveraged to examine the crystalline and amorphous characteristics of the material and its composite structures incorporating GO and rGO within the current study. The diffractogram was recorded in terms of 2θ in the 10°- 80° range using Cu-Kα radiations to acquire intensity data.

XRD is used for examining atomic spacing and crystal structure. These diffracted X-rays can provide information about a material's electronic dispersion. Bragg's law for the constructive interference between

a crystalline sample and a monochromatic X-ray, which is the foundation of X-ray diffraction analysis:

$$n\lambda = 2d \sin\theta \tag{1}$$

Here, the X-rays' wavelength is denoted as  $\lambda$ , the incident angle is  $\theta$ , the interplanar spacing responsible for the diffraction is d, and the diffraction order is n [12, 13].

XRD helps to identify and quantify the crystalline regions within a polymer. Polymers often have a mixture of crystalline and amorphous phases, and XRD can provide insights into the degree of crystallinity, which can influence the material's optical, mechanical, and thermal stability. All feasible lattice diffraction patterns are provided when the powdered material is oriented randomly and the sample is examined across a range of  $2\theta$  angles. The process of translating diffraction peaks to d-spacing, which is specific to a material, allows for additional material identification [14].

**3.3.3 Thermal Properties:** For analysing the thermal studies, Thermogravimetric analysis (TGA) and Differential Scanning Calorimetry (DSC) techniques.

3.3.3.1 Thermogravimetric analysis (TGA): This technique is employed to characterize materials by monitoring the variation in their mass as they are exposed to a regulated temperature environment. This technique provides valuable information about material's composition, stability, and behaviour under heating or cooling conditions. TGA enables the quantification of polymer weight loss as a function of temperature and time. Such weight variations can arise from physical phenomena, including vaporization, sublimation, and desorption, as well as chemical processes such as oxidation and decomposition within polymeric materials. The samples exhibit a mass loss as a result of numerous physical and chemical changes when the

temperature rises. As a result, the study is useful in figuring out the samples' thermal stability. It was observed that the horizontal line represents the temperature at which a material is more thermally stable, or the zone where there is no weight loss, and the vertical line represents where weight loss occurs due to evaporation, decomposition, or dehydration [15].

Perkin Elmer, TGA-4000 (Fig. 8(A)) having a scanning rate of 0.1 to  $200^{\circ}$ C/min, was used for the determination of percentage weight loss of polymer and its composites with GO and rGO from  $50^{\circ}$ C to  $600^{\circ}$ C temperature range. The polymeric sample is heated in an inert environment (N<sub>2</sub> presence) at the rate of  $10^{\circ}$  C/min. TGA monitors the weight loss of a sample under the fluctuation of temperature. This is particularly useful for analysing volatile components, such as solvents or water, that may evaporate upon heating.



Figure 8(A). TGA instrument used for current research and (B).

DSC Instrument used to measure thermal transitions

**3.3.3.2 Differential Scanning Calorimetry (DSC):** DSC-6000 (Perkin Elmer instrument, fig 8(B)), having a temperature range -70°C to 450°C, was used for measuring the exchange of heat energy of PAZ and its

composites with GO and rGO in the presence of  $N_2$  (inert atmosphere) under of 10° C/min rate.

This technique is employed to examine how polymers react to heat. DSC can be used to investigate the glass transition or the melting of a crystalline polymer. Thermal properties like melting, crystallization, glass transition temperature, and heat capacity of the polymer are examined by this technique [16].

It should be noted that not every polymer goes through all three of these changes when heated. Only polymers with the ability to form crystals exhibit melting and crystallization peaks. Crystalline polymeric materials typically encompass amorphous regions and exhibit a glass transition, in contrast to fully amorphous polymers, which only undergo a glass transition. While the crystalline domains solely experience melting, the amorphous segments solely exhibit the glass transition. The specific temperatures at which the polymer chains undergo these phase changes are determined by the polymer's structural characteristics. The graph of heat versus temperature for a completely crystalline polymer exhibits an upward discontinuity at its melting temperature. During the glass transition, the heat vs temperature curve is consistent but not smooth. Its slope indicates its heat capability. Given that T<sub>g</sub> (Glass Transition temperature) and T<sub>m</sub> (Melting point) have greater heat capacities, the slope rises after them **[17]**.

**3.3.4. Scanning Electron Microscopy (SEM):** SEM was employed to acquire a high-magnification image of the material, which is a valuable imaging technique. This is the best and most flexible technique for analyzing the samples' microstructure morphology [18].

A high-resolution (1.0 nm) and high-magnification (25X to 10<sup>6</sup>X) JEOL field emission SEM was utilized to characterize the morphological features of the materials.

The morphology of the polymer and its composite with GO and rGO were studied by varying the magnification from 500 to 25000 X.



Figure 9. SEM instrument used for morphological study of prepared materials

Given its widespread application in the study of failure mechanics and fracture, particle shape, and size, and scattering in polymer matrices, SEM is a crucial instrument for polymer investigation. Because of this, SEM is usually found in polymer investigation and manufacturing facilities. By exposing phases to solvents, phases can be selectively etched to produce the required phase transitions for SEM analysis of the microstructural characteristics of polymer systems [18].

3.4 Electrochemical Characterisation: Α multi-channel Potentiostat/galvanostat (Autolab PGSTAT204, Metrohm, Fig. 10) was used to identify the electrochemical behaviour of all the prepared materials. Polyazine and its composite's electrochemical behaviour were evaluated for supercapacitor applications using a three-electrode setup. Techniques employed included cyclic voltammetry (CV), galvanostatic charge-discharge (GCD), and electrochemical impedance spectroscopy (EIS). These were performed in 1M H<sub>2</sub>SO<sub>4</sub> electrolyte. CV was performed from 10, 60 and 100 mV/s scan rates. The GCD was carried out at 1 A/g, 0.5 A/g, and 0.25 A/g to determine the power and energy densities of the prepared material. EIS measurements were conducted under 100 MHz to 100 kHz frequency range, with an amplitude of 20 mV/s alternating current.



Fig 10. Instrument for electrochemical characterization

**3.4.1 Cyclic voltammetry (CV):** CV is an effective tool for probing the redox behavior of chemical species. This widely utilized method enables the investigation of electron transfer processes, making it a valuable tool for studying chemical reactions, including catalysis. Using a specified scan rate, the electrode potential is swept between limits  $V_1$  and  $V_2$  in this potential sweep approach [19]. The current versus potential graph that displays the redox process's threshold is called a

cyclic voltammogram. The measured peak current is indicative of that specific electrode reaction. The CV plots can be utilized for evaluating specific capacitance ( $C_{sp}$ ) with the assistance of equation (2).

$$C_{sp} = \frac{A}{2m\Delta Vk} \tag{2}$$

Where A is the area under the CV curve, m is the deposited mass of the electroactive material over CPE,  $\Delta V$  is the applied potential window, and k is the scan rate (in mV/s) [20, 21].

**3.4.2 Galvanostatic charge-discharge (GCD):** GCD is an effective technique that is extensively employed to assess the electrochemical performance of energy storage devices, encompassing batteries, supercapacitors, and other electrochemical systems. In battery applications, GCD analysis measures both charging and discharging durations at a steady current, making it easier to calculate capacity (mAh/g). For supercapacitors, GCD is utilized to calculate the specific capacitance or areal capacitance. Furthermore, the charge-discharge profiles derived from GCD can be employed to derive both power density and energy density. The voltage-time curves provide insights into the material's energy storage behaviour (e.g., battery-like vs. capacitor-like). By performing the GCD cycles over time, the cyclic stability of the material/device is evaluated, which is crucial for practical applications [22].

GCD measurements were conducted at diverse current densities within the designated working potential range. The obtained GCD profiles were leveraged to calculate the specific capacitance, which was subsequently utilized to evaluate the total energy density and power density of the electroactive material. Equation (3) is employed to determine the specific capacitance ( $C_{sp}$ ). Equation (4) is for energy density ( $E_g$ ), and equation (5) is employed for power density (P):

$$C_{sp\ (F/g)} = \frac{I\Delta t}{m\Delta V} \tag{3}$$

$$E_g (Wh/Kg) = \frac{c_{sp} \cdot \Delta V^2}{2} * \frac{1000}{3600}$$
 (4)

$$P (W/kg) = \frac{E_g}{\Lambda t} \times 3600 \tag{5}$$

Here, I represents the current density,  $C_{sp}$  symbolizes the specific capacitance, the potential window is denoted by  $\Delta V$ , the discharge time is denoted by  $\Delta t$ ,  $E_g$  stands for energy density, and P stands for power density [21, 22].

This technique is straightforward, reliable, and widely employed for investigating and comparing the behaviour of different energy storage systems.

In this current work, the charge-discharge behaviour of the PAZ and its composites was carried out at different current densities (1, 0.25, 0.5 A/g) with a 0 V to 1 V working potential window.

**3.4.3 Electrochemical Impedance Spectroscopy (EIS):** EIS is a useful method for examining how quickly charges are transferred and transported in electrochemical processes. It is also used for examining the properties of electrode reactions and for the characterization of conducting materials. EIS is a valuable analytical technique for examining the intricate processes of electron diffusion and transport that occur across the interface between the electrode and the electrolyte. This frequency domain approach clarifies how doping and redox additive electrolytes affect the supercapacitor's resistive and capacitive elements [23].

Nyquist plots are frequently employed in the investigation of polymers, particularly through the technique of EIS, to analyze and describe the electrical and electrochemical characteristics of polymer materials. In this context, the Nyquist plot represents the impedance response of the polymer as a function of frequency, providing insights into various material properties and behaviors. By using the Nyquist plot, polymer materials are designed for applications like energy storage, coatings, and advanced functional materials. A Bode plot is created when the magnitude of impedance and phase angle are plotted on a double-axis plot as a function of frequency. The plot is typically used to analyse the impedance response of an electrochemical system, such as batteries, fuel cells, or corrosion systems, over a range of frequencies [24, 25]. EIS measurements were conducted under a 100 MHz to 100 kHz frequency range, with a 20 mV/s amplitude of AC (alternating current).

#### References

- [1] Pastravanu, M., Dumitriu, M., & Lixandru, T. (1986). Synthesis and properties of new polyazine-III. *Eur. Polym. J*, 22(7),565—567.
- [2] Guerrero-Contreras, J., & Caballero-Briones, F. (2015). Graphene oxide powders with different oxidation degrees, are prepared by synthesis variations of the Hummers method. *Materials Chemistry and Physics*, 153, 209–220. doi:10.1016/j.matchemphys.2015.01.005
- [3] Mudila, H., Joshi, V. Rana, S., Zaidi, M. G. H., & Alam, S. (2014). Enhanced electrocapacitive performance and high power density of polypyrrole/graphene oxide nanocomposites prepared at reduced temperature. *Carbon Letters*, 15(3), 171-179. doi: 10.5714/CL.2014.15.3.171
- [4] Zaaba, N. I., Foo, K. L., Hashim, U., Tan, S. J., Liu, W.-W., & Voon, C. H. (2017). Synthesis of Graphene Oxide using Modified Hummers Method: Solvent Influence. *Procedia Engineering*, 184, 469–477. doi:10.1016/j.proeng.2017.04.118
- [5] Habte, A. T., & Ayele, D. W. (2019). Synthesis and Characterization of Reduced Graphene Oxide (rGO) Started from Graphene Oxide (GO) Using the Tour Method with Different Parameters. *Advances in Materials Science and Engineering*, 2019, 1–9. doi:10.1155/2019/5058163
- [6] Xue, J., Sun, Q., Zhang, Y., Mao, W., Li, F., & Yin, C. (2020). Preparation of a Polypyrrole/Graphene Oxide Composite Electrode by Electrochemical Codeposition for Capacitor Deionization. *ACS Omega*, 5(19), 10995–11004. doi:10.1021/acsomega.0c00817
- [7] Liu, G., Shi, Y., Wang, L., Song, Y., Gao, S., Liu, D., & Fan, L. (2019). Reduced graphene oxide/polypyrrole composite: an advanced electrode for high-performance symmetric/asymmetric supercapacitor. *Carbon Letters*, 30(4), 389–397. doi:10.1007/s42823-019-00108-x

- [8] Zayed, S. I. M., & Arida, H. A. M. (2013). Preparation of Carbon Paste Electrodes and Its Use in Voltammetric Determination of Amiloride Hydrochloride Using in the Treatment of High Blood Pressure. *International Journal of Electrochemical Science*, 8, 1340-1348. doi:10.1016/S1452-3981(23)14102-2
- [9] Mohamed, M. A., Jaafar, J., Ismail, A. F., Othman, M. H. D., & Rahman, M. A. (2017). Fourier Transform Infrared (FTIR) Spectroscopy. *Membrane Characterization*, 3–29. doi:10.1016/b978-0-444-63776-5.00001-2
- [10] Barrios, V. A. E., Méndez, J. R. R., Aguilar, N. V. P., Espinosa, G. A., & Rodríguez, J. L. D. (2012). FTIR An Essential Characterization Technique for Polymeric Materials. Infrared Spectroscopy Materials Science, *Engineering and Technology*. doi:10.5772/36044
- [11] Gong, Y., Chen, X., & Wu, W (2024). Application of Fourier transform infrared (FTIR) spectroscopy in sample preparation: Material characterization and mechanism investigation. *Advances in Sample Preparation*, 11, 100122. doi:10.1016/j.sampre.2024.100122.
- [12] Abhilash, V., Rajender, N., & Suresh, K. (2016). X-ray diffraction spectroscopy of polymer nanocomposites. *Spectroscopy of Polymer Nanocomposites*, 410–451. doi:10.1016/b978-0-323-40183-8.00014-8
- [13] Holder, C. F., & Schaak, R. E. (2019). Tutorial on Powder X-ray Diffraction for Characterizing Nanoscale Materials. *ACS Nano*, 13(7), 7359–7365. doi:10.1021/acsnano.9b05157
- [14] Widjonarko, N. E. (2016). Introduction to Advanced X-ray Diffraction Techniques for Polymeric Thin Films. *Coatings*, 6(4), 54. doi:10.3390/coatings6040054
- [15] Ng, H. M., Saidi, N. M., Omar, F. S., Ramesh, K., Ramesh, S., & Bashir, S. (2018). Thermogravimetric Analysis of Polymers.

- Encyclopedia of Polymer Science and Technology, 1–29. doi:10.1002/0471440264.pst667
- [16] Vanden Poel, G., & Mathot, V. B. F. (2007). High-performance differential scanning calorimetry (HPer DSC): A powerful analytical tool for the study of the metastability of polymers. *Thermochimica Acta*, 461(1-2), 107–121. doi:10.1016/j.tca.2007.04.009
- [17] Schick, C. (2009). Differential scanning calorimetry (DSC) of semicrystalline polymers. *Analytical and Bioanalytical Chemistry*, 395(6), 1589–1611. doi:10.1007/s00216-009-3169-y
- [18] Guise, O., Strom, C., & Preschilla, N. (2011). STEM-in-SEM method for morphology analysis of polymer systems. *Polymer*, 52(5), 1278–1285. doi:10.1016/j.polymer.2011.01.
- [19] Elgrishi, N., Rountree, K. J., McCarthy, B. D., Rountree, E. S., Eisenhart, T. T., & Dempsey, J. L. (2017). A Practical Beginner's Guide to Cyclic Voltammetry. *Journal of Chemical Education*, 95(2), 197–206. doi:10.1021/acs.jchemed.7b00361
- [20] Ullah, R., Khan, N., Khattak, R., Khan, M., Khan, M. S., & Ali, O. M. (2022). Preparation of Electrochemical Supercapacitor Based on Polypyrrole/Gum Arabic Composites. *Polymers*, 14, 242. doi:10.3390/polym14020242
- [21] Bashid, A., Assyaima, H., Lim, H. N., Kamaruzaman, S., Rasid, S. A., Yunus, R., Huang, N. M., Yin, C. Y., Rahman, M. M., Altarawneh, M., Jiang, Z. T., & Alagarsamy, P. (2017). Electrodeposition of Polypyrrole and Reduced Graphene Oxide onto Carbon Bundle Fibre as Electrode for Supercapacitor. *Nanoscale Research Letters*, 12(1), 246.

doi:10.1186/s11671-017-2010-3

[22] Wang, P., Zheng, Y., & Li, B. (2013). Preparation and electrochemical properties of polypyrrole/graphite oxide composites

- with various feed ratios of pyrrole to graphite oxide. *Synthetic Metals*, 166, 33–39. doi:10.1016/j.synthmet.2013.01.002
- [23] Lazanas, C. A., & Prodromidis, I. M. (2023). Electrochemical Impedance Spectroscopy—A Tutorial. *ACS Measurement Science Au*, 3 (3), 162-193. doi: 10.1021/acsmeasuresciau.2c00070
- [24] Mei, B.-A., Munteshari, O., Lau, J., Dunn, B., & Pilon, L. (2017). Physical Interpretations of Nyquist Plots for EDLC Electrodes and Devices. *The Journal of Physical Chemistry C*, 122(1), 194–206. doi:10.1021/acs.jpcc.7b10582
- [25] Li, T., Qin, Z., Liang, B., Tian, F., Zhao, J., Liu, N., & Zhu, M. (2015). Morphology-dependent capacitive properties of three nanostructured polyanilines through interfacial polymerization in various acidic media. *Electrochimica Acta*, 177, 343–351. doi:10.1016/j.electacta.2015.03.169

### 4.1 FOURIER TRANSFORM INFRARED SPECTROSCOPY (FTIR):

The infrared spectra of all the prepared materials were noted through FTIR spectroscopy, having 0.5 cm<sup>-1</sup> resolution and a wavenumber range of 8300-350 cm<sup>-1</sup>. This analysis was conducted with the Diamond ATR accessory and the Spectrum 10 software.

**4.1.1 FTIR of Polyazine (PAZ):** The synthesized polymer was confirmed by the FTIR spectroscopy. Fig 11. represents the FTIR of the PAZ synthesized from *p*-benzoquinone and hydrazine hydrate. The absorption with maxima peaks at 3213, 1567.7, and 1505.7 cm<sup>-1</sup>, ascribed by the Ar-H, -C=N, and C-C ring stretching vibration respectively **[1, 2]**, and the absorption band at 1467.4, 1348.3, and 1201.1 cm<sup>-1</sup> corresponds to N-N stretching vibration, -C-N stretching **[3]**, Phenolic C-O stretching vibration respectively **[1]**. The intensity was observed to decrease from 821.7 to 608.3 cm<sup>-1</sup>, attributable to aromatic C-H vibrations, and further decreased at 457.8 cm<sup>-1</sup> due to bending

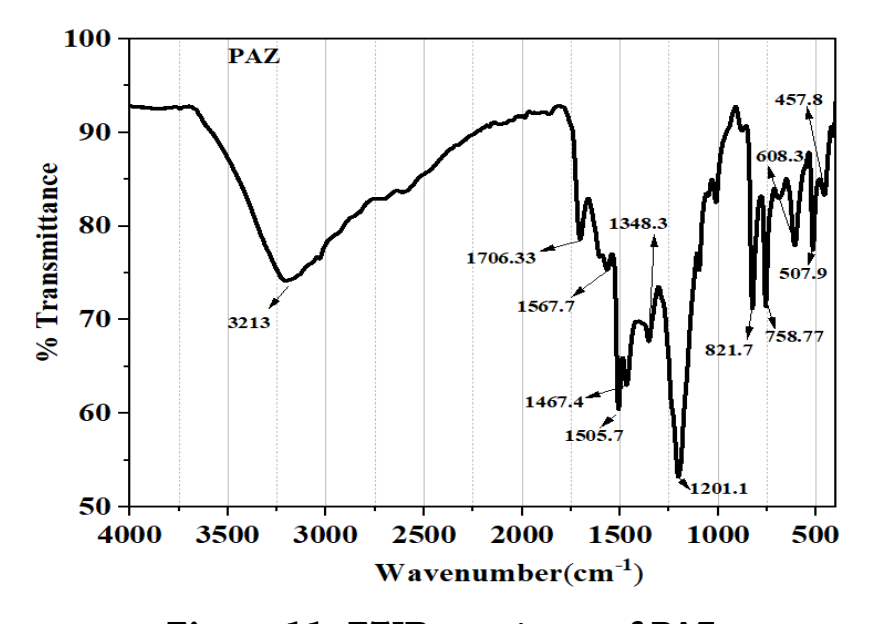


Figure 11. FTIR spectrum of PAZ

vibration of the C-H bond **[4, 5]**, while the peak appeared at 507.9 cm<sup>-1</sup>, indicative of the residual Zn-Cl bond present in the sample.

**4.1.2 FTIR of Graphene Oxide (GO):** GO was synthesized through the oxidation of graphite, facilitated by potassium permanganate. The oxygen-containing functional groups present on the GO surface were confirmed using FTIR spectroscopy. Fig.12. appear for FTIR of GO which shows a broad absorption maxima near about 3204 cm<sup>-1</sup> corresponding to OH peaks and this broad peak may be due to the hydrogen bonding, 1717.7 cm<sup>-1</sup> corresponding to the presence of CO stretching carboxyl group, 1620.38 cm<sup>-1</sup> corresponding to CO of ketone group, CO stretching vibration of carboxyl groups, C=C remained before and after the oxidation process **[6-8]**. The absorption peak that appears at 1383.37 cm<sup>-1</sup> is attributed to the alkoxy group's (C-O-C) stretching vibration, while the absorption at 1225.37 cm<sup>-1</sup> is ascribed to the ester group's C-O stretching. Additionally, the band at 1049.01 cm<sup>-1</sup> is associated with the CO stretching (alcohols and phenols) mode **[6, 9, 10]**.

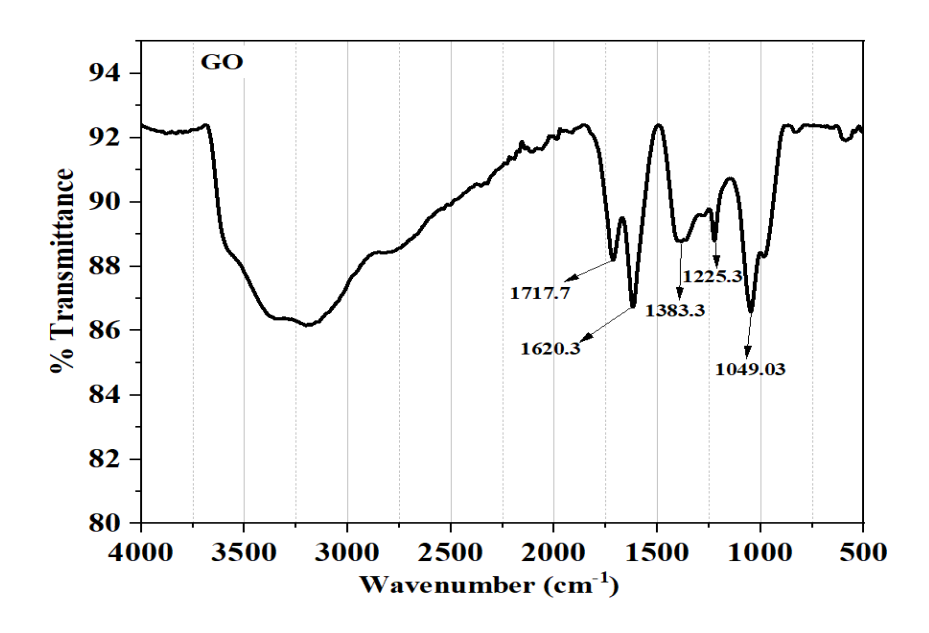


Figure 12. FTIR spectrum of GO

# 4.1.3 FTIR of Reduced Graphene Oxide (rGO):

Figure 13 depicts the FTIR spectra of rGO. The prominent peaks observed in graphene oxide near 3204 cm<sup>-1</sup> are absent in rGO, indicating successful deoxygenation. Additionally, additional peaks emerge in the rGO spectra at approximately 1708 cm<sup>-1</sup> and 1560.53 cm<sup>-2</sup> <sup>1</sup>, which can be responsible for the appearance of skeletal vibrations of the graphene backbone chain and the C=C stretching vibrations, respectively. After the reduction process, the peaks appeared at 1207.02 cm<sup>-1</sup> and 1017.09 cm<sup>-1</sup>, ascribed to CO stretching of the remaining carbonyl groups. The GO's stretching vibrations indicated by the peaks observed in the range of 1207 cm<sup>-1</sup> to 1017.09 cm<sup>-1</sup> are skeletal vibrations from the unoxidized graphitic domain. Consequently, the oxygen-containing functional moieties were effectively reduced to some degree, and the rGO's peripheral structure and basal plane still contained small amounts of functional group residue. This provides additional proof that GO can be reduced chemically [11, 12].

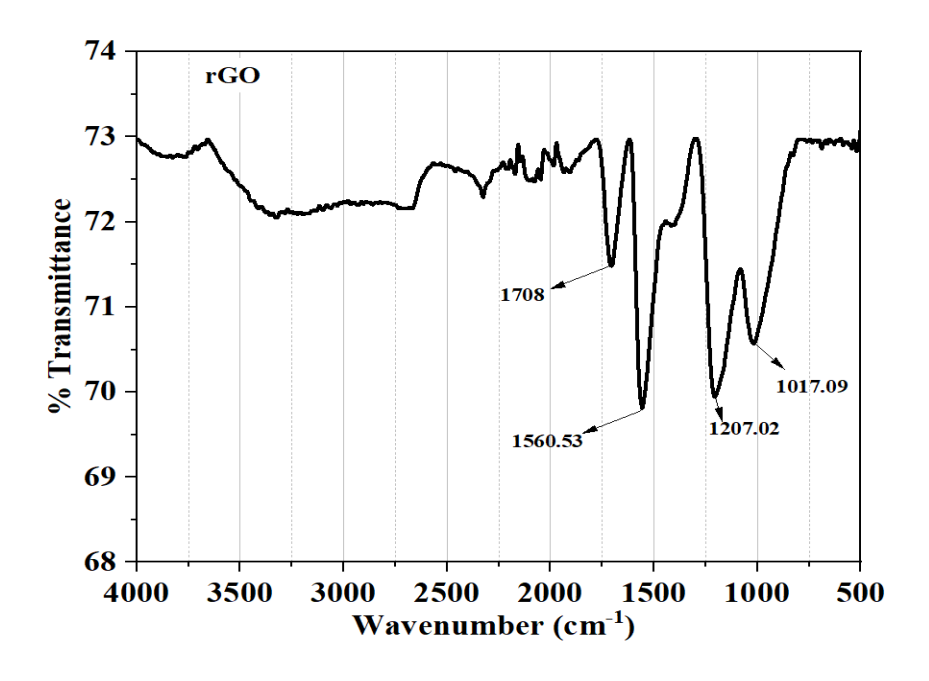


Figure 13. FTIR spectrum of rGO

**4.1.4 FTIR of Polyazine composite with GO (PG):** Fig. 14 represents the FTIR spectrum of PAZ, GO, and its composite PG. Now, in the FTIR data of PG, it is observed that a broad absorption band appears in the range of 3500-3000 cm<sup>-1</sup>, which indicates the peak of GO, and it may be due to the OH functional groups present in GO, and this broadening may be due to intermolecular hydrogen bonding, which is common in composite materials. The shift from 1700 cm<sup>-1</sup> to 1709 cm<sup>-1</sup> suggests that the carboxyl groups in PG because of additional conjugation and hydrogen bonding of the -C=O group with other functional groups [6, 7]. The slight shift from 1567.7 cm<sup>-1</sup> to 1570 cm<sup>-1</sup> suggests that the electronic environment of the imine bond has changed due to conjugation and H-bonding. The peak appearing at 1400 cm<sup>-1</sup> is ascribed to N-N stretching vibrations, which are characteristic of PAZ, and these changes suggest the successful formation of PG [13, 14]. At 1206 cm-1 (1201.1 cm-1) ascribed to the phenolic CO, while the absorption peak appeared at 1042.57 cm<sup>-1</sup> (1046.86 cm<sup>-1</sup>) is due to the CO stretching group of alcohols and phenols [1, 4]. The shift in peaks may be due to the formation of the H-bonding or resonance. Compared with the infrared spectra of GO and PAZ, the IR spectra of PG show that the absorption corresponds to the peaks of C=N, -C=O, OH, N-N, and shifting toward higher or lower wavenumbers, indicating the formation of PG. Overall, these spectral shifts indicate chemical bonding interactions or structural modifications in PG compared to GO and PAZ, confirming its successful formation [8, 15].

## 4.1.5 FTIR of Composite of Polyazine with reduced Graphene oxide

**(PrG):** FTIR spectrum confirms the formation of the composite of PAZ with rGO, as shown in Fig. 15. In PrG, the absorption bands at 1567 and 1505.7 cm<sup>-1</sup> belong to the PAZ are somewhat moved to 1566.54 and 1506 cm<sup>-1</sup>. The FTIR spectrum of composite PrG shows the absorption bands at 1566.54 cm<sup>-1</sup>, associated with the conjugated -C=N stretching vibration, and 1504.67 cm<sup>-1</sup> associated with the C-C

stretching vibrations. The absorption band appearing at 1195.45 cm<sup>-1</sup> corresponds to the phenolic -C=O stretching vibration, and the absorption peak at 814 cm<sup>-1</sup> due to the -C=O bending vibrations corresponds to the shift in the wavenumber of the rGO sheet. Compared with the infrared spectra of rGO and PAZ, the infrared spectra of composite PrG show the peaks of CH=N, CO, and C=C shifting toward higher or lower wavenumbers, indicating the formation of PrG [16].

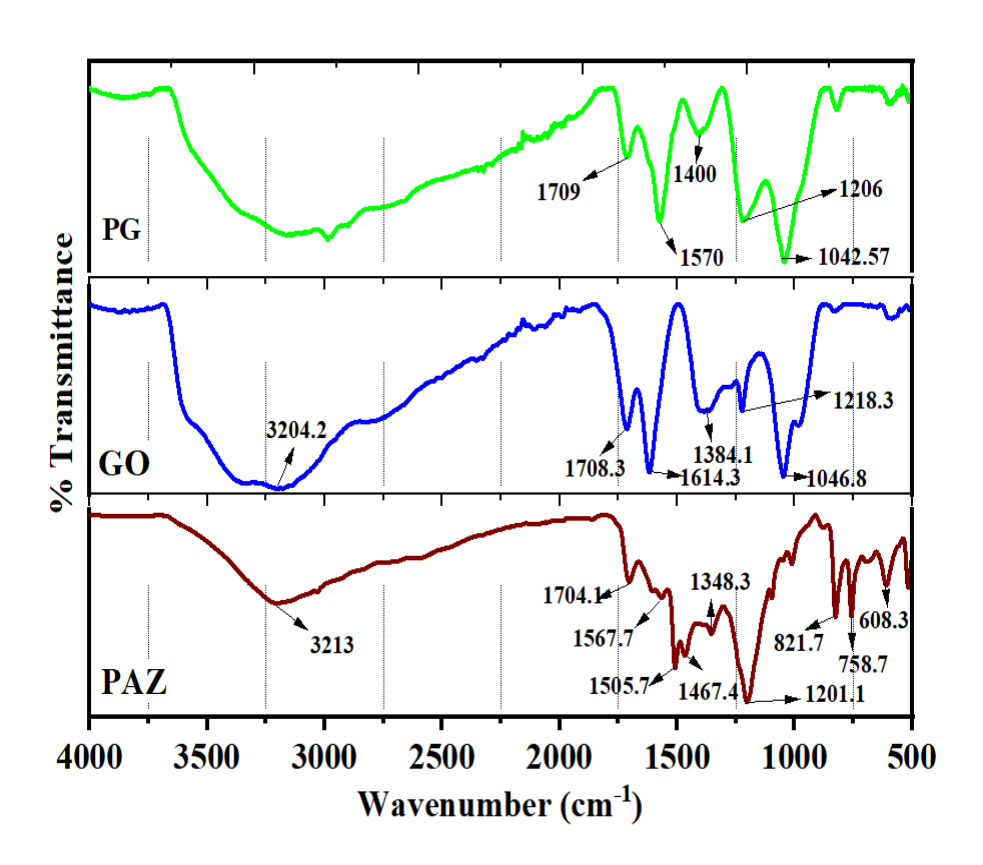


Figure 14. FTIR spectrum PAZ, GO and PG

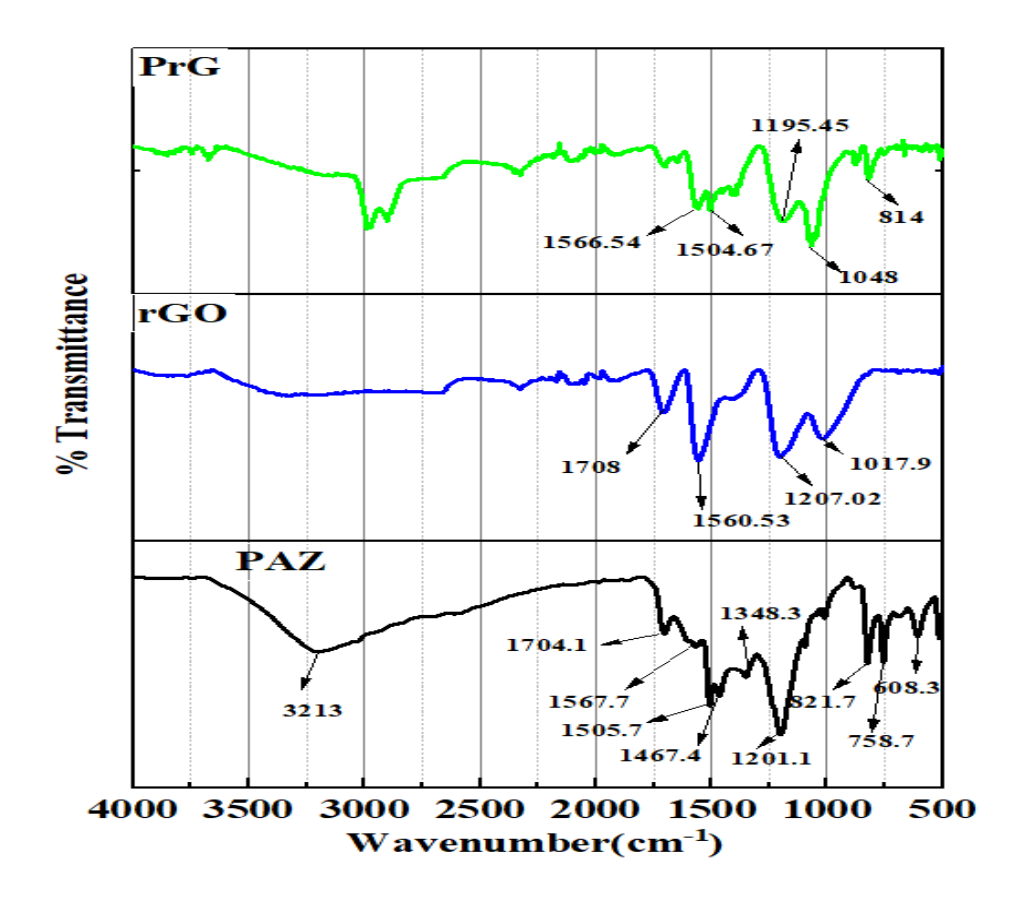


Figure 15. FTIR spectrum of PAZ, rGO, and PrG

- **4.2 MORPHOLOGICAL STUDIES:** The morphology of the prepared PAZ, GO, rGO, and their composites was studied by using two major techniques. Out of which is X-ray diffraction (XRD), and the other is Scanning Electron Microscope (SEM).
- **4.2.1 XRD of PAZ:** A Bruker powder X-ray diffractometer was used to study the nature of the PAZ (crystalline/amorphous) in the current investigation. The diffractogram was recorded in terms of  $2\theta$  with a  $10^{\circ}$   $80^{\circ}$  range using Cu-Ka radiations to acquire intensity data. The diffractogram of this PAZ shows maxima reflection at  $2\theta$ =22.384°, which corresponds to lattice planes (431) with spacing d=3.96 Å as determined by equation 1. The XRD of the prepared PAZ shows a typical pattern of peaks in the broad  $2\theta$  range of 20-30°, like polypyrrole and

polyaniline, thus representing the similar nature of the PAZ to other conducting polymers [17].

$$n\lambda = 2d \sin\theta \tag{1}$$

Here, n represents an integer defined by the order provided,  $\theta$  represents the angle between the scattering planes and incident ray,  $\lambda$  is the CuKa radiation source's wavelength, and d is the distance between atomic layers [17].

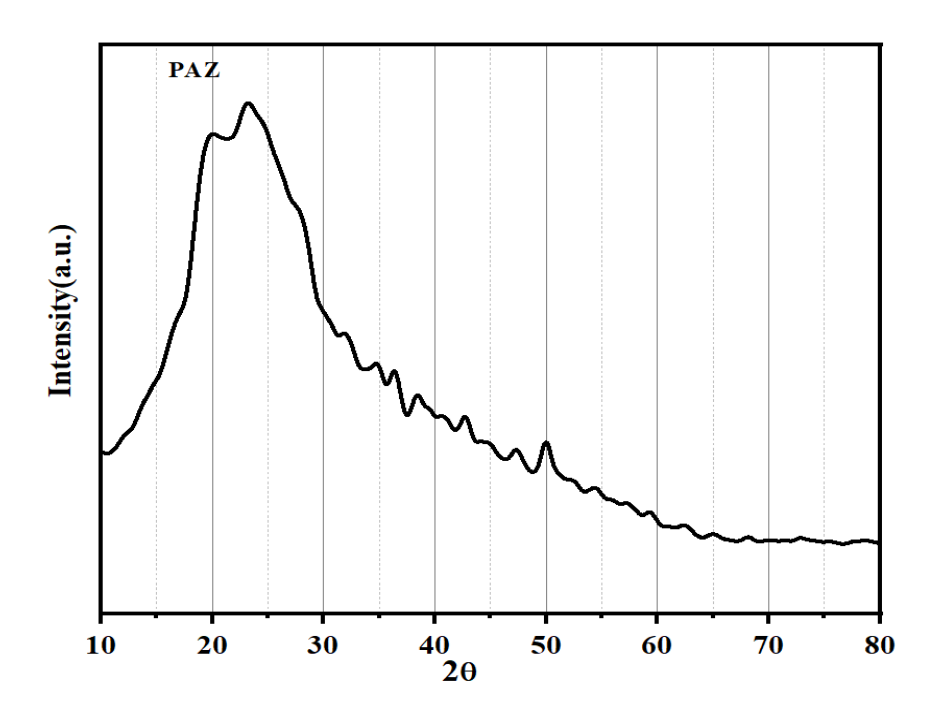


Figure 16. XRD of PAZ

The polymeric chains of azine are dispersed at interplanar spacing, resulting in broad peaks that are indicative of the amorphousity of the prepared polymer (Fig. 16). Certain intense peaks in the XRD spectra are present due to the remaining ZnCl<sub>2</sub> in the polymer, thus representing a somewhat crystalline character. The average particle size

calculated by Scherrer's formula (equation 2) indicates that the results obtained by SEM are in coordination with XRD results.

$$D = \frac{K\lambda}{\beta \cos \theta} \tag{2}$$

The symbols D,  $\theta$ , K, and  $\lambda$  are the crystallite size, diffraction angle, shape factor, and wavelength of X-ray, respectively.  $\beta$  denotes the FWHM (full width at half maximum) [18].

**4.2.2 XRD of GO:** X-ray diffraction (XRD) represents one of the most extensively employed techniques for the characterization of GO. This method functions by monitoring the variation in X-ray intensity versus scattering angle. A critical factor in evaluating the structural characteristics of graphene is the interlayer spacing. The interlayer spacing of the GO (Fig. 17) is approximately 7.7Å due to the roughness of the atomic-scale surface resulting from composition defects (sp<sup>3</sup> bonding) introduced on the initially atomically smooth graphene sheet, as well as the attachment of oxygen-containing functional groups on both sides of the graphene sheet. Due to the manufacture of carboxyl, epoxy, and hydroxyl groups, GO has a wide interlayer distance. The characteristic peak of the graphite at  $2\theta = 26.4^{\circ}$  with an interlayer spacing of 3.34 Å shifts to  $2\theta = 11.45^{\circ}$ , which explains the non-uniform crystal structure with the addition of an oxygen functional group with an interlayer spacing of 7.7 Å along the orientation (001) in the GO. The incorporation of oxygen-containing functional groups like epoxy, carboxyl, carbonyl, and hydroxyl groups, added to the carbon basal plane in the chemical oxidation process led to an expansion in the separation between neighbouring carbon layers. Furthermore, the diffraction peak that appears at 42.36° suggests the presence of shortrange order among all the stacked layers of graphene [7].

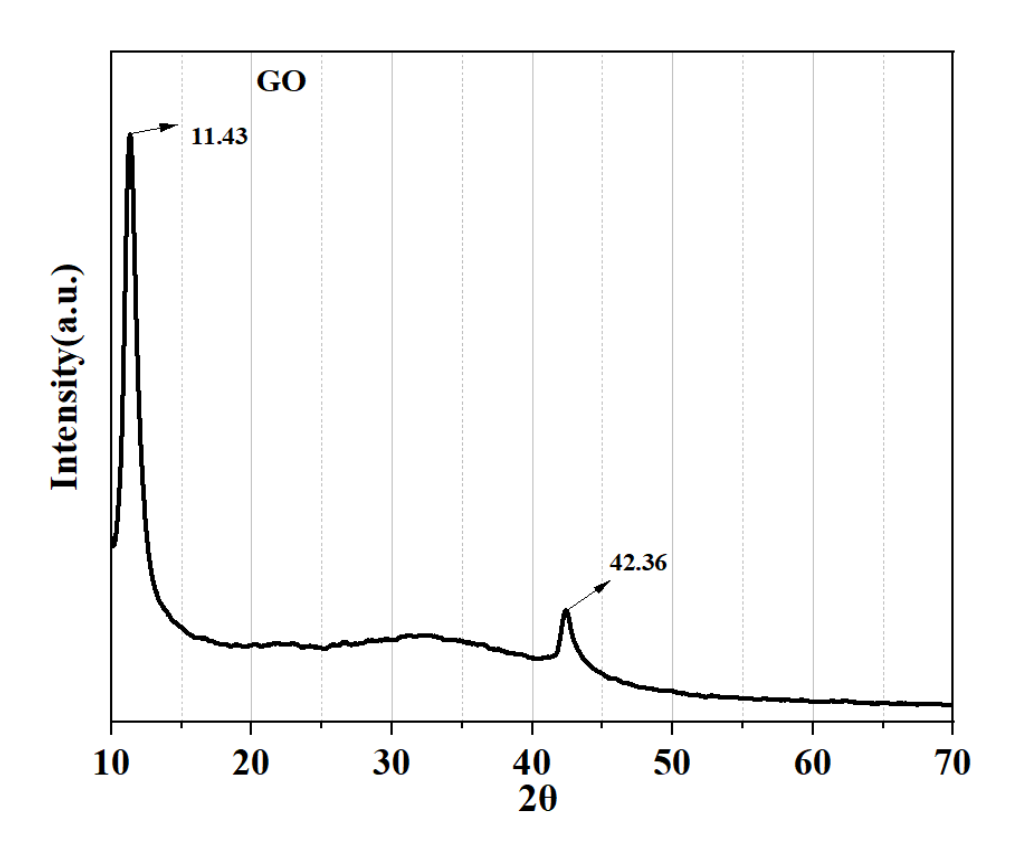


Figure 17. XRD of GO

**4.2.3 XRD of rGO:** The reduction of the GO is responsible for this change in the interlayer spacing, as the rGO pack becomes tighter than the GO (Fig. 18). Even though the interlayer spacing is smaller than in GO, rGO's basal spacing is greater than in well-ordered GO (single-layer pristine graphene). The remaining oxygen functional groups could be the cause of the increased basal spacing, which would suggest that GO has not been completely reduced. This suggests that the samples exhibit a highly disordered stacking orientation [19].

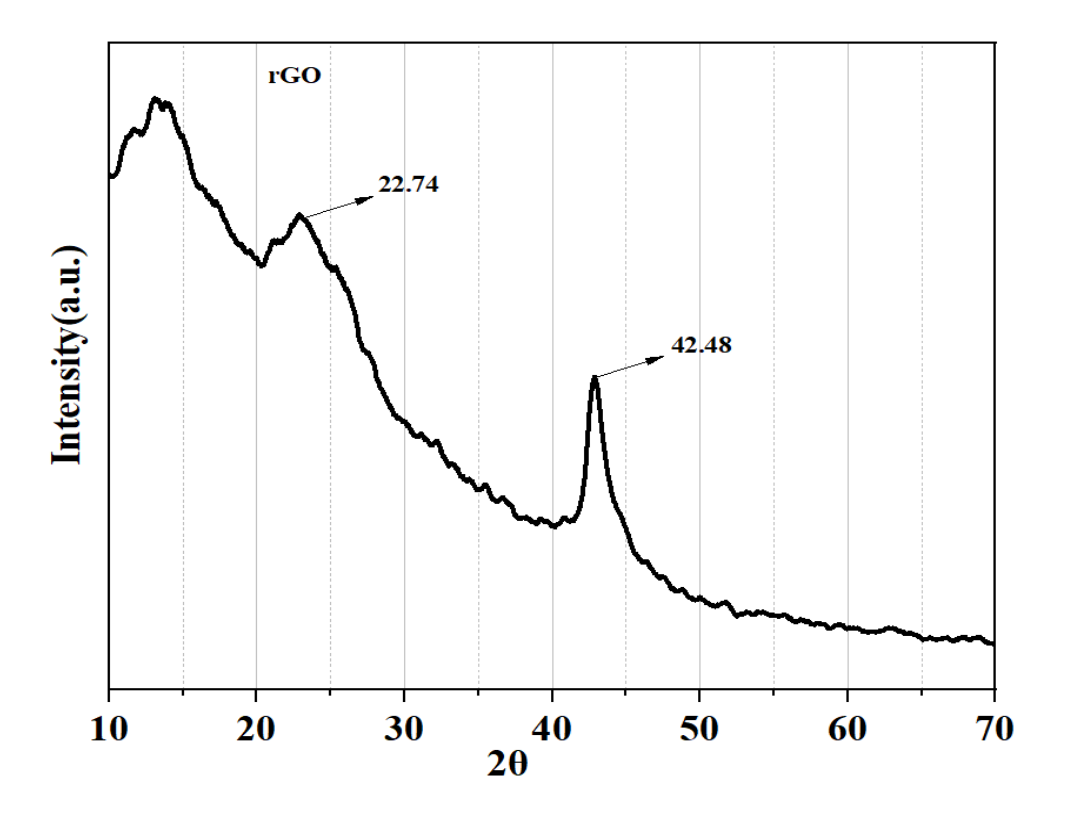


Figure 18. XRD of rGO

Furthermore, rGO exhibited a decrease in d-spacing from 7.7 Å to 2.1 Å, indicating the successful elimination of functional groups containing oxygen. It also showed strong Van der Waals interactions present between every layer, which caused the thin rGO nanosheets to stack on top of one another to form thick heaps. At  $2\theta = 42.48^{\circ}$  with (004) orientation, another, less intense peak is visible, ascribed to the turbostratic band of disordered carbon materials. The diffraction peak at 42.48° with an interlayer spacing of 2.1 Å suggests a short-range ordered arrangement of the graphene layers. The broad peaks near about  $2\theta = 22.74^{\circ}$  with (002) orientation, along with an interlayer spacing of 3.9 Å, and a small broad peak between 10-15° appeared, and due to these broad peaks, it is found to be amorphous in nature [20].

**4.2.4 XRD of the composite of PAZ with GO (PG):** The prepared PAZ, XRD displays a characteristic pattern of peaks in the wide  $2\theta$  range of  $20-30^{\circ}$ , comparable to polypyrrole and polyaniline, indicating the PAZ's similar nature.

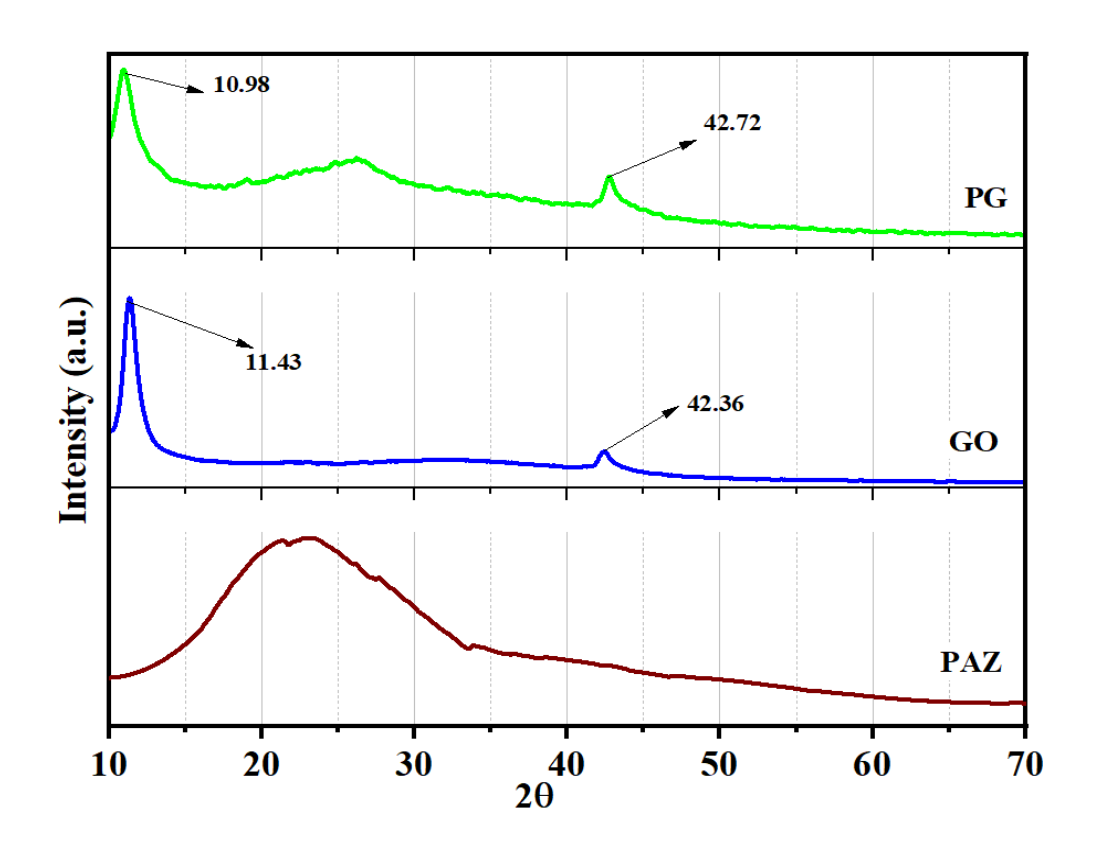


Figure 19. XRD of PAZ, GO, and PG

In the XRD pattern of composite made from PAZ and GO (as shown in Fig. 19), the diffraction peak at  $2\theta = 11.43^{\circ}$  shifted to  $2\theta = 10.98^{\circ}$  (characteristic peak of GO) with an interlayer spacing of 8.04 Å, a broad peak was observed between 20-30° same as in case of PAZ and a peak at  $2\theta$ =42.36° shifts to 42.72° (characteristic peak of GO). The decrease in intensity of the peaks in PG may be due to the lesser content of GO compared to PAZ in the composites **[21].** 

**4.2.5 XRD of a composite of PAZ with rGO (PrG):** The XRD of the prepared PAZ shows a typical pattern of peaks in the broad  $2\theta$  range of  $20-30^{\circ}$  like polypyrrole and polyaniline, thus representing the similar nature of the PAZ [17].

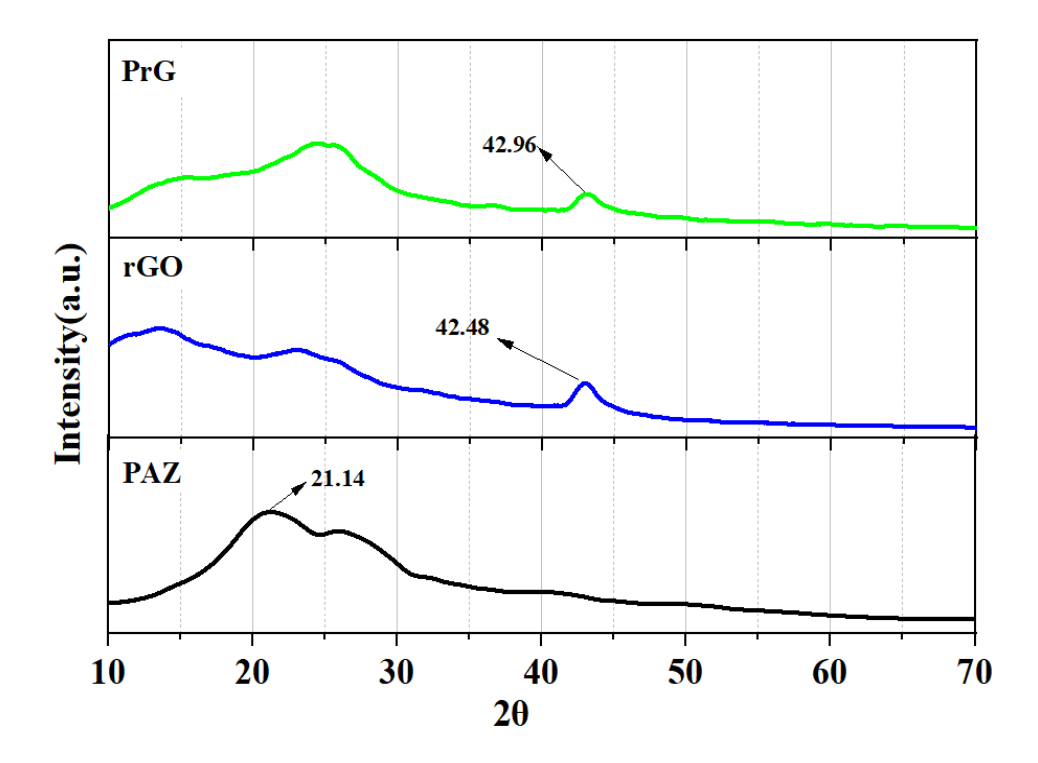


Figure 20. XRD of PAZ, rGO and PrG

A broader peak is visible for rGO near about  $2\theta = 22.74^{\circ}$  (diffraction peak of rGO) after the removal of oxygen-containing groups throughout the chemical reduction process. A second, less prominent peak with a (001) orientation is visible at  $2\theta = 42.48^{\circ}$ , and it is thought to be caused by the turbostratic band of disordered carbon materials to other conducting polymers [20]. Fig 20. represent the XRD pattern of composite PrG, a broad peak was observed between 20-30°, same as in the case of PAZ, and a peak at  $2\theta = 42.48^{\circ}$  shifts to  $42.96^{\circ}$  (characteristic peak of rGO). The intensity of the peaks in composite decreases may be due to the lesser content of rGO as compared to PAZ [21].

- **4.3. SCANNING ELECTRON MICROSCOPY (SEM):** The material's morphological features were examined using a high-resolution (1.0 nm (15 kV), 1.3 nm (1 kV), and 3.0 nm (15 kV)) Jeol field emission SEM throughout the analysis, and magnification ranges from 25 to 1,000,000 with probe currents ranging from a few pA to 200nA. By utilizing a high-energy electron beam, SEM generates a variety of signals on the sample's surface, enabling the creation of detailed, high-resolution images. The sample's exterior appearance, topography, chemical composition, and crystalline structure are all shown by the image.
- **4.3.1 SEM of PAZ:** The JEOL field emission SEM having a high resolution (1.0 nm), and magnification (25X to 10<sup>6</sup>X) was used to determine the morphology of the material. The morphology of the PAZ was studied by varying the magnification from 500 to 25000 X (Fig. 21 A-C). The prepared PAZ was observed to have flaky morphology which determines its amorphous nature, which is somewhat similar to other conducting polymers such as polypyrrole [22]. The small pieces present over the flaky polymer represent the small fragments of dimers and oligomers. The small flakes were observed to have an average length of 0.862 mm while the average area of flakes was 2473 mm<sup>2</sup>.

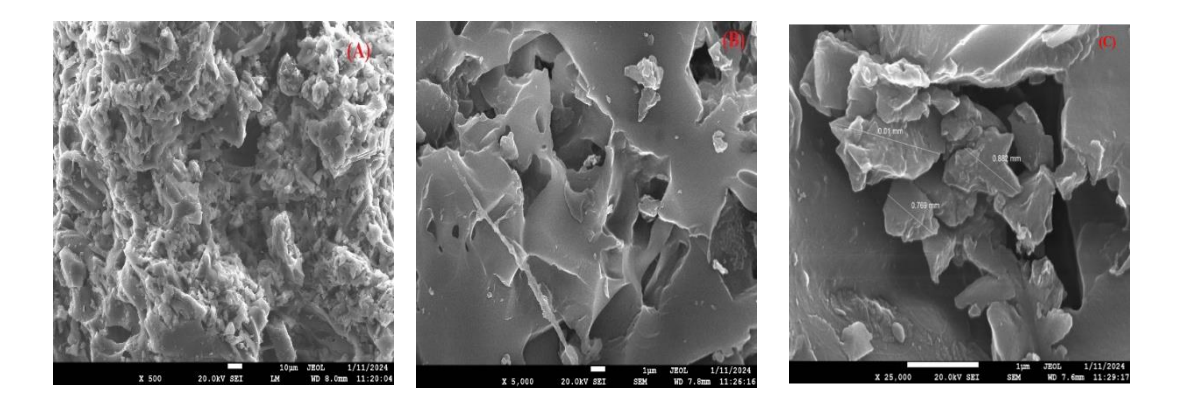


Figure 21(A-C). SEM images of PAZ at 500, 5000, and 25000 magnifications

**4.3.2 SEM of GO:** SEM was utilized to characterize the morphological properties of a sample of GO. The material known as graphite is made up of rough flakes that spread in different irregular sizes. After oxidation and sonication, graphite is converted into GO. The thickness of GO is due to the presence of oxygen functional groups that bind to the plane. This showed that throughout the oxidation process, graphite had peeled off. The SEM of GO was run at a working distance of 7.6 mm (the distance between the sample surface and the bottom of the SEM column) with an accelerating voltage of 20 kV. The morphology of GO was examined by altering the magnification between 500 and 25000. Fig. 22 (A-C) depicts the microstructure of GO, the average size of the film is about 10 µm, and its morphology is non-uniform at the magnification of 500 to 2500. The size is 1µm with a non-uniform structure at the magnification of 5000 to 25000 and the GO was found to be crystalline. As seen in the figure, the GO displayed multilayer stacking and wrinkles, with lateral size approaching several micrometers [23, 24].

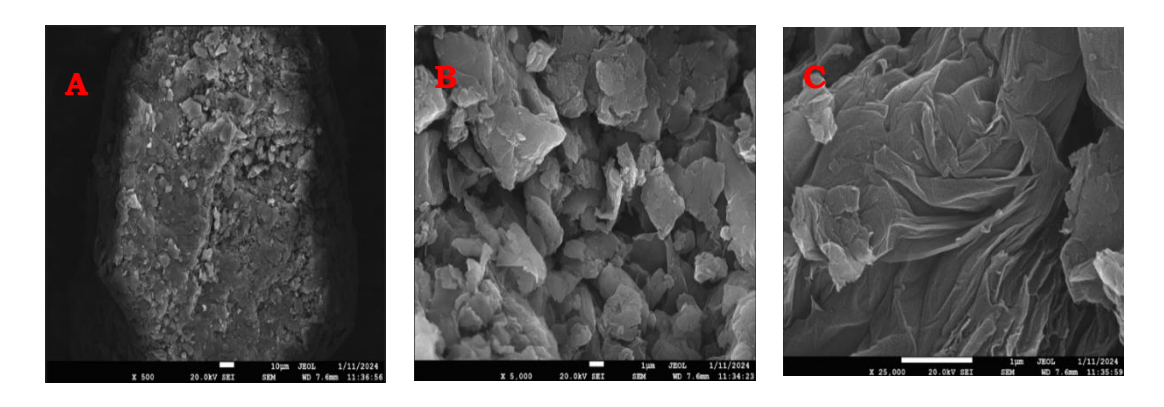
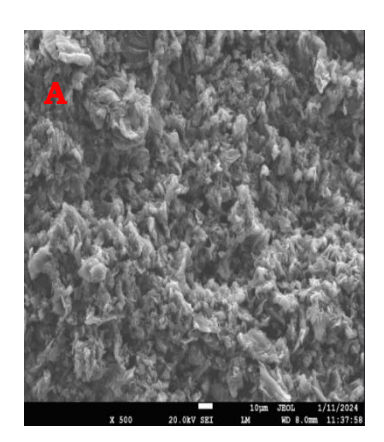
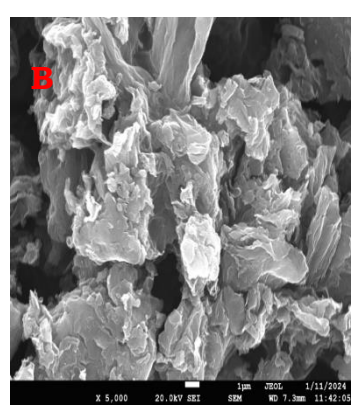


Figure 22(A-C). SEM images of GO at 500, 5000, and 25000 magnifications

**4.3.3 SEM of rGO:** The morphology of reduced graphene was investigated by varying the magnification between 500 and 25000. The average thickness of the film is approximately  $10~\mu m$ , and at

magnifications of 500 to 2500, its shape is uniform throughout. It was discovered that the rGO was found to be amorphous in nature and had a size of 1µm with a uniform structure at magnifications ranging from 5000 to 25000. In the case of rGO, the findings demonstrated that fewer the number of graphene layers in GO resulted in FESEM images depicting an opener framework and enhanced diffusion compared to graphite. Following the deoxygenation of GO, FESEM pictures of rGO displayed a distinct, extremely wrinkled surface. Upon increasing the magnification, the prepared rGO showcased a uniform shape and smooth surface, with the sinuate structural features of rGO becoming more pronounced after reduction. This transformation may be due to the elimination of functional groups containing oxygen in rGO. The rGO morphology, which is displayed in Fig. 23(A-C), then shows that the space between layers is decreasing and that rGO has a thin sheet morphology in comparison to GO [25, 26].





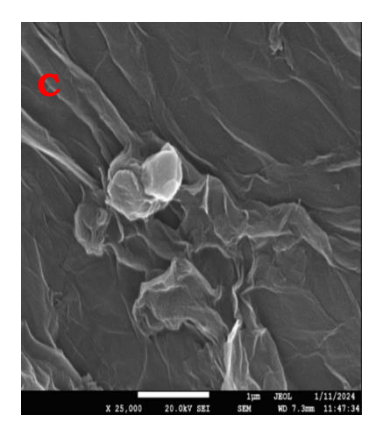


Figure 23(A-C). SEM images of rGO at 500, 5000, and 25000 magnifications

**4.3.4 SEM of the composite of PAZ with GO (PG):** Fig. 24(A-C) shows the SEM images of PG composites. It was readily apparent that GO aggregated in the PG composite. Its morphology is uniform throughout and is found to be amorphous. Microscopic imaging reveals a phase-

separated structure with a flaky appearance, suggesting the intercalation of GO into the layers of PAZ [27].

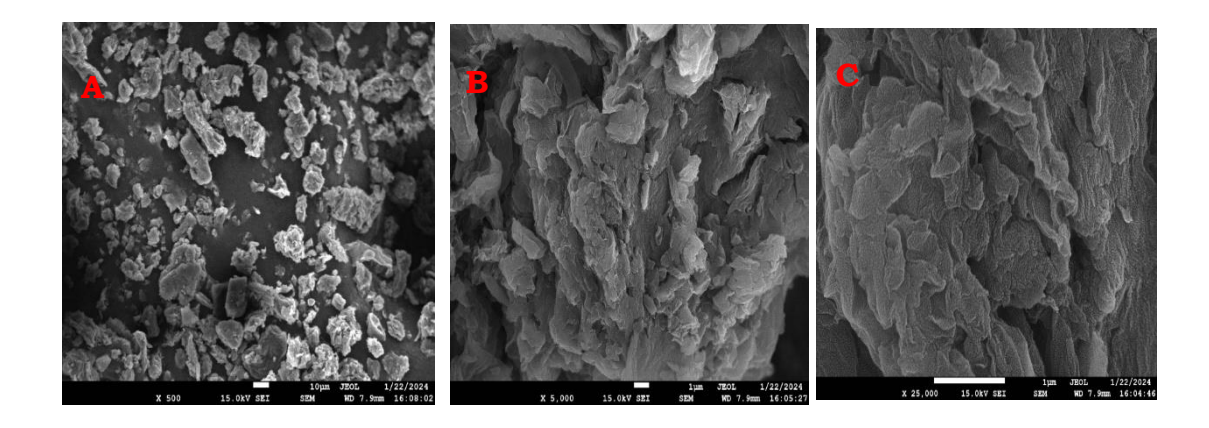


Figure 24(A-C). SEM images of PG at 500, 5000, and 25000 magnifications

**4.3.5. SEM of the composite of PAZ with rGO (PrG)**: In the case of PrGs composite, when PAZ particles are adorning the rGO sheets, a fairly coarse and flaky structure is seen (Fig.25(A-C)), indicating the PAZ particles successfully developed on the rGO surface shows that it is uniform throughout and was found to be amorphous **[28].** 

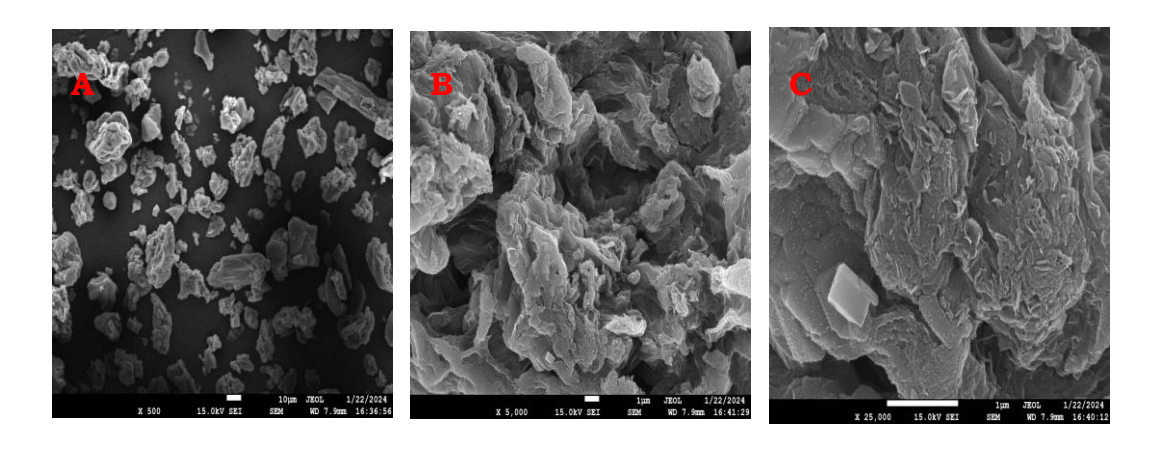


Figure 25(A-C). SEM images of PrG at 500, 5000, and 25000 magnification

**4.4 THERMAL PROPERTIES:** The thermal stability of PAZ was determined by the two most commonly used techniques,

Thermogravimetric analysis (TGA) and Differential Scanning Calorimetry (DSC).

**4.4.1 TGA of PAZ:** Perkin Elmer, TGA-4000 having a scanning rate of 0.1 to 200°C/min, was employed to determine the percentage weight loss with the variation of temperature from 50°C to 600°C. The polymeric sample is heated in air at a 10°C/min rate. The TGA curve of PAZ is represented by Fig 26. The results indicate that the initial weight decline (~ 3%) of PAZ was attributed to the evaporation of absorbed moisture in the 28–100°C range. Further degradation in mass (34.32%) of PAZ appears from 100°C to 220°C attributed to the decomposition of possible impurities of low molecular weighted molecules (monomer/oligomer units) remaining in the polymer matrix, as that of most widely studied CPs like PANI and PPY [29, 30].

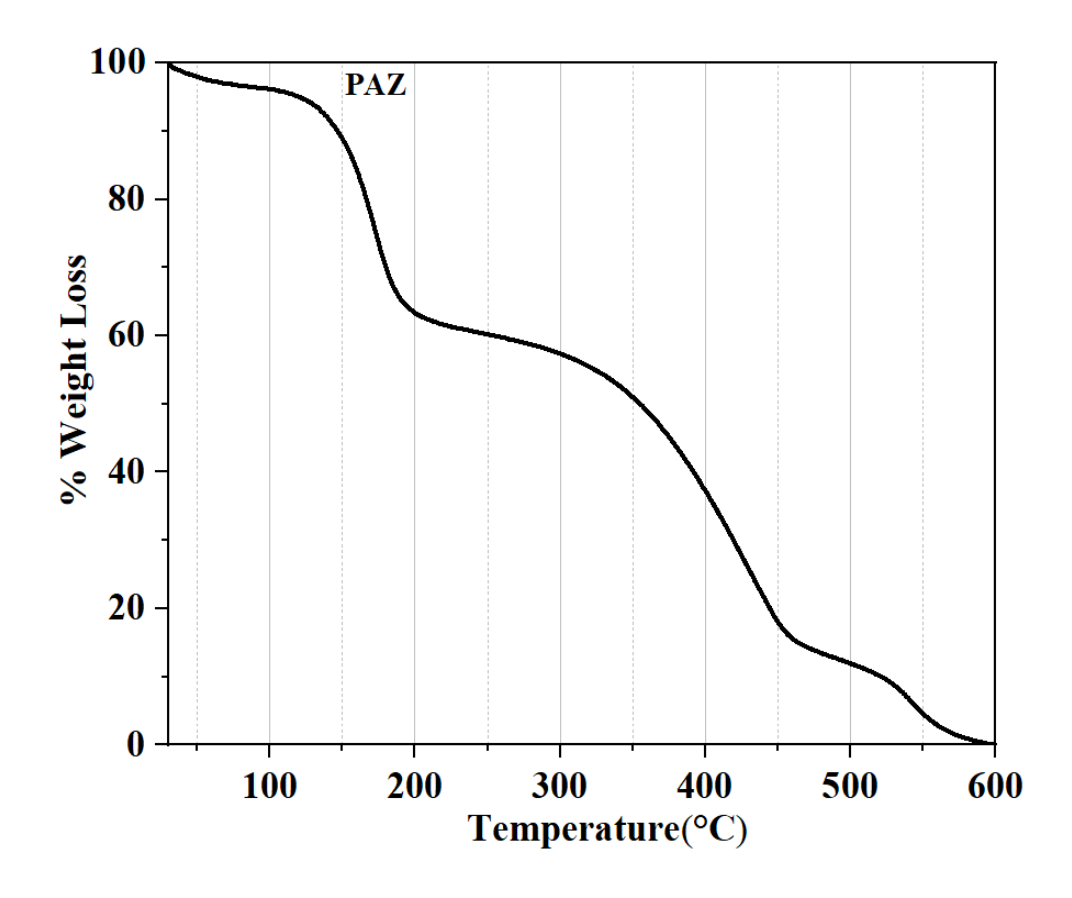


Figure 26. TGA plot of PAZ

An additional weight reduction (47.08%) was appeared from 220°C to 470°C temperature range, which could be attributed to the release of degraded product, viz. CO<sub>2</sub> and CO from the PAZ structure [31, 32], resulted in a remaining carbon material of ~15%, which was nearly completely lost (0.23% residue) during further thermal degradation, which is generally observed if the TGA is carried in the air. However, the thermal degradation of PAZ would depend upon the nature of the monomer and the structure complexity of the obtained polymer [29].

**4.4.2 TGA of GO:** Perkin Elmer, TGA-4000 having a scanning rate of 0.1 to 200°C/min, was used for the determination of percentage weight loss in the 50- 600°C temperature range. The polymeric sample is heated in an inert environment (N<sub>2</sub> presence) at the rate of 10° C/min.

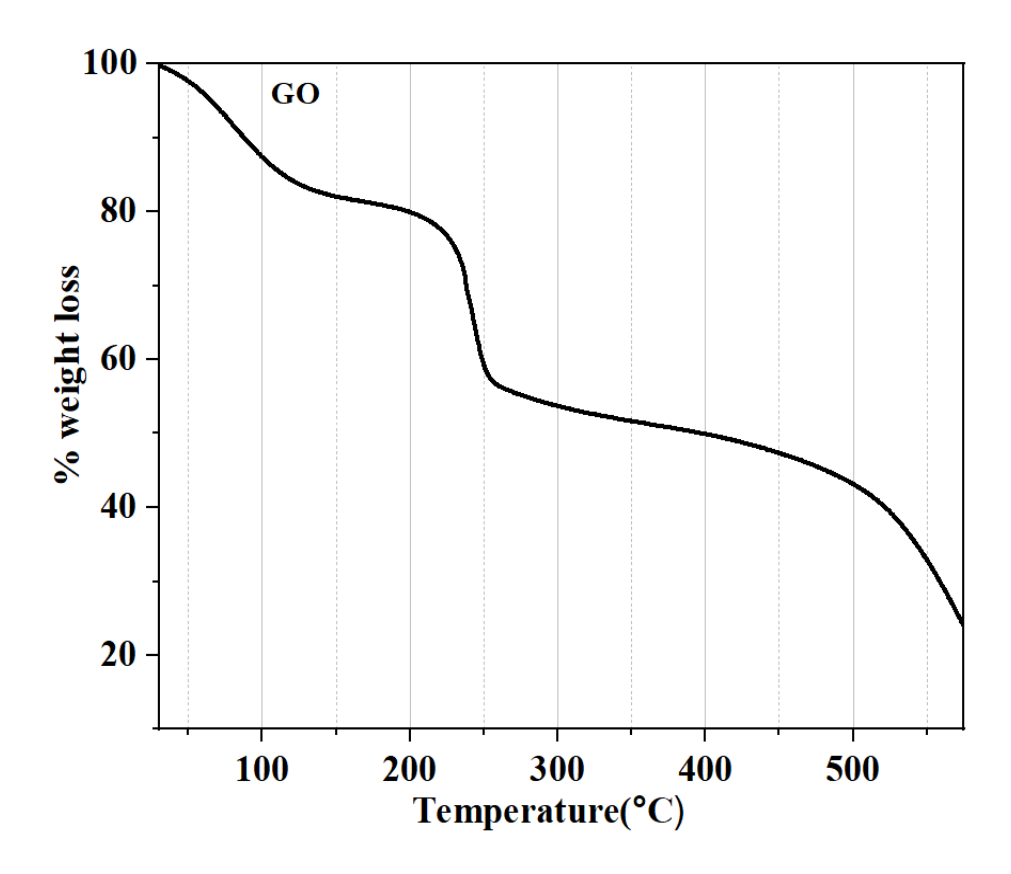


Figure 27. TGA plot of GO

The TGA analysis of GO (Fig. 27) indicates the first weight loss of  $95\text{-}120^{\circ}\text{C}$ , attributed to the evaporation of water molecules. Additionally, a 28.45% weight reduction was observed in the temperature range from  $120^{\circ}\text{C}$  to  $270^{\circ}\text{C}$ , which can be due to the chemical decomposition of oxygen-containing functional groups or the complete and abrupt cleavage of epoxy and hydroxyl groups from the ring structure. The further mass degradation i.e. 12% occurs at  $270\text{-}575^{\circ}\text{C}$  can be linked to the oxidative pyrolysis of carbon frameworks like CO and  $CO_2$  [33].

**4.4.3 TGA of rGO:** The TGA of rGO exhibits greater thermal stability than GO's because of its lower concentration of oxygen-containing groups.

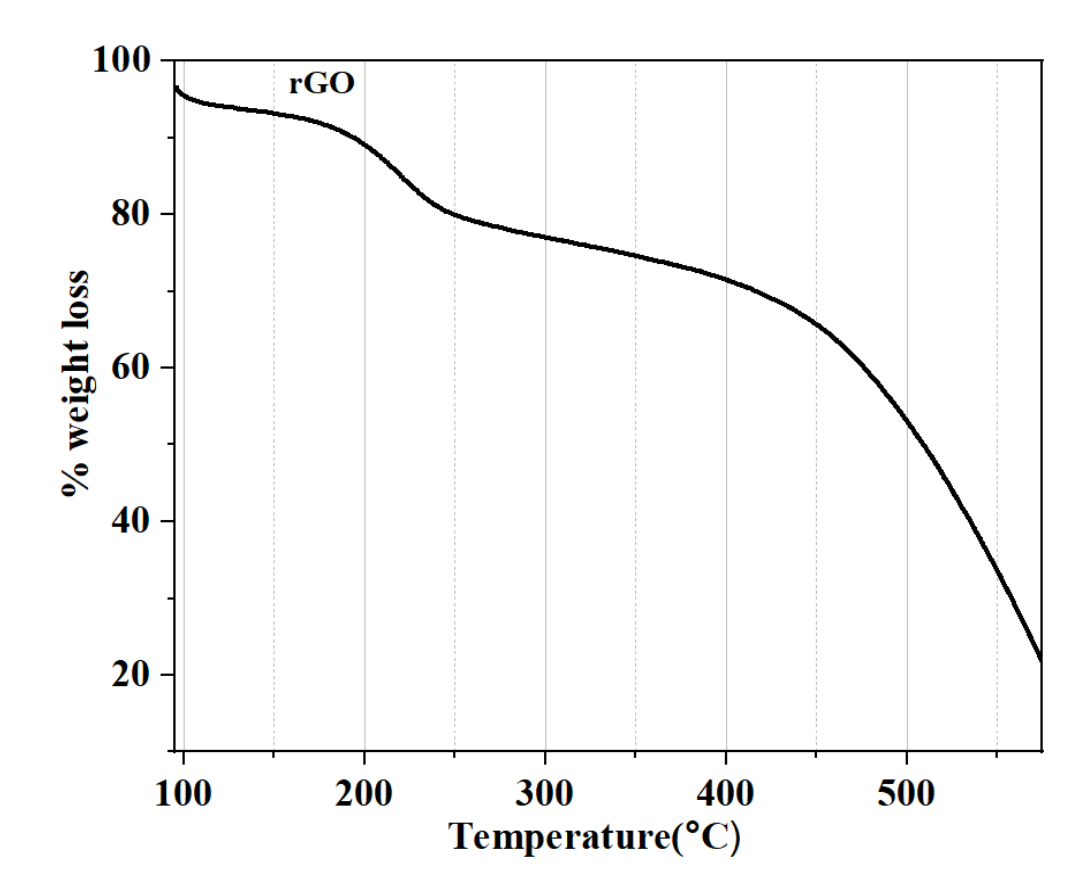


Figure 28. TGA plot of rGO

Because they had fewer oxygen functional groups upon reduction, the rGO samples displayed significantly less weight loss. The TGA plot of rGO (Fig. 28) shows that the initial weight loss (16.45%) was observed from 95-250 °C attributed to the thermal decomposition of functional groups incorporating oxygen to the production of CO, H<sub>2</sub>O, and CO<sub>2</sub> gases. The final mass loss of 46.37% appeared from the 250-575°C temperature range, which arises from the elimination of functional groups like C-OH groups and epoxy groups that are more stable [34].

**4.4.4 TGA of PG along with PAZ and GO:** In the case of PG composite, less weight reduction was observed (as shown in Fig. 29) with the rise in the temperature. Initial weight loss (8.34%) at 50-110°C due to the evaporation of surface-absorbed water molecules. After that, the weight loss of 17.76% at 110-255 °C due to the degradation of low molecular weight impurities and chemical decomposition of oxygen-containing groups. The major weight loss (41.34%) was observed at 255-575 °C due to the degradation of the PAZ backbone. Concurrently, the PAZ exhibits a substantial mass reduction of 94% from 100 to 575°C. In comparison, the PG composite displays a weight loss of 60% within the same temperature range of 100 to 575°C. Furthermore, the PG demonstrates enhanced thermostability compared to the PAZ, which may be attributable to the robust bond interaction between the PAZ and the GO sheets [33, 35, 36].

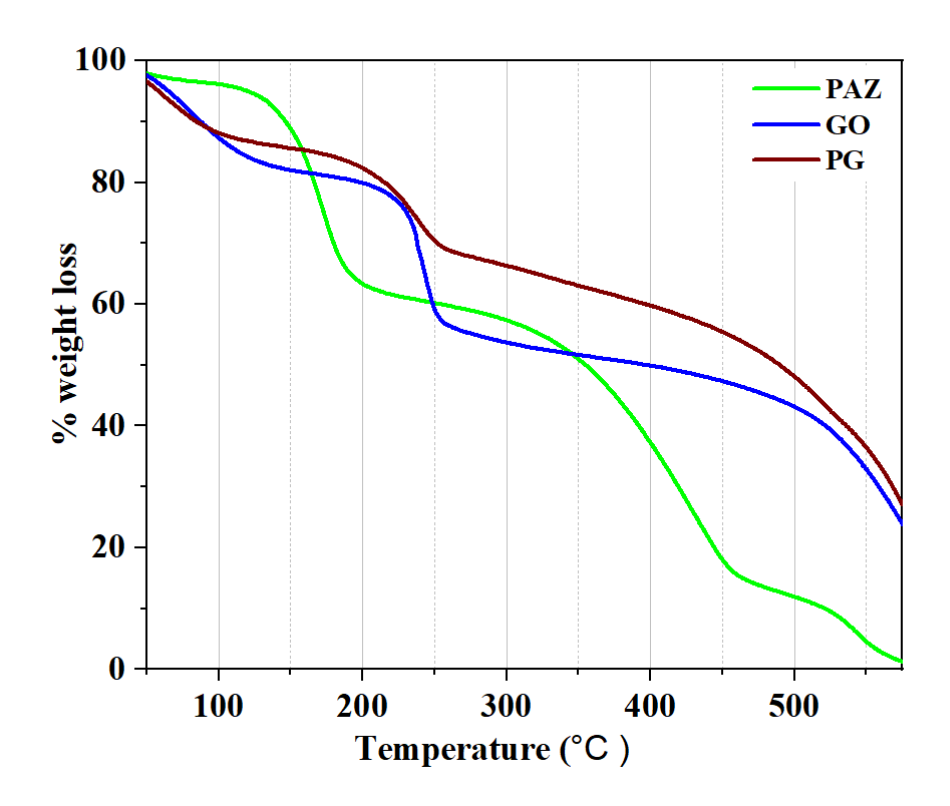


Figure 29. TGA plot of PAZ, GO, and PG composite

**4.4.5 TGA** of PrG along with PAZ and rGO: The TGA analysis method was used for studying the PrG composite's thermal stability. Fewer weight reduction was observed for PrG composite as compared to pure PAZ as shown in Fig. 30. It shows that the initial weight reduction (12.7%) was observed from 50-220°C because of the loss of surface adsorbed water molecules and solvent content of PAZ in both PAZ and PG [28]. The material exhibited a further weight reduction of 12.48% from 220°C to 415°C temperature due to the uniform distribution of polymer chains in both PAZ and PrG. The final weight loss (45%) was observed from 415-575 °C for PrG composite and pure PAZ, completely losing weight at temperatures above 415°C. However, the PG composite keeps around 28% of its weight at a temperature above 415°C. When the temperature is between 415 and 575 °C, the PrG composite exhibits a very low weight reduction. The PrG composite is more stable than pure PAZ at higher temperatures [37, 38].

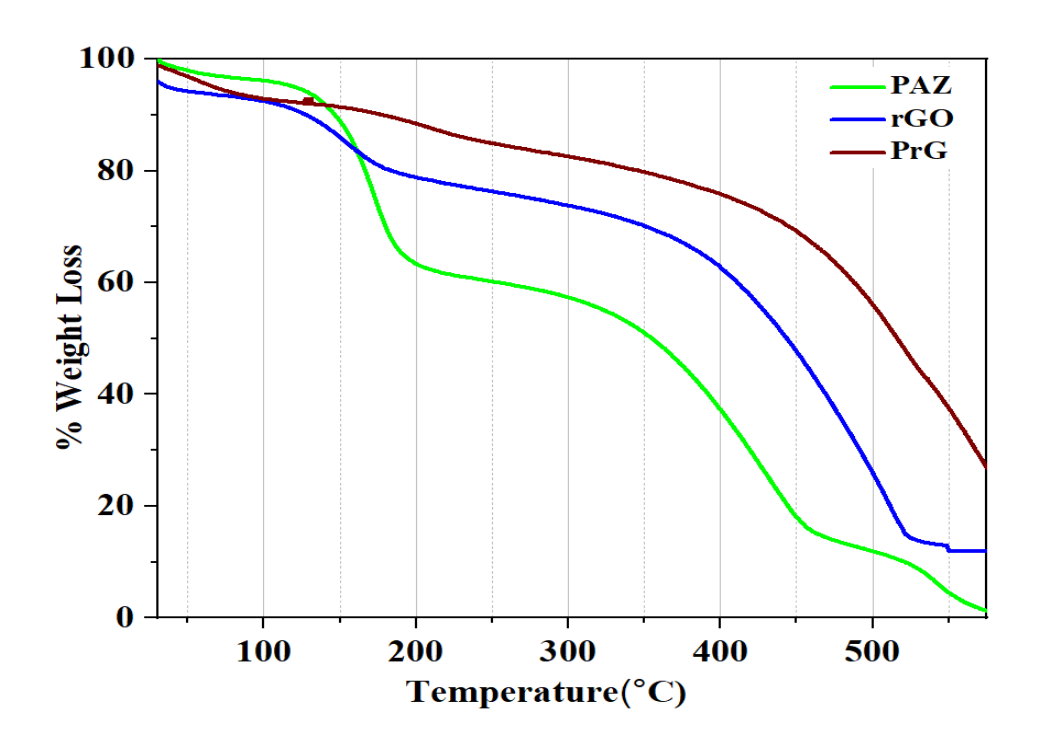


Figure 30. TGA plot of PAZ, rGO, and PrG composite

**4.5 DIFFERENTIAL SCANNING CALORIMETRY (DSC):** The heat flow related to phase transitions in polymeric materials versus temperature is determined by employing the DSC thermal investigation method. DSC-6000 (Perkin Elmer) having a temperature range -70°C to 450°C, was used for measuring the exchange of heat energy in the presence of  $N_2$  (inert atmosphere) at the rate of 10° C/min.

**4.5.1 DSC of PAZ:** The plot of heat flow against temperature was implemented to observe the PAZ's heat transition. Fig 31. represent the DSC curve of PAZ. The DSC curve shows that the glass transition temperature (T<sub>g</sub>) occurred at 169.33°C. Below 169.33°C, a large endothermic peak was seen in the PAZ, which could be attributed to the ejection of moisture and other tiny particles. PAZ was found to be decomposed at 436.8°C, which indicates the high thermal stability of the prepared PAZ, which is comparable to polyaniline-type conducting polymer [39].

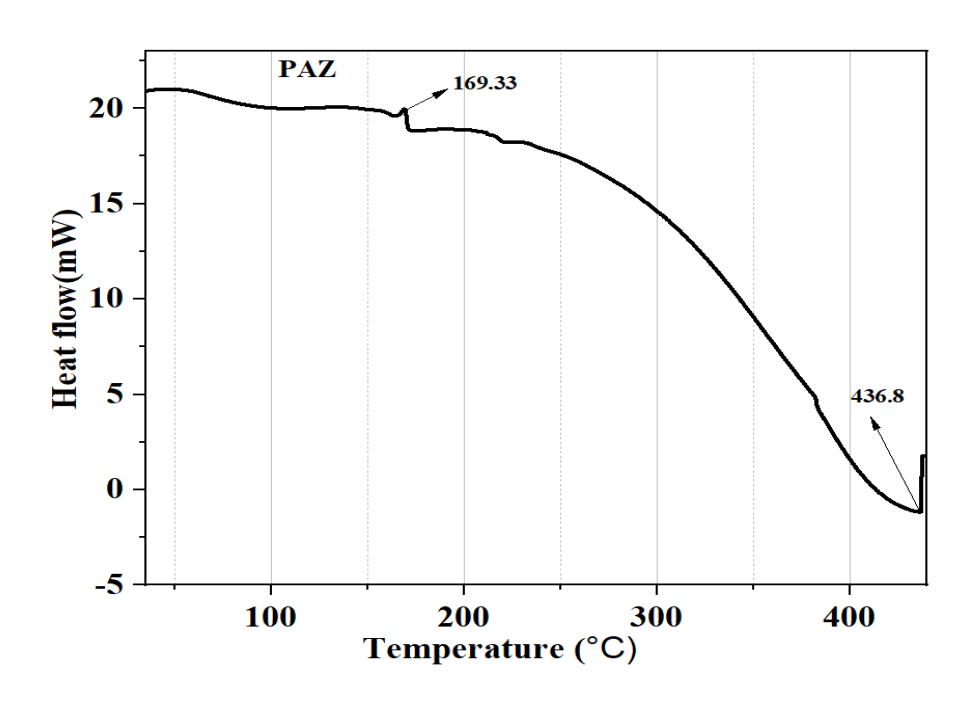


Figure 31. DSC curve of PAZ

**4.5.2 DSC of GO:** The thermal characteristics of materials, such as phase transitions, can be evaluated using DSC, which measures heat flow by varying temperatures. GO is a layered material with various functional groups containing oxygen such as hydroxyl (OH), epoxide (-O-), carboxyl (COOH), and carbonyl (C=O), present on its basal planes. These groups disrupt the regular structure of graphite, making GO more reactive and hydrophilic compared to pristine graphite. When studying GO via DSC, the DSC curve shows the preparation of GO from graphite was an exothermic reaction.

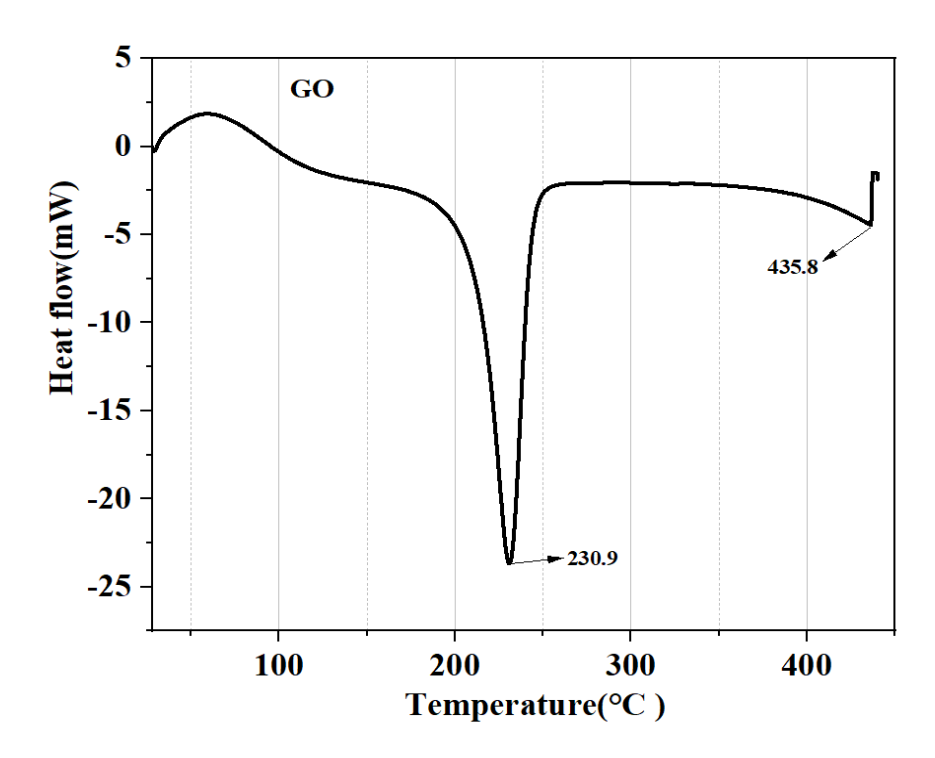


Figure 32. DSC curve of GO

A highly exothermic peak is observed in the DSC curves near about 230.9°C attributed to the reduction of oxygen-containing groups (like hydroxyl, epoxide, and carboxyl), which could lead to the formation of rGO. The DSC curve (Fig. 32) exhibits an exothermic peak which is due to the result of the reduction process, signifying the energy release linked to the elimination of oxygen groups. If the heating is continued to higher temperatures, GO decomposes at around 435.8°C, with a sharp exothermic indicating the breakdown of the material, possibly releasing gases like CO<sub>2</sub>, CO, or other volatile organic compounds [28].

**4.5.3 DSC of rGO:** The DSC curve (Fig. 33) shows the reduction of GO into rGO was an exothermic reaction. DSC curve shows an exothermic peak (around 210 °C) seen in the case of rGO due to absorbed moisture and the loss of oxygenated functional groups. However, because there were fewer -OH and -COOH groups, these peaks were not as strong as those seen in GO. Peak intensity occurs from a decrease in the number

of functional groups caused by the conversion of GO into rGO. The melting point of rGO was found to be 439.8°C which shows that it has higher thermal stability than GO [28, 40].

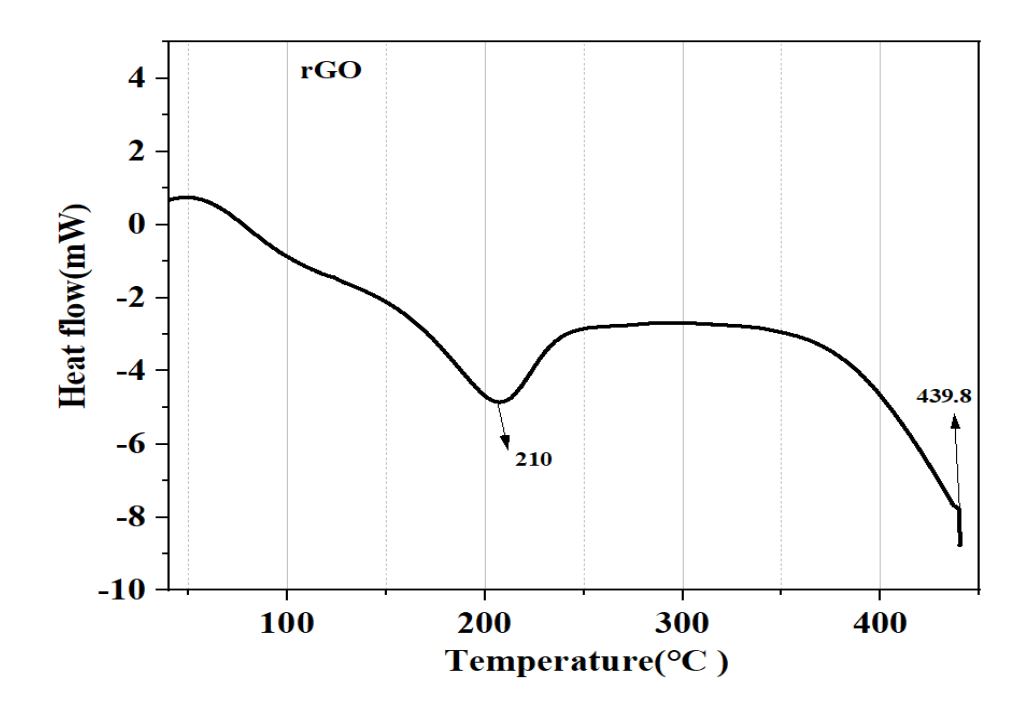


Figure 33. DSC curve of rGO

**4.5.4 DSC of PG, PAZ and GO:** A cross-linking reaction produces thermodynamic stability when GO and PAZ are combined at lower temperatures. The DSC curve (Fig. 34) shows that the composite of PG shows high thermal stability as compared to pure PAZ and GO. The binary composite displayed an exothermic peak at 224.99°C from the release of specific gases (like CO, H<sub>2</sub>O, and CO<sub>2</sub>) and an exothermic peak at 439.5 °C from the breakdown of the polymer's backbone, all of which indicate that the binary composite was successfully formed. The composite decomposes at a higher temperature than pure PAZ, which means the thermal stability of PG is higher than PAZ **[41].** 

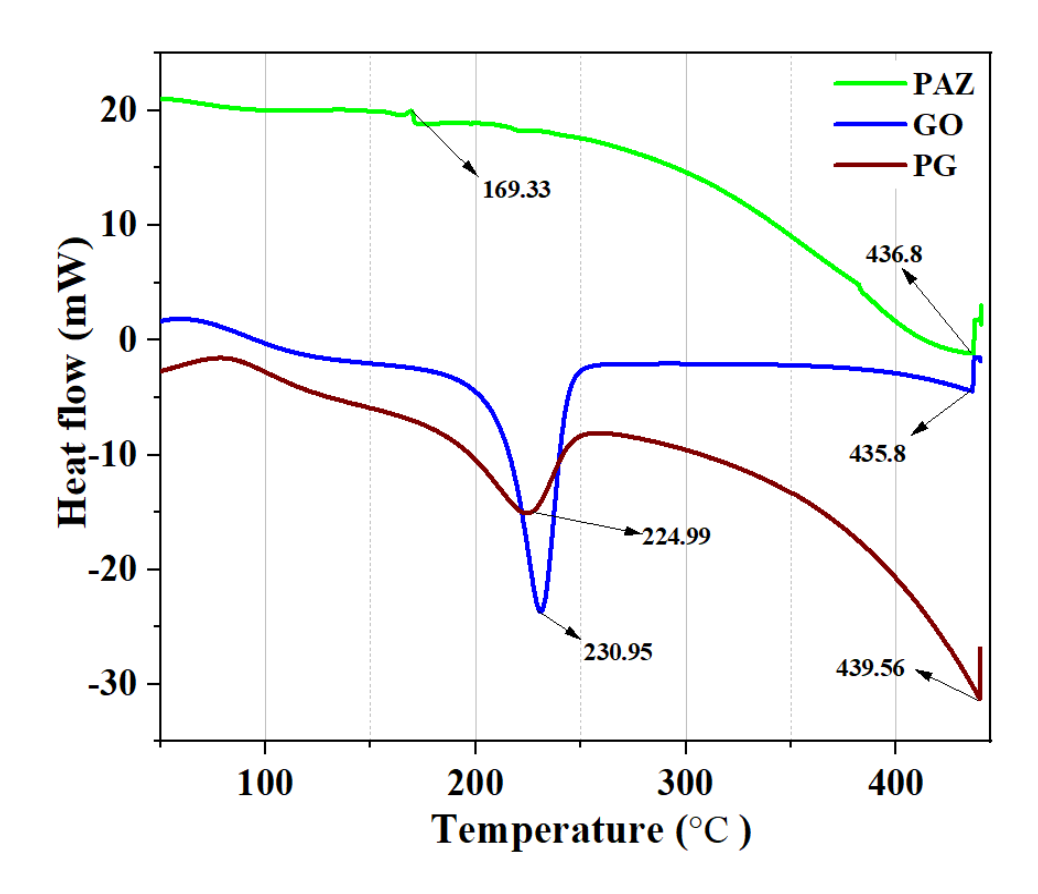


Fig 34. DSC curve of PAZ, GO, and PG composite

**4.5.5 DSC of PrG along with PAZ and rGO:** Another binary composite PrG in the DSC curve depicts an exothermic peak at 248.17 °C (Fig 35). The peak intensity was found to be lower because of enhancement in thermal stability. The temperature rise shows that it was also highly thermally stable like PAZ and rGO due to its high melting point, which is 438.7°C **[9, 42]**.

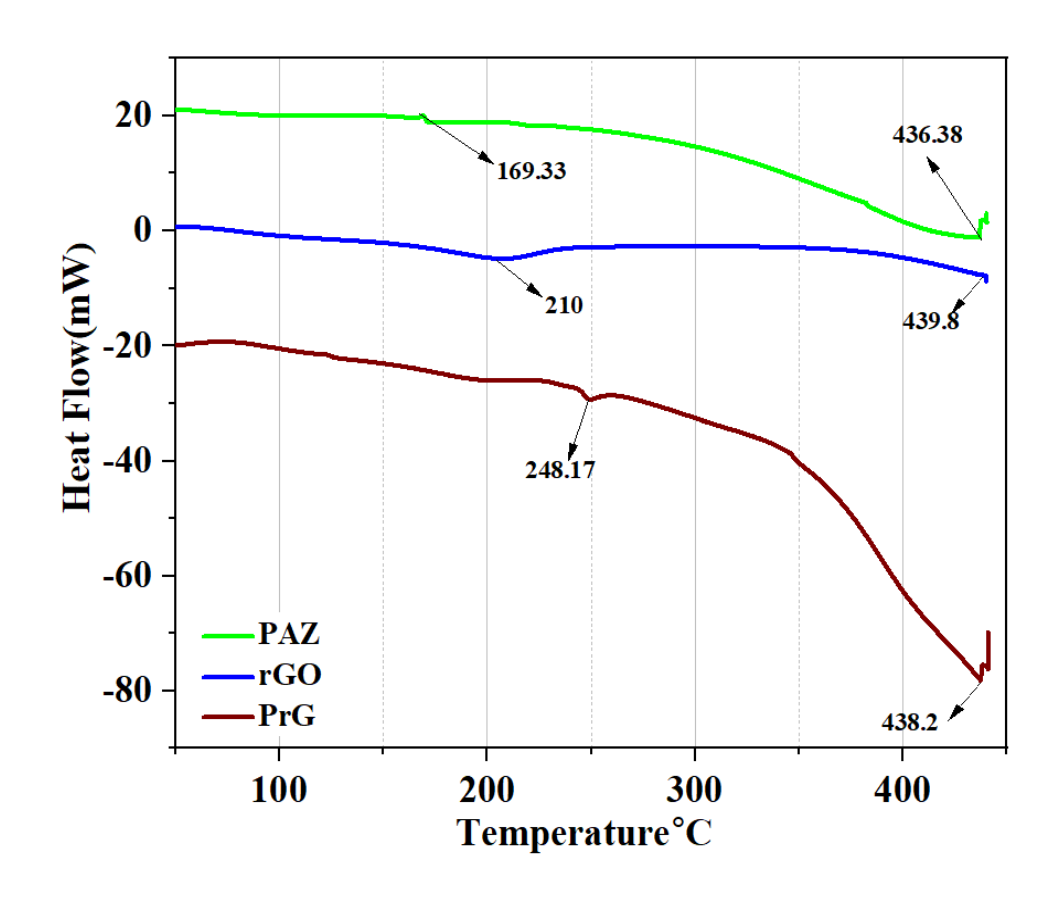


Figure 35. DSC curve of PAZ, rGO, and PrG composite

## 4.6 ELECTROCHEMICAL STUDIES:-

multi-channel Potentiostat/galvanostat (Autolab PGSTAT204, Metrohm) was used for electrochemical measurements. The electrochemical behaviour of PAZ and its composites with GO and rGO for supercapacitor applications were examined by using a threeelectrode system by EIS, GCD and CV techniques in 1M H<sub>2</sub>SO<sub>4</sub> taken as an electrolyte. CV was performed at varying scan rates from 10 to 100 mV/s using a reference electrode of Ag/AgCl. The GCD measurements were performed at varying current densities (1, 0.5, 0.25 A/g) to evaluate the power and energy density of the electrode material. EIS measurement was performed at a frequency range of 100 MHz to 100 kHz, with 20 mV/s amplitude of AC. A mass loading of 1±0.1 mg of PAZ, GO, rGO, PGs, and PrGs over CPE was deposited to determine the electrochemical behavior.

**4.6.1 CYCLIC VOLTAMMETRY (CV):** CV is used to quantify the electrochemical response of a redox-active solution to a potential sweep cycled between two or more predetermined values. To evaluate the electrochemical performance of PAZ, GO, rGO, PGs, and PrGs as an electroactive material for supercapacitor electrodes deposited over earlier fabricated CPE. The cyclic voltammograms measured for the electroactive material in a 1M H<sub>2</sub>SO<sub>4</sub> electrolyte in the potential window of 0 to 1.0 V exhibited a nearly rectangular (quasi-rectangular) shape across various scan rates. This behaviour confirms the material's Faradaic redox activity, leading significant to pronounced pseudocapacitive properties and efficient ion transport characteristics [43, 44]. The CV plots can be utilized for evaluating specific capacitance  $(C_{sp})$  with the assistance of equation (2).

$$C_{sp} = \frac{A}{2m\Delta V k} \tag{3}$$

Where A is the area under the CV curve, m is the deposited mass of the electroactive material over CPE,  $\Delta V$  is the applied potential window and k is the scan rate (in mV/s) [45, 46].

**4.6.1.1 CV of PAZ:** Using CV in a three-electrode cell layout, the electrochemical characteristics of PAZ were examined at room temperature in  $1M\ H_2SO_4$  at a common 10, 60, and  $100\ mV/$  scan rates in 0 to 1.0V potential window. Redox transitions between a semiconducting and conducting state cause cathodic and anodic peaks. The CV curves of the PAZ electrode exhibit Faradaic redox reactions, displaying anodic peaks associated with oxidation and a cathodic peak attributed to the reduction of PAZ. The CV results show that when the scan rate increases from  $10\ mV/s$  to  $100\ mV/s$ , the specific capacitance

of PAZ declines. The specific capacitance was found to be maximum, i.e. 35.42 F/g at 10 mV/s, and minimum, i.e. 4.8 F/g at 100 mV/s. As the scan rate increases from 10 to 100 mV/s, Figure 36 demonstrates that the area and specific capacitance drop, suggesting an inverse relationship between the two parameters. At lower scan rates, the electrolyte ions can interact with the entirety of the active surface area due to their improved penetration, and at larger scan rates, the electrolyte ions are diffusion-limited and time-constrained to the electrode's porous structure.

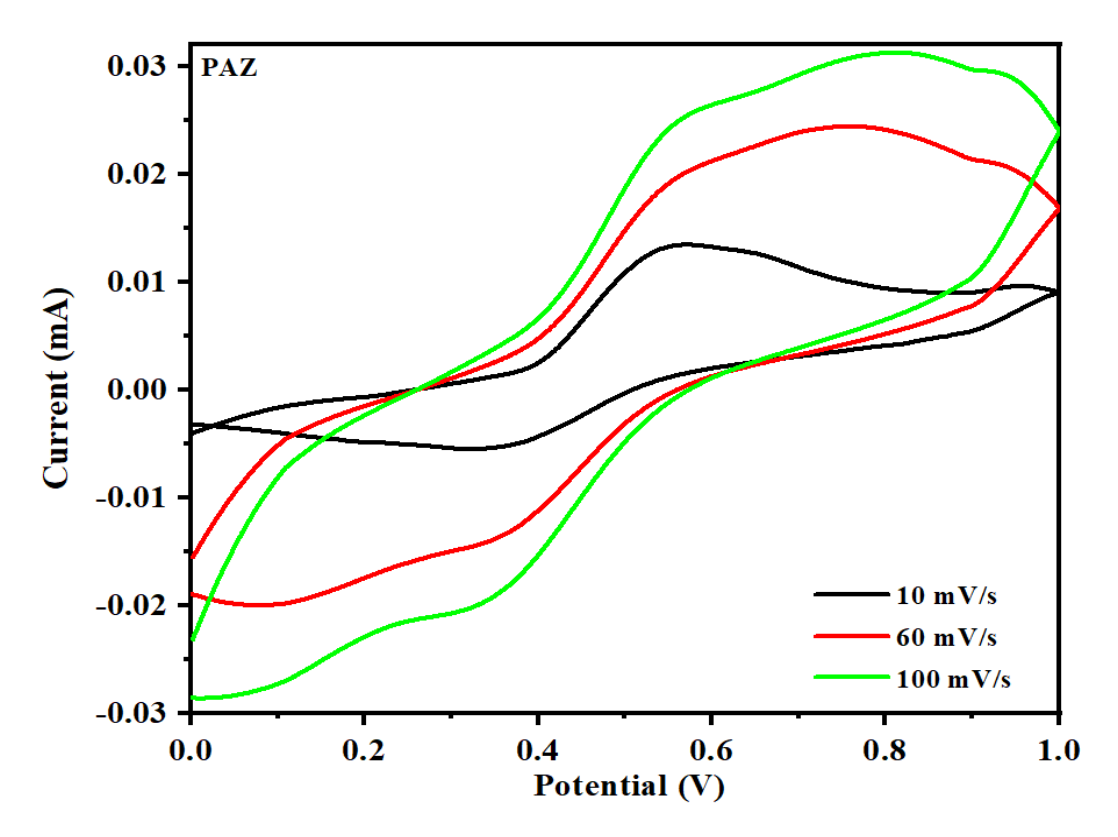


Figure: 36 CV of PAZ at a varying scan rate

The impressive electrochemical behaviour of PAZ may be due to its extended conjugation within the polymer structure and its large surface area of 2473 mm<sup>2</sup>, which offers an effective location for charge carrier

interaction and improved charge transfer. However, this is to be noticed that the high resistance of CPE leads to comparably low capacitance [47]. The result makes this polymer comparable to some of the existing conducting polymers such as polythiophene [48] and polyindole [49], which depend upon the synthetic method, substrate's resistance, the surface area of the active polymeric material, etc.

**4.6.1.2 CV of GO:** The electrochemical behaviour of GO over a carbon paste electrode was examined with a three-electrode cell setup in 1M sulfuric acid (H<sub>2</sub>SO<sub>4</sub>) at different scan rates of 10, 60, and 100 mV/s, within a potential window of 0 to 1V. Reversible redox transitions of GO give rise to cathodic and anodic peaks in the CV curves. Faradaic redox processes are evident in the CV data of the GO electrode, exhibiting a cathodic peak corresponding to the reduction and anodic peaks due to the oxidation process. GO typically shows capacitive behaviour due to the redox-active oxygen groups on its surface. The functional groups enable the adsorption and desorption of ions from the electrolyte during the scan, leading to a current response [50]. This is often observed as a pair of peaks or broad humps in the CV of GO. The electrochemical properties of GO studied via CV are important for applications in energy storage devices such as supercapacitors, batteries, and fuel cells. GO's ability to undergo redox reactions allows it to contribute to energy storage mechanisms, though its capacitance is often lower than rGO. Higher redox peaks in a CV indicate higher electrochemical reaction activity. The specific capacitance of GO was calculated using equation (3) and it was observed that when the scan rate rises from 10 mV/s to 100 mV/s, the specific capacitance of GO drops [45, 46].

The investigation of GO revealed that its electrochemical behaviour was influenced by the scan rate, and the findings demonstrated that GO exhibited superior specific capacitance compared to PAZ across all the tested scan rates (Fig. 37). This superiority can be attributed to GO's

enhanced electron transport within its matrix structure [35]. At 10 mV/s, the maximum  $C_{\rm sp}$  of 247.2 F/g was encountered for GO in Table 5.

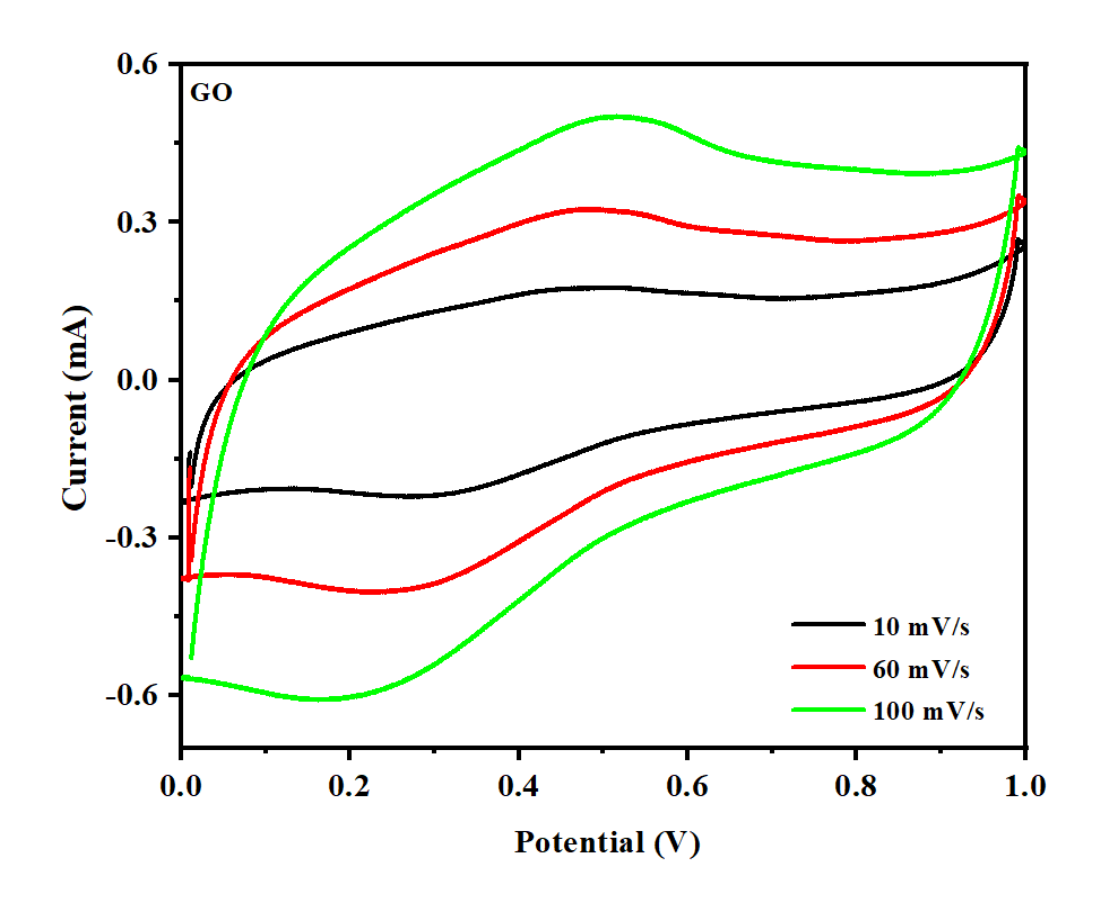


Figure: 37 CV curve of GO at a various scan rate

Table: 5 Specific capacitance of GO at various scan rates

Scan Rate(mV/s)	s) Specific Capacitance(F/g)	
10 mV/s	247.20 F/g	
60 mV/s	101.54 F/g	
100 mV/s	33.53 F/g	

It was observed that GO has a maximum  $C_{sp}$  of 247.20 F/g at 10 mV/s and a minimum (33.53 F/g) at 100 mV/s scan rate.

**4.6.1.3 CV of rGO:** The electrochemical behaviour of rGO over a carbon paste electrode was examine with a three-electrode cell setup in 1M sulfuric acid ( $H_2SO_4$ ) from 10 mV/s to 100 mV/s, within a potential window of 0 to 1V. During cycling, the anodic peak corresponds to the oxidation of the rGO, while the cathodic peak corresponds to its reduction. These peaks shed light on rGO's electrochemical activity and capacity for charge storage. The specific capacitance ( $C_{sp}$ ) of rGO was evaluated by using equation (3) and it was observed that the  $C_{sp}$  of rGO diminishes as the scan rate is augmented from 10 mV/s to 100 mV/s as shown in Fig. 38.

Analysis revealed that the reduction process, which restores a sizable amount of the graphene's sp<sup>2</sup> hybridized carbon network and enhances its electrical conductivity, is the reason why the specific capacitance of rGO is substantially larger than that of GO and they shows better charge transport. The deoxygenation of GO results in the partial removal of oxygenated functional groups in reduction process, which in turn leads to a decrease in the number of structural defects and a more well-preserved graphene-like configuration. This helps enhance the material's electrochemical stability and reversible charge storage capabilities as an electrode material. CV is an essential technique for evaluating the electrochemical properties of rGO, helping to understand its behaviour in applications like energy storage, sensors, and catalysis [50].

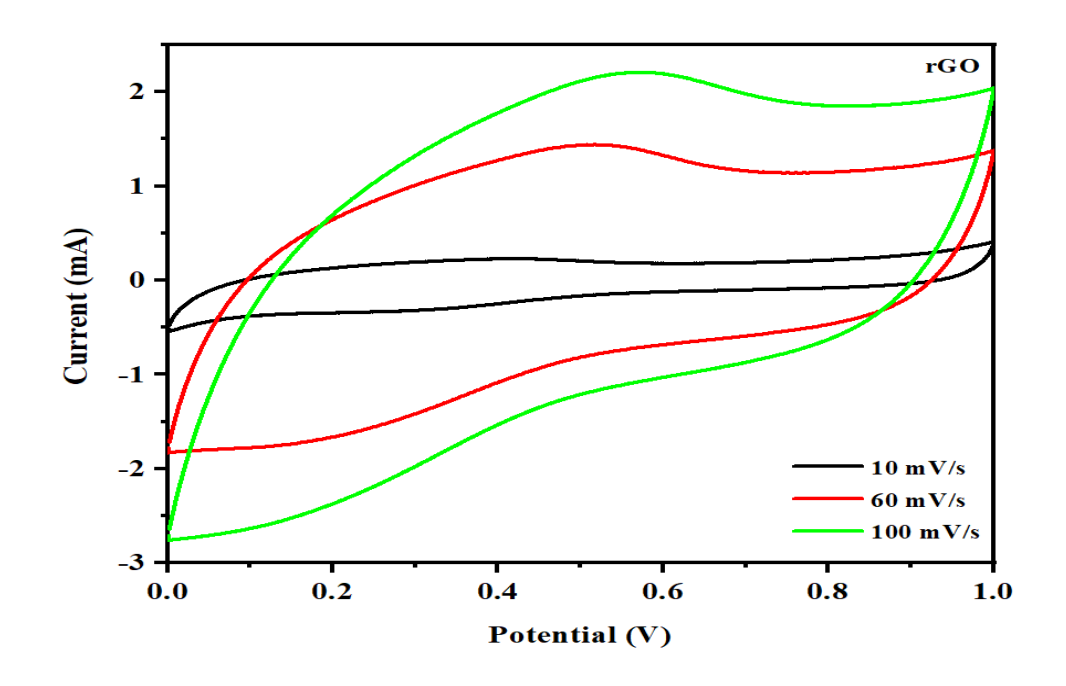


Figure: 38 CV of rGO at a varying scan rate

It was observed that rGO has a maximum value 383.21 F/g of  $C_{sp}$  at 10 mV/s and a minimum (48.77 F/g) value at 100 mV/s from Table 6.

Table: 6 Specific capacitance of rGO at various scan rates

Scan rate	Specific capacitance(F/g)	
10 mV/s	383.21	
60 mV/s	167.37 F/g	
100 mV/s	48.77 F/g	

**4.6.1.4 CV of composites of PAZ with GO (PGs):-** The electrochemical characteristics of composites of PAZ and GO were also examined at room temperature in  $1M\ H_2SO_4$  electrolyte and from  $10\ to\ 100\ mV/s$  scan rate with  $0\ 10\ 1.0\ V$  working potential window. The  $C_{sp}$  values of the materials, including PAZ, GO, and their composites, demonstrate a

progressive increase due to their structural properties that facilitate the availability of free electrons for electrical conduction. The materials' increased surface area and porous nature are responsible for this behaviour. The durability of the materials is demonstrated by the CV curves, which show a steady rise in the magnitude of the cathodic and anodic current with an expanded scan rate. However, this pattern is not continuous and results in a drop in specific capacitance.

•

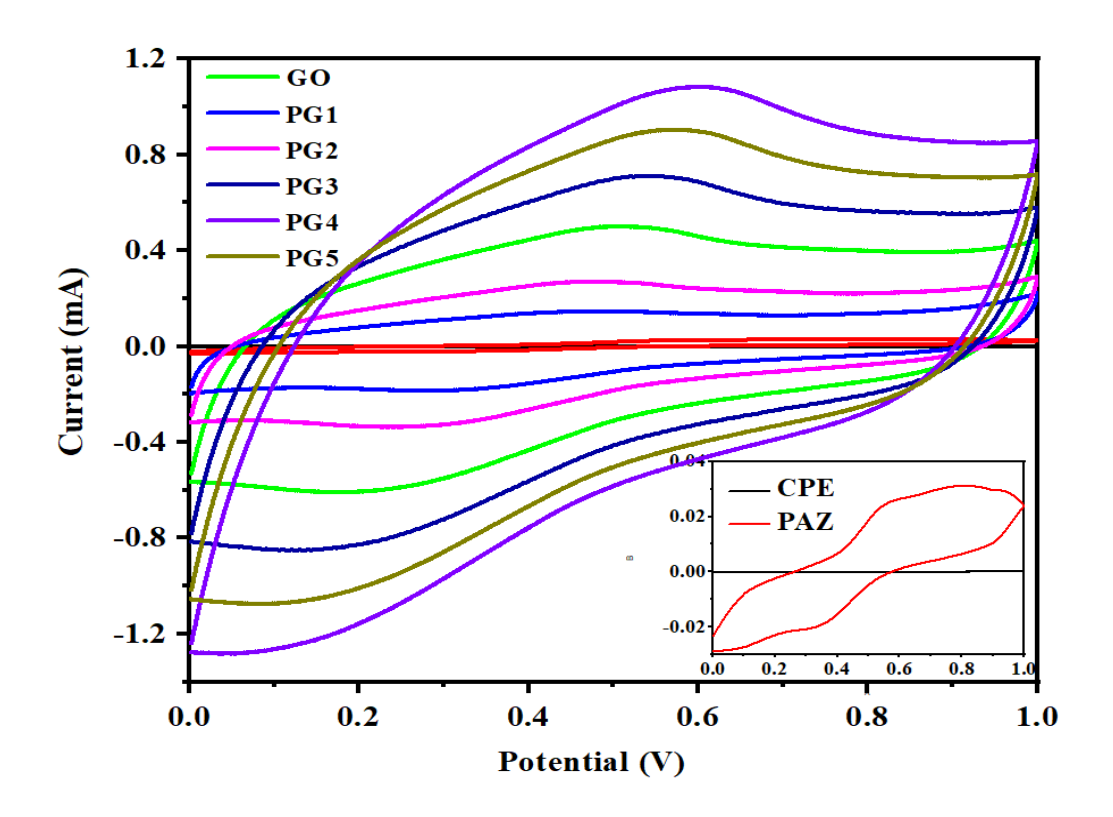


Figure: 39 CV of PGs at 10 mV/s scan rate

When specific weight percentages of GO are added to the PAZ matrix, their homogenous grafting enhances the surface area and raises the  $C_{sp}$  of the PAZ composite, however, this rise is not consistent. PG1 and PG2 had lower specific capacitance (77.48 and 140.20 F/g, respectively) than GO, possibly due to the lower amount of GO compared to PAZ in

these composites. As the ratio of GO was increased in the composite material, the specific capacitance was observed to be enhanced, confirming the effect of GO. The CVs of CPE, GO, PAZ, and all the PGs at 10 mV/s have been shown in Fig. 39 for comparative analysis.

Table:7 Specific capacitance of the PAZ, GO and PGs at various scan rates

Materials	Scan rates		
materials	100 mV/s	60 mV/s	10 mV/s
PAZ	4.8	13.16	35.42
GO	33.53	101.54	247.20
PG-1	10.52	29.84	77.48
PG-2	18.90	55.78	140.20
PG-3	45.30	124.39	332.05
PG-4	63.10	173.89	475.61
PG-5	55.11	156.01	407.56

When specific weight percentages of GO are added to the PAZ matrix, their homogenous grafting enhances the surface area and raises the specific capacitance, however, after a certain addition of GO to PAZ there was a fall in specific capacitance. The maximum value of C<sub>sp</sub> was achieved for PG-4, which further started to decrease as the amount of GO increased in the composite PG-5 (depicted in Table 7). Adding more graphene oxide layers to PAZ can potentially reduce the specific capacitance. This is because the increased GO layers may hinder electrical conductivity and diminish the available surface area for

energy storage. PGs that are aligned well function very well as electrode materials.

4.6.1.4 CV of composites of PAZ with rGO (PrGs):- The electrochemical characteristics of PAZ and rGO composites were examined at room temperature in 1M H<sub>2</sub>SO<sub>4</sub>, across the potential window of 0 to 1.0 V, and with standard scan rates of 10, 60, and 100 mV/s (Fig.40). Because of their structural characteristics, which include the availability of free electrons for electric conduction, specific capacitance values gradually rise from PAZ to rGO and their composites. This can be explained by the increased surface area and porous structure of all the materials. CV curves demonstrate a consistent rise in the cathodic and anodic current range with increased scan rate; however, this tendency was not uniform, and the materials' stability was indicated by a decrease in specific capacitance.

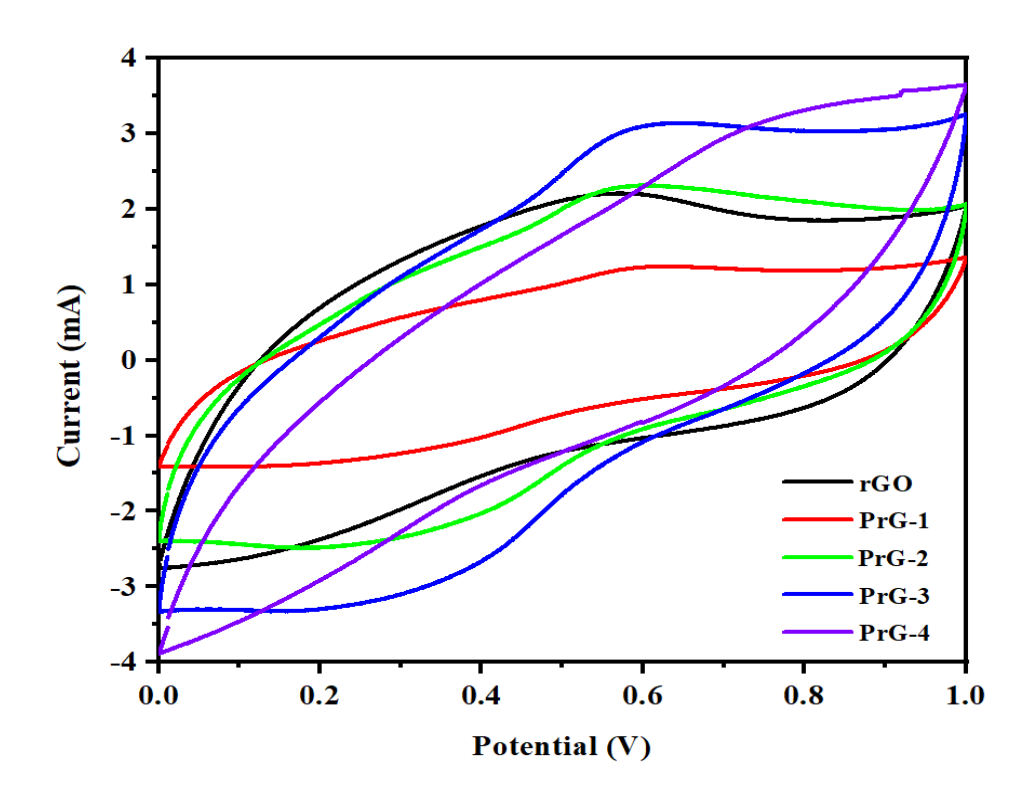


Figure: 40 CV of PrGs at 10 mV/s scan rate

The C<sub>sp</sub> values of PAZ, rGO, and their composites show the highest capacitance values of 35.42, 383.21, and 689.21 F/g, respectively at 10 mV/s, and the values decrease regularly with the rise in scan rate from 10 to 100 mV/s. The homogeneous grafting of rGO at specified weight percentages increases the specific capacitance of PAZ and improves its surface area, although this rise is not constant. After PrG-3 (1:1) reached its maximum specific capacitance value of 689.21 F/g, extra rGO layers were added to PAZ, which inhibited conduction and reduced the active surface area. This resulted in a fall in C<sub>s</sub>. PrGs that are properly aligned perform admirably as electrode materials concluded from Table 8.

Table:8 Specific capacitance of the PAZ, rGO and PrGs at various scan rates

Materials	Scan rates		
materials	100 mV/s	60 mV/s	10 mV/s
PAZ	4.8	13.16	35.42
rGO	48.77	167.37	383.21
PrG-1	20.11	48.32	158.76
PrG-2	43.34	124.87	312.10
PrG-3	112.54	362.19	689.21
PrG-4	54.22	163.65	432.21

**4.6.2 GALVANOSTATIC CHARGE-DISCHARGE (GCD):** The term "galvanostatic charge and discharge" refers to a method of charging and discharging a battery or supercapacitor at a constant current. his method maintains a steady current supplied to the system throughout the process, and the voltage varies depending on the characteristics of

the energy storage device. This method is commonly used in testing battery performance, as it allows the study of how the device responds to a fixed current over time and in research to test the behaviour of various batteries, such as lithium-ion batteries, during charge and discharge cycles.

The GCD curves were employed for determining the specific capacitance, which was further utilized to determine the energy density and power density of electroactive materials. The following equations 4, 5, and 6 are used to determine the specific capacitance (C<sub>sp</sub>), energy density (E<sub>g</sub>), and power density(P) respectively:

$$C_{SP(F/g)} = \frac{I\Delta t}{m\Delta V} \qquad ----- \tag{4}$$

$$E_g (Wh/Kg) = \frac{C_{sp} \cdot \Delta V^2}{2} * \frac{1000}{3600}$$
 (5)

$$P (W/kg) = \frac{E_g}{\Delta t} \times 3600$$
 -----(6)

Where I stands for current density,  $\Delta t$  stands for discharge time,  $\Delta V$  stands for potential window,  $C_{sp}$  stands for specific capacitance,  $E_g$  stands for energy density, and P stands for power density [18, 45].

**4.6.2.1 GCD of PAZ:** The electrochemical charge-discharge performance of PAZ was investigated at various current densities (1, 0.5, 0.25 A/g), and in 0-1 V working potential window (Fig. 41).

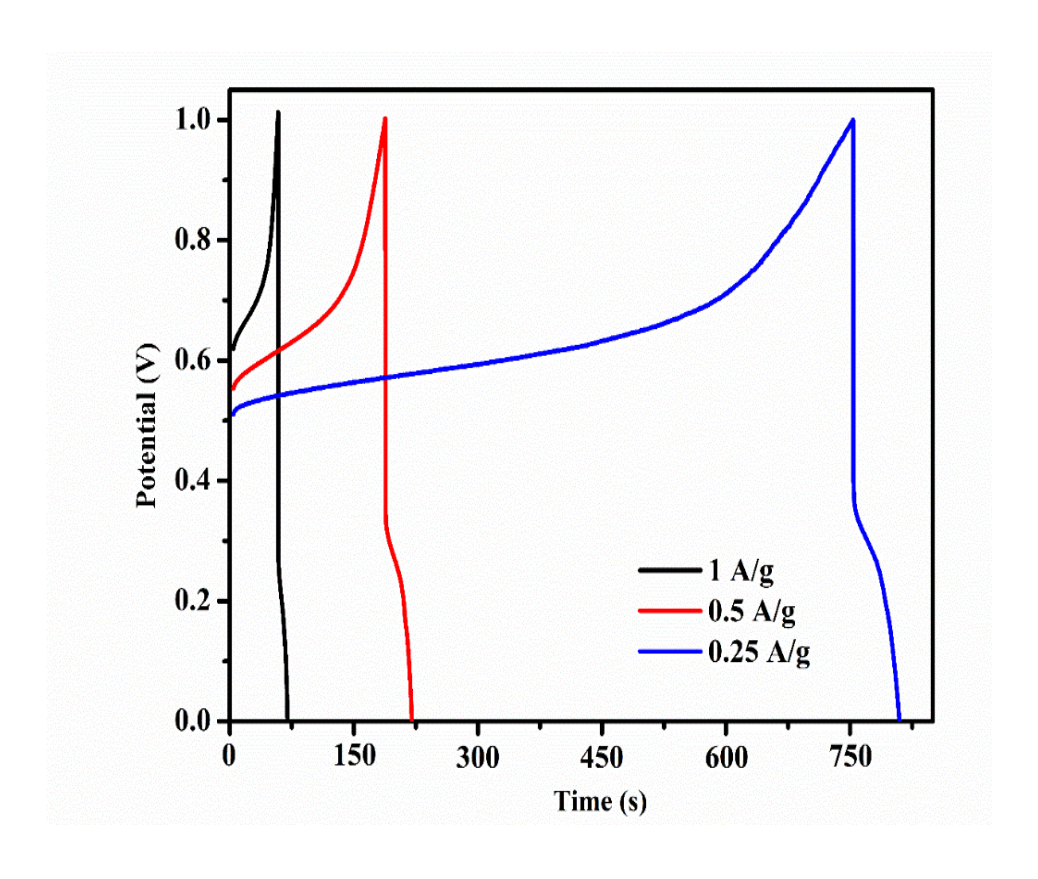


Figure: 41 GCD curve for PAZ at varying current density

Equations 4, 5, and 6 were used to evaluate the power, energy density, and specific capacitance of generated electrodes of PAZ at various current densities listed in Table 9.

Table: 9 Specific capacitance, energy, and power density of PAZ at varying current densities

Current density (A/g)	Specific capacitance (F/g)	Energy density (Wh/kg)	Power density (W/kg)
1	19.9	2.76	499.99
0.5	31.8	4.41	249.99
0.25	28.37	3.94	124.99

**4.6.2.2 GCD of GO along with PAZ and PG-4:** The charge-discharge characteristics of PAZ, GO, and PG-4 were investigated with 0-1 V working potential window and 1 A/g current density, as depicted in Fig. 42. The specific capacitance values were derived from the GCD measurements, and these data were subsequently employed to determine the overall energy density and power densities of the electroactive materials.

Equations 4, 5, and 6 were used to evaluate the power, energy density, and specific capacitance of generated electrodes of all the prepared materials at various current densities listed in Table 10.

Table 10: Specific capacitance, energy, and power density of PAZ, GO, and PG-4 at the current density of 1 A/g

Materials	Specific	Energy density	Power
	capacitance	(Wh/kg)	density
	(F/g)		(W/kg)
PAZ	19.90	2.76	499.99
GO	22.39	5.06	856.33
PG-4	37.26	10.35	1007.02

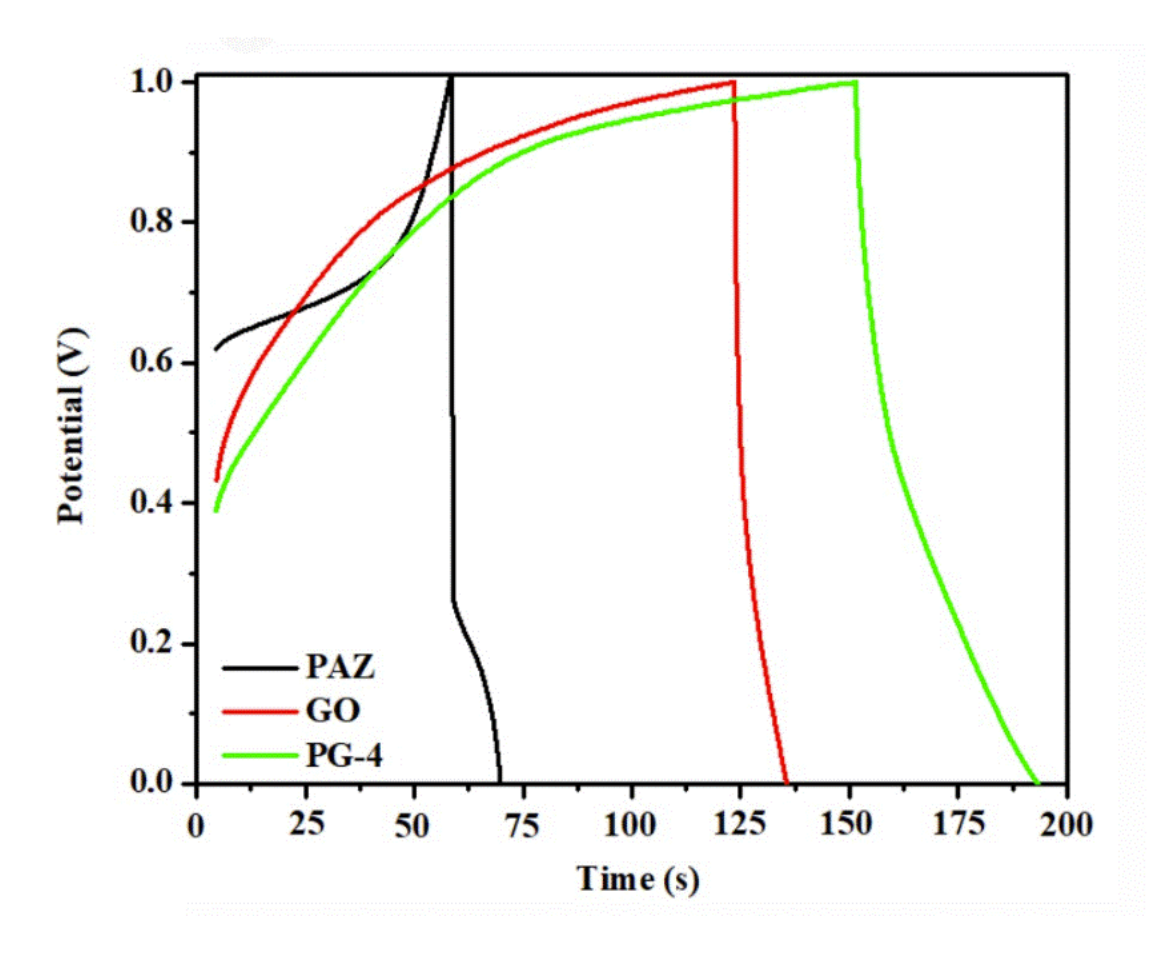


Figure: 42 GCD curves of PAZ, GO, and representative PG-4 at 1 A/g

**4.6.2.3 GCD of rGO, PAZ, and PrG-3:** Electrochemical behaviour of various generated electrodes of prepared materials and the GCD curves of rGO and PrG-3 for the supercapacitor device at a current density of 1 A/g are represented by the GCD curve as shown in Fig. 43.

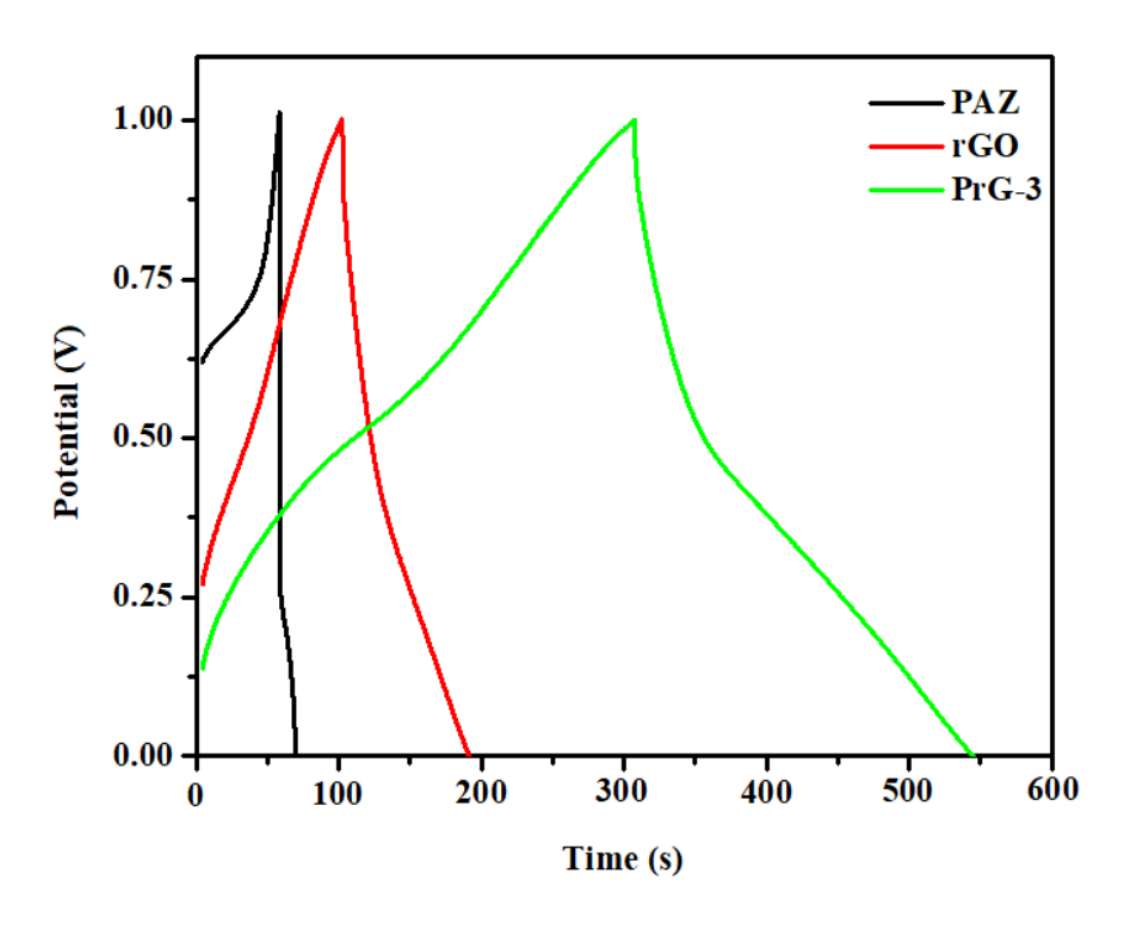


Figure: 43 GCD curves of PAZ, rGO, and representative PrG-3 at 1 A/g

Equations 4, 5, and 6 were used to evaluate the power, energy density, and specific capacitance of generated electrodes of all the prepared materials at various current densities listed in Table 11.

Table:11 Specific capacitance, energy, and power density of PAZ, rGO, PrG-3 at the current density of 1A/g

Materials	Specific	Energy density	Power
	capacitance	(Wh/kg)	density (W/
	(F/g)		kg)
PAZ	19.90	2.76	499.99
rGO	90.11	12.52	500.00
PrG-3	235.31	32.68	499.99

4.6.3 ELECTROCHEMICAL IMPEDANCE SPECTROSCOPY (EIS): EIS uses a tiny sinusoidal alternating current pulse at various frequencies to assess the impedance of electrochemical systems. EIS is a valuable technique for studying reaction kinetics and battery properties. Nyquist plot and Bode plot are the methods for visualizing impedance spectrums in EIS. A Nyquist plot maps the real and imaginary impedance thus revealing the reaction mechanisms and kinetics involved in the electrochemical system, while Bode plots represent the phase and magnitude changes with change in frequency. EIS is used for studying the properties of electrode reactions and for the characterization of conducting materials [51].

**4.6.3.1 EIS of PAZ:** EIS is a useful method for analyzing the mechanisms behind charge transport and the frequency of charge transfer in electrochemical systems. It is a procedure that impacts a device with alternating current (AC) and obtains the AC response from it. EIS is used for studying the properties of electrode reactions and for the characterization of conducting materials [51, 52]. Fig. 44 represents the Nyquist plot for the PAZ, where the absence of a semicircular region indicates the low faradaic resistance offered. EIS measurement was performed under the 100 mHz -100 kHz frequency range, and a 20 mV/s amplitude of AC. At low frequency the optimally polarizable capacitor yields a near-linear (straight) response, with the curve aligning closely(parallel) with the imaginary axis, thus representing a typical quasi-ideal capacitor; the nonideal capacitance's resistive component is what causes the inclination towards the real axis. The internal resistance of the electrode and the ohmic resistance of the electrolyte are represented by the intersection point (Rs, resistance offered by solution) on the real axis at high frequencies. The parallel connection of the double-layer capacitance ( $C_{\text{DL}}$ ), and the interfacial charge transfer resistance (R<sub>CT</sub>), results in the slight semicircular behaviour in the high- to midfrequency range.

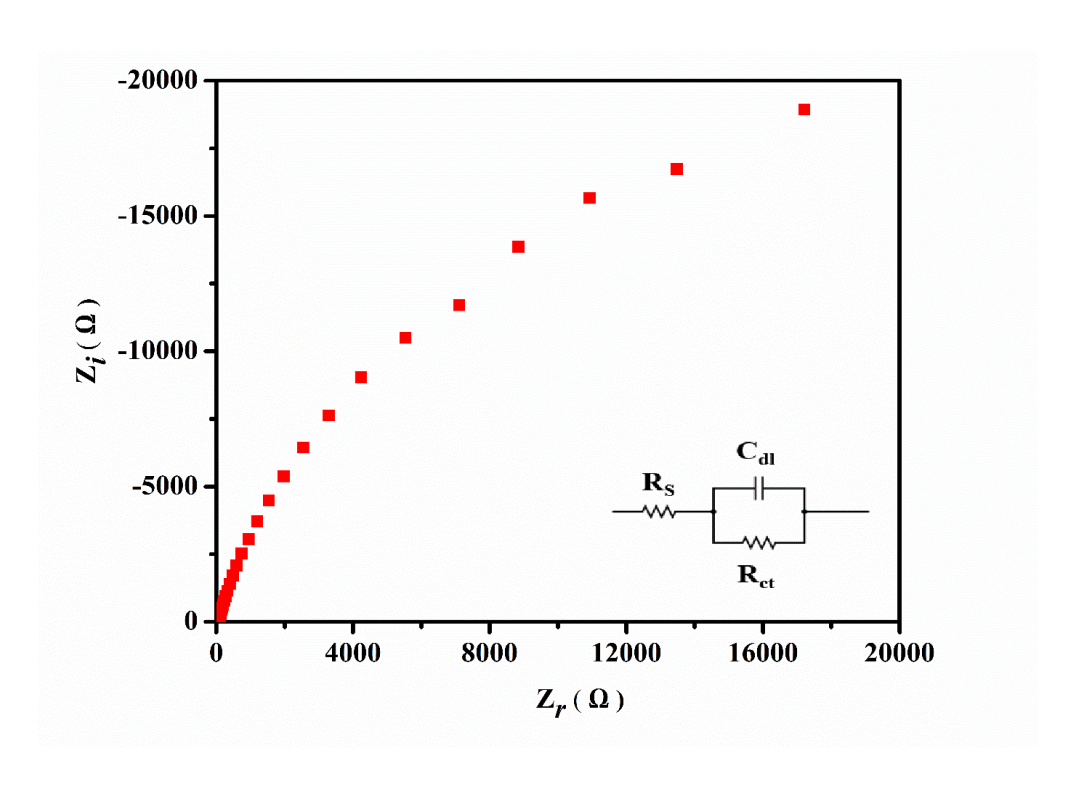


Figure 44: Nyquist plot of PAZ

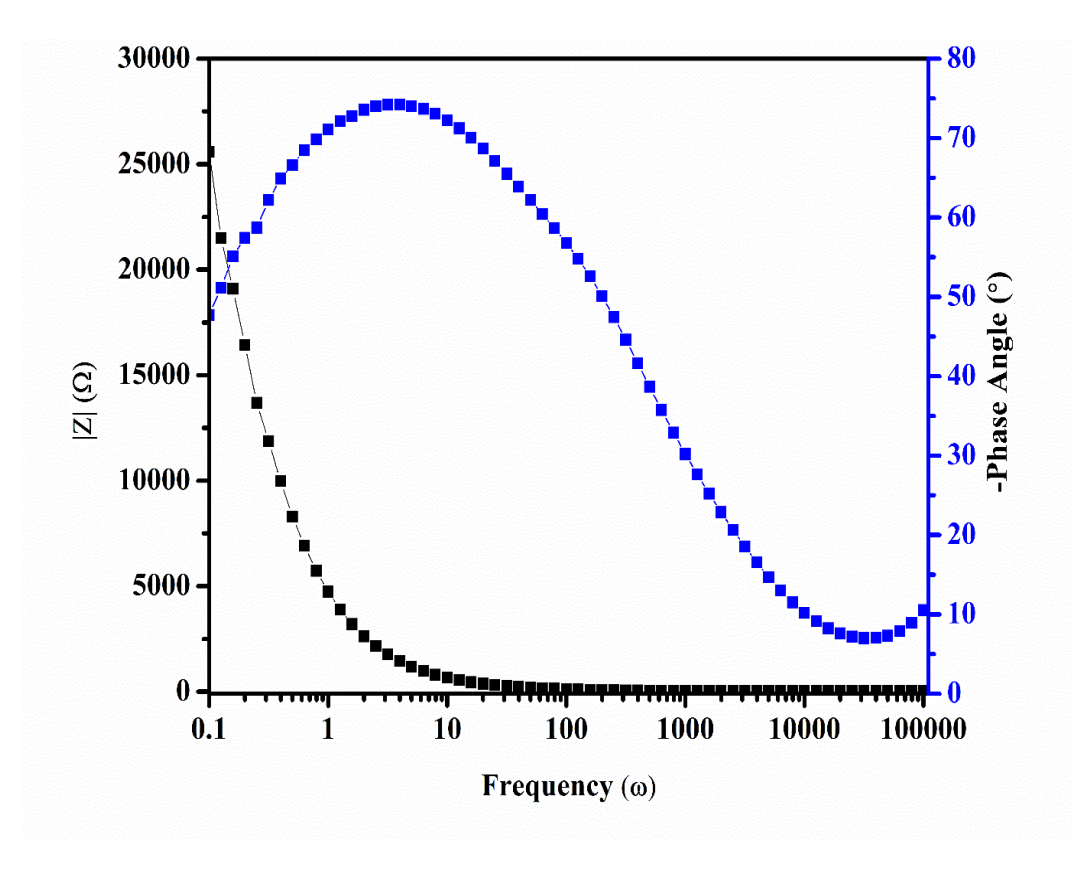


Figure 45: Bode plot of the prepared PAZ representing the typical relation between impedance, frequency, and phase angle

A Bode plot (fig 45) was used to further examine the PAZ capacitance performance. A phase angle of -75° was noted which is close to that of an ideal capacitor (-90°), indicating improved charge transfer because of the electrode and electrolyte's advantageous contact **[52]**. The plot represents low resistance offered at higher frequencies, thus confirming the results obtained in the Nyquist plot of the polymer. The plot suggests that little resistance to the electron transfer is provided.

## 4.6.3.2 EIS of PAZ, GO and PG-4:

An AC amplitude of 20 mV/s was used for EIS studies, which were conducted from 100 mHz to 100 kHz, obtained in an aqueous solution of 1M H<sub>2</sub>SO<sub>4</sub>. The Nyquist plot for PAZ, GO, and PG-4 is shown in Fig. 46, which provides information about the charge transfer resistance and capacitance at high and low frequencies, respectively. The lack of semicircle indicates that there was low faradaic resistance or no barrier to charge transfer for these materials [53, 54]. In the present study, the imaginary component Z<sub>r</sub> exhibits a sharp and near-vertical line at low frequencies range, a low ( $R_{ct}$ ) value of 23.18  $\Omega$  was obtained for the PG-4 composite which is far as lower as compared to 122.49  $\Omega$  and 180.87  $\Omega$  encountered for GO and PAZ respectively, representing very small charge transfer resistance. A zoomed-in view of the impedance data at lower resistance and capacitance regions is shown in the inset in Fig. 46. The inset figure highlights refined differences between the electroactive materials, particularly in their high-frequency response. PG-4 appears to be the most efficient material in terms of electrochemical performance, while PAZ shows the highest resistance and potentially lower electrochemical activity.

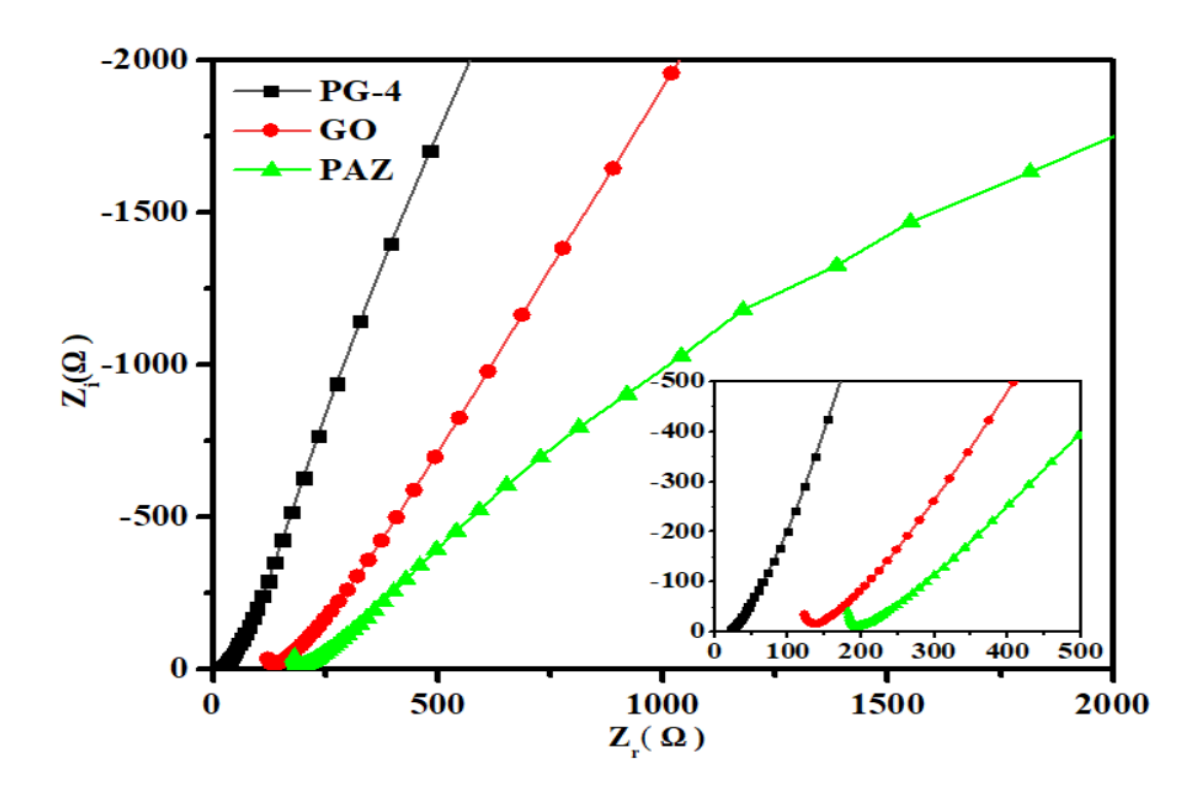


Figure 46: Nyquist plot of PAZ, GO, and representative PG-4

For perfect capacitors in a series RC circuit, the capacitive impedance shows a dependence on the inverse of the capacitance, indicating that the Nyquist diagram must be vertical. Likewise, for low frequencies, the phase angle in the Bode figure(plot) is expected to get closer to 90° [54]. The performance of the PAZ's capacitance was further investigated using a Bode plot. A phase angle of -75° was observed for polyazine, which is nearly equal to the phase angle of an ideal capacitor (-90°), suggesting enhanced charge transfer as a result of the beneficial contact between the electrode and electrolyte [52]. The plot illustrates low resistance provided at higher frequencies, supporting the findings seen in the polymer's Nyquist plot. The plot implies that there isn't much resistance to the electron transfer.

Fig. 47 displays impedance data against frequency i.e. Bode plot, illustrating the electrical characteristics of PAZ, GO, and PG-4 on a logarithmic scale ranging from approximately 0.1 to 10<sup>-5</sup> Hz. PAZ, GO, and PG-4 show a decrease in impedance (Z) with increasing frequency.

Among all the electroactive materials, PG-4 represents a lower impedance value across the frequency range as compared to PAZ and GO, which indicates better charge/discharge and smoother electron or during abilities for PG-4. ion transport energy storage The phase curves, display an increase in frequency, indicating a change in electrical behavior for each sample at different frequencies. A phase angle that increases with frequency suggests that the material can better manage changes in frequency, indicating better performance in conditions. PG-4 also represents favorable dynamic phase characteristics as compared to other samples.

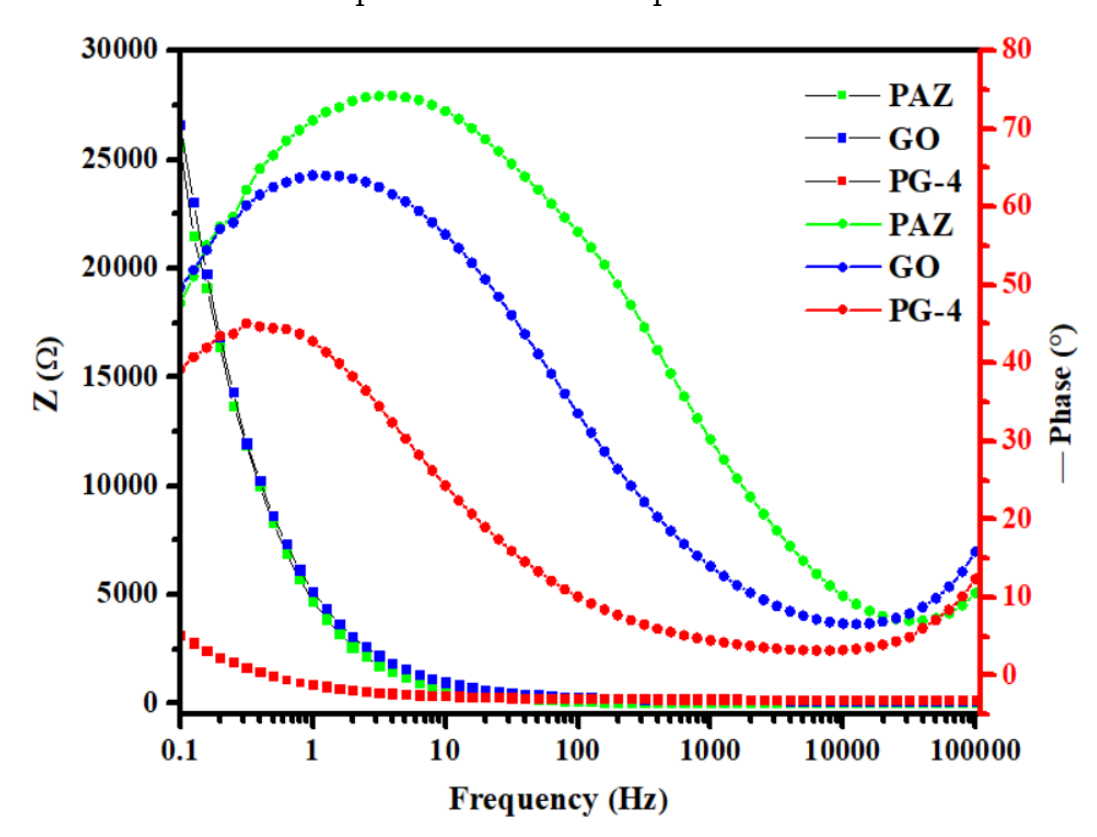


Figure 47: Bode plot of PAZ, GO, and representative PG-4

**4.6.3.3 EIS of PAZ, rGO, and PrG-3:** EIS was employed to analyze the electrochemical performance of PAZ, rGO, and its constructed composite, PrG-3. The EIS was conducted at open circuit potential throughout a frequency range of 100 kHz to 100 mHz. The frequency response in the electrode material/electrolyte system is displayed by

the Nyquist plot, which compares the imaginary part (-Z') of resistance with its real part (Z). An AC amplitude of 20 mV/s was used for EIS studies, which were conducted from 100 mHz to 100 kHz frequency range.

In the Nyquist plot (Fig. 48) of PAZ, rGO and its composite PrG-3 show the absence of a semicircle suggests that these compounds had either no barrier to charge transmission or low faradaic resistance [52].

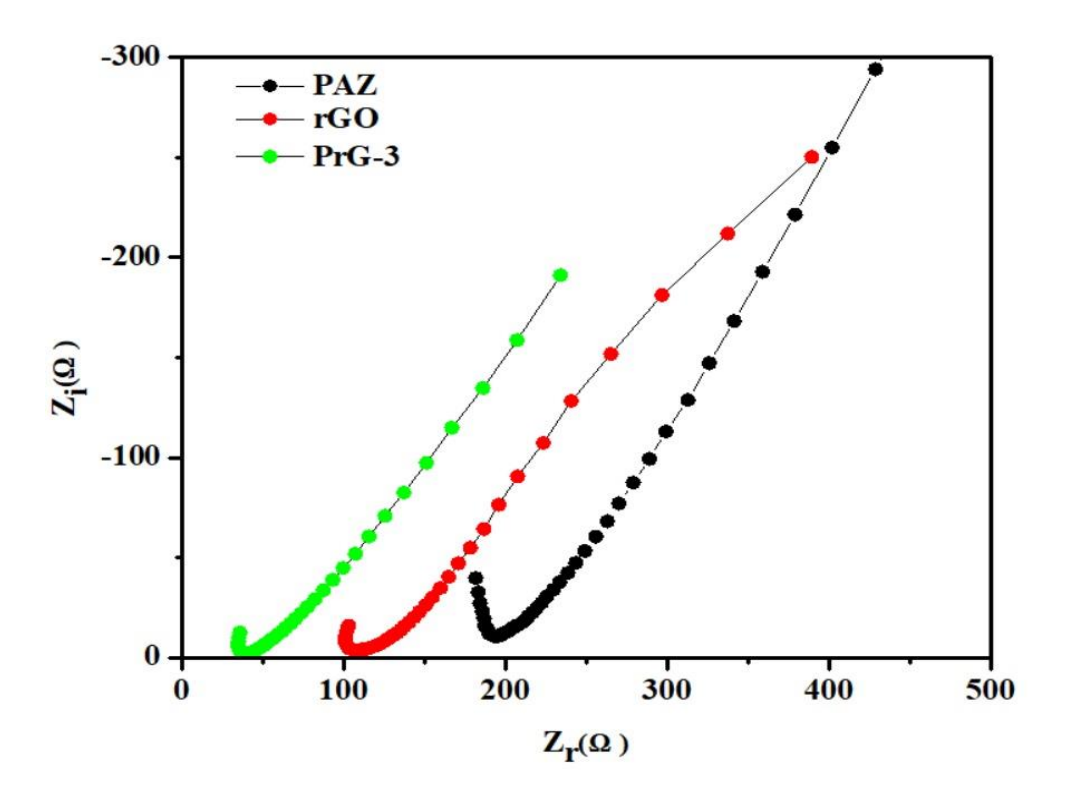


Figure 48. Nyquist plot of PAZ, rGO and PrG-3

Fig. 49 displays impedance data against frequency i.e. Bode plot, illustrating the electrical characteristics of PAZ, and PrG-3 on a logarithmic scale ranging from approximately 0.1 to 10<sup>-5</sup> Hz.

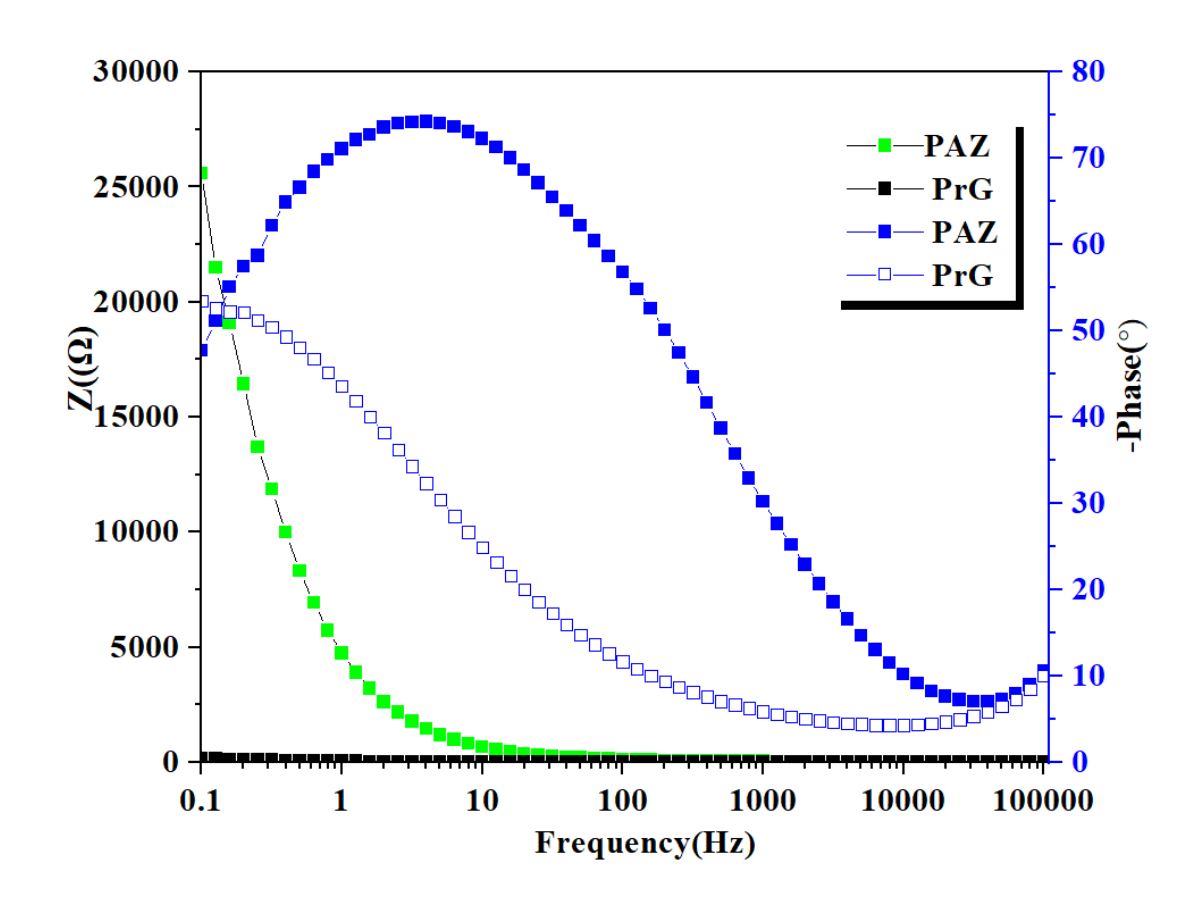


Figure 49. Bode plot of PAZ, and PrG-3

Among all the electroactive materials, PrG-3 represents a lower impedance value across the frequency range as compared to pure PAZ which indicates better charge/discharge and smoother electron or ion transport during energy storage abilities for PrG-3.

## References

- [1] Dineshkumar. S., & Muthusamy. A. Investigation of aggregation induced emission in 4-hydroxy-3-methoxybenzaldehyde azine and polyazine towards application in (opto) electronics: synthesis, characterization, photophysical and electrical properties, *Designed Monomers* and *Polymers*, 2016, 20(1), 234–249. doi:10.1080/15685551.2016.1231039
- [2] Miraqyan, N. A., Arakelyan, R. H., Durgaryan, N. A., & Durgaryan, A. H. (2018). Synthesis and investigation of poly(p-phenylenediamine)—poly(1,4-benzoquinonediimine-N,N-diyl-1,4-phenylene). *Chemical Papers*, 72(6), 1517–1524. doi:10.1007/s11696-017-0378-2
- [3] Chauhan, N. P. S., Ametab, R., Ametac, R., & Ameta, S. C. (2011). Thermal and conducting behaviour of emeraldine base (EB) form of polyaniline (PANI). *Indian Journal of Chemical Technology*, 18, 118-122.
- [4] Chougule, M. A., Pawar, S. G., Godse, P. R., Mulik, R. N., Sen, S., & Patil, V. B. (2011). Synthesis and Characterization of Polypyrrole (Ppy) Thin Films. *Soft Nanoscience Letters*, 1(1), 6–10. doi:10.4236/snl.2011.11002
- [5] Islam, M., Naushad, M., & Patel, R. (2014). Polyaniline/basic oxygen furnace slag nanocomposite as a viable adsorbent for the sorption of fluoride from aqueous medium: equilibrium, thermodynamic and kinetic study. *Desalination and Water Treatment*, 54(2), 450–463. doi:10.1080/19443994.2014.887034
- [6] Rattana, Chaiyakun, S., Witit-anun, N., Nuntawong, N., Chindaudom, P., Oaew, S., kedkeaw, C., & Limsuwan, P. (2012). Preparation and characterization of graphene oxide nanosheets. *Procedia Engineering*, 32, 759–764. doi:10.1016/j.proeng.2012.02.009
- [7] Nazri, S. R. B., Liu, W.-W., Khe, C.-S., Hidayah, N. M. S., Teoh, Y.-P., Voon, C. H., Lee, H. C., & Adelyn, P. Y. P. (2018). Synthesis,

- characterization and study of graphene oxide. *AIP Conference Proceedings*, 2045, 020033. doi:10.1063/1.5080846
- [8] Surekha, G., Krishnaiah, K. V., Ravi, N., & Padma Suvarna, R. (2020). FTIR, Raman and XRD analysis of graphene oxide films prepared by modified Hummers method. *Journal of Physics: Conference Series*, 1495, 012012. doi:10.1088/1742-6596/1495/1/012012
- [9] Habte, A. T., & Ayele, D. W. (2019). Synthesis and Characterization of Reduced Graphene Oxide (rGO) Started from Graphene Oxide (GO) Using the Tour Method with Different Parameters. *Advances in Materials Science and Engineering*, 2019, 1–9. doi:10.1155/2019/5058163
- [10] Paulchamy, B., Arthi, G., & Lignesh, B. D. (2015). A Simple Approach to Stepwise Synthesis of Graphene Oxide Nanomaterial. Journal of Nanomedicine & Nanotechnology, 6, 253. doi: 10.4172/2157-7439.1000253
- [11] Bindumadhvan. K., Srivastava, S., & Srivastva, I. (2013). Green Synthesis of Graphene. *Journal of Nanoscience and Nanotechnology*. doi: 10.1166/jnn.2013.7461
- [12] Thema, F. T., Moloto, M. J., Dikio, E. D., Nyangive, N. N., Kotsedi, L., Mazza, M & Khenfouch, M. (2012). Synthesis and Characterization of graphene thin films by chemical reduction of exfoliated and intercalated graphite oxide. *Journal of Chemistry*, 2013(1), 150536. doi:10.1155/2013/150536
- [13] Zayed, S. I. M., & Arida, H. A. M (2013). Preparation of Carbon Paste Electrodes and Its Using in Voltammetric Determination of Amiloride Hydrochloride Using in the Treatment of High Blood Pressure. *International Journal of Electrochemical Science*, 8, 1340-1348. doi:10.1016/S1452-3981(23)14102-2

- [14] Miraqyan, N. A., Arakelyan, R. H., Durgaryan, N. A., & Durgaryan, A. H (2018). Synthesis and investigation of poly(p-phenylenediamine)—poly(1,4-benzoquinonediimine-N,N-diyl-1,4-phenylene). *Chemical Papers*, 72(6), 517–1524. doi:10.1007/s11696-017-0378-2
- [15] Guerrero-Contreras, J., & Caballero-Briones, F. (2015). Graphene oxide powders with different oxidation degree, prepared by synthesis variations of the Hummers method. *Materials Chemistry and Physics*, 153, 209–220. doi:10.1016/j.matchemphys.2015.01.005
- [16] Shah, A. ul H. A., Ullah, S., Bilal, S., Rahman, G., & Seema, H. (2020). Reduced Graphene Oxide/Poly(Pyrrole-co-Thiophene) Hybrid Composite Materials: Synthesis, Characterization, and Supercapacitive Properties. *Polymers*, 12(5), 1110. doi:10.3390/polym12051110
- [17] Sood, Y., Mudila, H., Katoch, A., Lokhande, P. E., Kumar, D., Sharma, A., & Kumar, A. (2023). Eminence of oxidants on structural-electrical property of Polypyrrole. *Journal of Materials Science Materials in Electronics*, 34(18). doi:10.1007/s10854-023-10834-8
- [18] Ullah, R., Khan, N., Khattak, R., Khan, M., Khan, M. S., & Ali, O. M. (2022). Preparation of Electrochemical Supercapacitor Based on Polypyrrole/Gum Arabic Composites. *Polymers*, 14(2), 242. doi:10.3390/polym14020242
- [19] Gurunathan, S., Woong Han, J., Abdal Daye, A., Eppakayala, V., & Kim, J. (2012). Oxidative stress-mediated antibacterial activity of graphene oxide and reduced graphene oxide in Pseudomonas aeruginosa. *International Journal of Nanomedicine*, 5901. doi:10.2147/ijn.s37397
- [20] Hidayah, N. M. S., Liu, W.-W., Lai, C.-W., Noriman, N. Z., Khe, C.-S., Hashim, U., & Lee, H. C. (2017). Comparison on graphite, graphene oxide and reduced graphene oxide: Synthesis and characterization. *AIP Conference Proceedings*, 1892, 150002. doi:10.1063/1.5005764

- [21] Han, Y., & Lu, Y. (2007). Preparation and characterization of graphite oxide/polypyrrole composites. *Carbon*, 45(12), 2394–2399. doi:10.1016/j.carbon.2007.07.007
- [22] Samwang, T., Watanabe, N. M., Okamoto, Y., Srinives, S.,& Umakoshi, H. (2023). Study of Chemical Polymerization of Polypyrrole with SDS Soft Template: Physical, Chemical, and Electrical Properties. *ACS Omega*, 8 (51), 48946-48957. doi:10.1021/acsomega.3c06511.
- [23] Shruthi, B., & Madhu, B. J. (2020). Dielectric, AC conductivity and electromagnetic interference shielding behavior of graphite oxide/polyvinylpyrrolidone composites. *SN Applied Sciences*, 2(4). doi:10.1007/s42452-020-2342-y
- [24] Imran, S. M., Kim, Y., Shao, G. N., Hussain, M., Choa, Y., & Kim, H. T. (2013). Enhancement of electroconductivity of polyaniline/graphene oxide nanocomposites through in situ emulsion polymerization. *Journal of Materials Science*, 49(3), 1328–1335. doi:10.1007/s10853-013-7816-5
- [25] Chuah, R., Gopinath, S. C. B., Anbu, P., Salimi, M. N., Yaakub, A. R. W., & Lakshmipriya, T. (2020). Synthesis and characterization of reduced graphene oxide using the aqueous extract of Eclipta prostrata. *Biotech*, 10(8). doi:10.1007/s13205-020-02365-4
- [26] Sharma, D., Kanchi, S., Sabela, M. I., & Bisetty, K. (2016). Insight into the biosensing of graphene oxide: Present and future prospects. *Arabian Journal of Chemistry*, 9(2), 238–261. doi:10.1016/j.arabjc.2015.07.015
- [27] Mudila, H., Zaidi, M. G. H., Rana, S., Joshi, V., & Alam, S. (2013). Enhanced electrocapacitive performance of graphene oxide polypyrrole nanocomposites. *International Journal of Chemical and Analytical Science*, 4(3), 139–145. doi:10.1016/j.ijcas.2013.09.001

- [28] Nisha, Singh, G., Kumar, A., Prasher, P., & Mudila, H. (2023). Synthesis of PANI-GO and PANI-rGO nanocomposites and their electrochemical performance. *Bulgarian Chemical Communications*, 55(A), 94-101. doi: 10.34049/bcc.55.A.0015
- [29] Dinesh kumar, S., & Muthusamy, A. (2017). Investigation of aggregation induced emission in 4-hydroxy-3-methoxybenzaldehyde azine and polyazine towards application in (opto) electronics: synthesis, characterization, photophysical and electrical properties. *Designed Monomers and Polymers*, 20(1), 234–249.

doi:10.1080/15685551.2016.1231039

- [30] Chougule, M. A., Pawar, S. G., Godse, P. R., Mulik, R. N., Sen, S., & Patil, V. B. (2011). Synthesis and Characterization of Polypyrrole (Ppy) Thin Films. *Soft Nanoscience Letters*, 1(1), 6–10. doi:10.4236/snl.2011.11002
- [31] Islam, M., Naushad, M., & Patel, R. (2014). Polyaniline/basic oxygen furnace slag nanocomposite as a viable adsorbent for the sorption of fluoride from aqueous medium: equilibrium, thermodynamic and kinetic study. *Desalination and Water Treatment*, 54(2), 450–463. doi:10.1080/19443994.2014.887034
- [32] Arumugam, A., Yogalaksha, P., Furhanashereen, M., & Ponnusami, V. (2020). Statistical optimization and enhanced synthesis of polyhydroxyalkanoates from Ceiba pendantra oil as novel non-edible feedstock. *Biomass Conversion and Biorefinery*, 12, 2071–2080, doi:10.1007/s13399-020-00742-w
- [33] Li, J., Liu, D., Li, B., Wang, J., Han, S., Liu, L., & Wei, H. (2015). A bio-inspired nacre-like layered hybrid structure of calcium carbonate under the control of carboxyl graphene. *CrystEngComm*, 17(3), 520–525. doi:10.1039/c4ce01632g.

- [34] Xiang, M., Yang, Z., Chen, J., Zhou, S., Wei, W., & Dong, S. (2020). Polymeric Thermoelectric Composites by Polypyrrole and Cheap Reduced Graphene Oxide in Towel-Gourd Sponge Fibers. *ACS Omega*, 5(46), 29955–29962. doi:10.1021/acsomega.0c04356
- [35] Mudila, H., Joshi, V. Rana, S., Zaidi, M. G. H., & Alam, S. (2014). Enhanced electrocapacitive performance and high power density of polypyrrole/graphene oxide nanocomposites prepared at reduced temperature. *Carbon Letters*, 15(3),171-179.

doi: 10.5714/CL.2014.15.3.171

- [36] Wu, W., Yang, L., Chen, S., Shao, Y., Jing, L., Zhao, G., & Wei, H. (2015). Core–shell nanospherical polypyrrole/graphene oxide composites for high-performance supercapacitors. *RSC Advances*, 5(111), 91645–91653. doi:10.1039/c5ra17036b
- [37] Liu, F., Cao, Y., Yi, M., Xie, L., Huang, W., Tang, N., Zhong, W., & Du, Y. (2013). Thermostability, Photoluminescence, and Electrical Properties of Reduced Graphene Oxide–Carbon Nanotube Hybrid Materials. *Crystals*, 3(1), 28–37. doi:10.3390/cryst3010028
- [38] Loryuenyong, V., Khadthiphong, A., Phinkratok, J., Watwittayakul, J., Supawattanakul, W., & Buasri, A. (2019). The fabrication of graphene-polypyrrole composite for application with dye-sensitized solar cells. *Materials Today: Proceedings*, 17, 1675–1681.

doi:10.1016/j.matpr.2019.06.198

[39] Vargas, L. R., Poli, A. K. D. S., Dutra, R., de, C. L., De Souza, C. B., Baldan, M. R., & Gonçalves, E. S. (2017). Formation of Composite Polyaniline and Graphene Oxide by Physical Mixture Method. *Journal of Aerospace Technology and Management*, 9(1), 29–38. doi:10.5028/jatm.v9i1.697

- [40] Gupta, R., Pancholi, K., Prabhu, R., Pancholi, M., Huo, D., Jha, V., & Latto, J. (2017). Integrated self-healing of the composite offshore structures. *OCEANS* 2017 Aberdeen, 1-4. doi:10.1109/oceanse.2017.8084828
- [41] Yin, K., Li, H., Xia, Y., Bi, H., Sun, J., Liu, Z., & Sun, L (2011). Thermodynamic and Kinetic Analysis of Low-temperature Thermal Reduction of Graphene Oxide. *Nano-Micro Letters*, 3(1), 51-55. doi:10.5101/nml.v3i1.p51-55
- [42] De Silva, K. K. H., Huang, H.-H., & Yoshimura, M. (2018). Progress of reduction of graphene oxide by ascorbic acid. *Applied Surface Science*, 447, 338–346. doi:10.1016/j.apsusc.2018.03.243
- [43] Wu, W., Yang, L., Chen, S., Shao, Y., Jing, L., Zhao, G., & Wei, H. (2015). Core–shell nanospherical polypyrrole/graphene oxide composites for high performance supercapacitors. *RSC Advances*, 5(111), 91645–91653. doi:10.1039/c5ra17036b
- [44] Zhou, H., Han, G., Xiao, Y., Chang, Y., & Zhai, H.-J. (2014). Facile preparation of polypyrrole/graphene oxide nanocomposites with large areal capacitance using electrochemical codeposition for supercapacitors. *Journal of Power Sources*, 263, 259–267. doi:10.1016/j.jpowsour.2014.04.03
- [45] Abdul Bashid, A. H., Lim, N. H., Kamaruzaman, S., Abdul Rashid, S., Yunus, R., Huang, M. N., Yin, Y. C., Rahman, M. M., Altarawneh, M., Jiang, T. Z., & Alagarsamy, P. (2017). Electrodeposition of polypyrrole and reduced graphene oxide onto carbon bundle fibre as electrode for supercapacitor. *Nanoscale Research Letters*, 12, 246. doi: 10.1186/s11671-017-2010-3.
- [46] Báez, C., Navarro, F., Fuenzalida, F., Aguirre, M. J., Arévalo, M. C., Afonso, M., García, C., Ramírez, G., & Palenzuela, J. A. (2019). Electrical and Electrochemical Behavior of Carbon Paste Electrodes

- Modified with Ionic Liquids Based in N-Octylpyridinium Bis(trifluoromethylsulfonyl)Imide, A Theoretical and Experimental Study. *Molecules*, 24(18), 3382. doi: 10.3390/molecules24183382
- [48] Shindalkar, S. S., Reddy, M., Singh, R., Nainar, M. A. M., &Kandasubramanian, B. (2023). Polythiophene blends and composites as potential energy storage materials. *Synthetic Metals*, 299. doi:10.1016/j.synthmet.2023.117467
- [49] Mudila, H., Prasher, P., Kumar, M., Kumar, A., Zaidi, M. G. H., & Kumar, A. (2019). Critical analysis of polyindole and its composites in supercapacitor application. *Materials for Renewable and Sustainable Energy*, 8(9), 1-19. doi:10.1007/s40243-019-0149-9
- [50] Xu, B., Yue, S., Sui, Z., Zhang, X., Hou, S., Cao, G., & Yang, Y. (2011). What is the choice for supercapacitors: graphene or graphene oxide? *Energy and Environmental Science*, 4(8), 2826. doi:10.1039/c1ee01198g
- [51] Ch. Lazanas, A., & Prodromidis, M. I. (2023). Electrochemical Impedance Spectroscopy—A Tutorial. *ACS Measurement Science Au*, 3 (3), 162-193. doi: 10.1021/acsmeasuresciau.2c00070
- [52] Allagui, A., Freeborn, T. J., Elwakil, A. S., Fouda, M. E., Maundy, B. J., Radwan, A. G., Said, Z., & Abdelkareem, M. A. (2018). Review of fractional-order electrical characterization of supercapacitors. *Journal of Power Sources*, 400, 457–467. doi:10.1016/j.jpowsour.2018.08.04
- [53] Laishevkina, S., Shevchenko, N., Iakobson, O., Dobrodumov, A., Chelibanov, V., & Tomšík, E. (2022). Influence of the Nature and Structure of Polyelectrolyte Cryogels on the Polymerization of (3,4-Ethylenedioxythiophene) and Spectroscopic Characterization of the Composites. *Molecules*, 27(21), 7576.

doi.org/10.3390/molecules27217576

[54] Bo, Z., Wen, Z., Kim, H., Lu, G., Yu, K., & Chen, J. (2012). One-step fabrication and capacitive behavior of electrochemical double layer capacitor electrodes using vertically-oriented graphene directly grown on metal. *Carbon*, 50(12), 4379-4387. doi:10.1016/j.carbon.2012.05.014

## 5.1 Summary

Considering the growing worldwide requirement for energy, we must focus particular attention on technologies for storing energy these days. As portable electronics, long-distance hybrid cars, spacecraft, and other vehicles become more capable, high-power density and energy electrical energy storage technologies are needed. To meet the demands of various applications in terms of energy, cycle life, power, cost, and safety, developments in electrode and electrolyte materials must be taken into account. Electrochemical technologies for storing energy are among the most promising for these kinds of applications. Although performance advancements and a fundamental knowledge of the constituent substances have advanced significantly in recent years, there are still many obstacles to be addressed. The current work attempts to create a highly effective hybrid supercapacitive material by utilizing the specific area and cyclic stability of carbon-based material in favour of strong pseudocapacitance via redox reactions of a pseudocapacitive material. This is part of the continuing effort to develop an efficient energy material to address the global energy shortage. The pseudocapacitive material in a hybrid system provides the majority of the specific capacitance.

In the present thesis titled "Poly(quinone-hydrazine) based composites for energy storage applications" the polyazine and its composites with graphene Oxide and reduced graphene were synthesized and characterized by using different spectroscopic techniques. The composites based on polyazine, graphene oxide, and reduced graphene have been evaluated for supercapacitor applications. This thesis contains five chapters.

The first chapter covers the basic introduction to conducting polymers and their properties. This chapter has more focus on the quinone-based conducting polymers (like 1,4-Benzoquinone, 1,4-naphthoquinone, and 9,10- anthraquinone) for energy storage purposes and their redoxactive properties which depend on various parameters.

The second chapter provides detailed information about the various quinone-based materials for energy storage. After conducting numerous literature reviews, it was discovered that adding an electrondonating group to quinones can raise their redox potential. However, adding more functional groups usually results in a higher molecular weight rather than more active sites, which lowers specific capacity. It was also observed that apart from the methods of polymerization and solidification, merging quinone compounds with conductive materials like graphene, carbon nanotubes, porous carbon, conducting polymer, etc., provides a practical approach to reducing quinone compound dissolution while simultaneously improving electrical conductivity. Additionally, it was noted that polyazine conducting materials have lately been studied by the scientific community to look into their possible application in EES. Conjugated polyazines are a novel class of semiconductor materials that show great promise for use in organic thin-film transistors and supercapacitors. The findings indicate the potential utilization of polyazine as a material for supercapacitor applications.

Chapter three provides an in-depth description of the materials and characterization methods utilized for the synthesis of conducting polymer polyazine, graphene oxide, reduced graphene oxide, and their composites. The experimental method of synthesis of polyazine, graphene oxide, reduced graphene oxide, and their composites is also covered in this chapter. P-benzoquinone and hydrazine hydrate were polycondensed using a catalytic quantity of ZnCl<sub>2</sub> at 110–115 °C to

create electroactive polyazine. Some basic concepts about the characterization techniques were also explained in this chapter. The following characterisation techniques are used in this current study: FTIR, XRD, SEM, TGA, and DSC. Electrochemical techniques like CV, GCD, and EIS were used for the detection of their electrochemical behaviour.

The fourth chapter includes the results and discussion part of the current work. The synthesis polymer and its composites were confirmed by the FTIR spectroscopy. By FTIR spectroscopy, it was observed that the resultant polymer had azine-type linkage. XRD, and SEM have been used to analyze the resultant polymer and their composites to establish their structural morphology. Polyazine and reduced graphene oxide were found to be amorphous while graphene oxide was found to be crystalline based on their XRD spectra. TGA and DSC studies revealed that the polymer and its composites are thermally stable for the supercapacitor. The electrochemical properties of the prepared PAZ, GO, rGO, and their composites were investigated by CV, GCD, and EIS techniques. CV analysis shows a regular increment in specific capacitance in composites, after that a decrease is observed in composites. The specific capacitance of pure PAZ was found to be maximum, i.e. 35.42 F/g at 10 mV/s and minimum, i.e. 4.8 F/g at 100 mV/s. The maximum specific capacitance of GO was found to be 247.20 F/g at 10 mV/s and the minimum at 33.53 F/g at 100 mV/s. The specific capacitance was found to be 77.48, 140.20, 332.05, 475.61, and 407.56 F/g for PG-1, PG-2, PG-3, PG-4, and PG-5 respectively at a scan rate of 10 mV/s. The specific capacitance was found to be 10.52, 18.90, 45.30, 63.10, and 55.11 for PG-1, PG-2, PG-3, PG-4, and PG-5 respectively at a scan rate of 100 mV/s. It was observed that the maximum value of specific capacitance was achieved for PG-4, which further started to decrease as the amount of GO increased in the composite PG-5.

In the case of rGO, the maximum specific capacitance was found to be 383.21 F/g at 10 mV/s and the minimum at 48.77 F/g at 100 mV/s. The specific capacitance was found to be 158.76, 312.10, 689.21, and 432.21 F/g for PrG-1, PrG-2, PrG-3, and PrG-4 respectively at a scan rate of 10 mV/s. The specific capacitance was found to be 20.11, 43.34, 112.54, and 54.22 F/g for PrG-1, PrG-2, PrG-3, and PrG-4 respectively at a scan rate of 100 mV/s. It was found that PrG-3 had the highest specific capacitance value, which began to decline when the amount of rGO in the composite PrG-4 arose. The specific capacitance, energy density, and power density were determined by GCD curves at a specific current density. The energy density was found to be 2.76, 4.41, and 3.94 Wh/kg for PAZ at the current densities of 1, 0.5, and 0.25 A/g respectively. The power density was found to be 499.99, 249.99, and 124.99 W/kg for PAZ at the current densities of 1, 0.5, and 0.25 A/g respectively. The specific capacitance, energy density, and power density were found to be 22.39 F/g, 5.06 Wh/kg, and 856.33 W/kg for GO at a current density of 1 A/g respectively. The specific capacitance, energy density, and power density were found to be 37.26 F/g, 10.35 Wh/kg, and 1007.02 W/kg for PG-4 at a current density of 1A/g. The specific capacitance, energy density, and power density were 90.11 F/g, 12.52 Wh/kg, and 500 W/kg for rGO at a current density of 1 A/g. The specific capacitance, energy density, and power density were found to be 235.31 F/g, 32.68 Wh/kg, and 499.99 W/kg for PrG-3 at a current density of 1A/g. EIS analysis shows that PAZ has low faradic resistance between 100 MHz to 100 kHz with an AC amplitude of 20 mV/s and a phase angle of -75° was noted, which is close to that of an ideal capacitor (-90°), indicating improved charge transfer because of the electrode and electrolyte's advantageous contact. In comparison to pure PAZ, the Bode plot shows that the composite PG-4 and PrG-3 has a lower impedance value over the frequency range, indicating improved charge/discharge and smoother electron or ion transit during energy

storage capabilities. With a substantially higher specific capacitance than polymer alone, the PrG-3 and PG-4 composites (has lowest impedance) electrode may be the promising candidate for the development of future safe and reasonably priced batteries and electrochemical supercapacitors respectively.

Among all the electroactive materials, PrG-3 may be suitable for battery applications due to its high energy density, which enables longer energy storage and extended device operation and PG-4 shows better capacitive beahviour due to its high specific capacitance, high power density, and less impedance over a frequency range.

#### **5.2 FUTURE OUTLOOK**

Numerous opportunities for further study in this crucial field of conducting polymers for energy storage applications are opened by the current thesis. Future research on this subject will focus on precisely optimizing the manufacture of supercapacitor devices to improve the electrode material's electrochemical performance. Further research is necessary to confirm the practicality of the synthesized composites for energy storage applications.

- Another avenue for future research is the careful blending of these novel polymers (PAZ) with different Carbonaceous materials (CNT and activated carbon, etc.) investigations and their electrochemical characteristics.
- Improving the hybrid supercapacitive material's current density through synthesis.
- More electrochemical characterizations of modified PAZ with carbonaceous materials using GCD and EIS.

#### **List of Publications:**

- 1. Pooja, Anil Kumar, and Harish Mudila "Studying Possibilities of Poly(benzoquinone-hydrazine) for Electrochemical Energy Storage Application" was published in ES Energy and Environment. [SJR: 0.45, Q2]
- 2. Pooja, Anil Kumar, Parteek Prasher and Harish Mudila "Factors affecting the electrical conductivity of conducting polymers" Carbon letters, 33, pages 307–324 [I.F: 4.5, SJR: 0.58, Q2]
- 3. Pooja, Harish Mudila and Anil Kumar "Quinone Based Conducting Materials for Efficient Energy Storage" was published in AIP conference proceedings. [SJR: 0.16]

### **List of Conference:**

 Oral presentation at 6th International Conference on Recent Advances in Fundamental and Applied Sciences (RAFAS 2025) held at Lovely Professional University, Phagwara, April 18-19, 2025.



2. Participated in 3rd International Conference on Materials for emerging technologies(ICMET-21) held at Lovely Professional University, Phagwara organized by Department of Research Impact and outcome, Division of Research and development during June 18-19, 2022



 Oral presentation at 4th International Conference on Recent Advances in Fundamental and Applied Sciences (RAFAS 2023) held at Lovely Professional University, Phagwara, March 24-25, 2023.



4. Participated in 3rd International Conference on Recent Advances in Fundamental and Applied Sciences (RAFAS 2021) held at Lovely Professional University, Phagwara during June 25-26, 2021.



5. Participated in Integrated Approaches in Science and Technology for Sustainable Future held at J. C. Bose University Of Science and Technology, YMCA, Faridabad during 28 Feb - 01 March, 2022.



# List of workshops:

1. Participated in one week virtual International Workshop on "Research Writing and Publication" organized by Central University of Haryana, Mahendergarh, India from 14th to 18th November, 2022



2. Participated in MDP-2021 oganised by Eudoxia Research Centre India.

